Multiplexed analysis of diverse RNA classes via hybridization chain reaction

Thesis by
Aneesh Acharya

In Partial Fulfillment of the Requirements for the
degree of
Doctor of Philosophy

CALIFORNIA INSTITUTE OF TECHNOLOGY
Pasadena, California

2016
Defended May 19, 2016

Aneesh Acharya
ORCID: 0000-0002-4402-7147

ACKNOWLEDGEMENTS

I would like to first thank my advisor, Niles Pierce. Niles accepted me as a young graduate student into his lab and has always made me feel supported. Without his patience, enthusiasm, and guidance, this thesis would certainly not be possible.

I thank my thesis committee, Michael Elowitz, Scott Fraser, and Sarkis Mazmanian. Throughout my graduate career, all three were unceasingly enthusiastic and excited about the possibilities of the technologies I developed, and I am deeply grateful for their support, advice, and optimism.

It's important I thank the entire Pierce Lab. Since joining, I've felt honored to work with such mature, intelligent, and composed colleagues. Every day I learn from them and try and improve myself. Specifically, Harry Choi and Colby Calvert have been great co-workers and friends throughout my graduate life. Harry is one of my closest friends and was always available when I needed help.

I also thank my collaborator, Greg Donaldson, and students I had the privilege of mentoring, Siva Gangavarapu, Aditya Bhagavati, and George Artavanis.

Finally, and most importantly, I thank my friends and family for keeping me grounded and balanced – I'm truly fortunate to have maintained my closest friendships from grade school. I thank Srimoyee Ghosh, my girlfriend and best friend. Caltech is not always the easiest place to be, but she has always been there for me, and I will never forget that. And I thank my family – my father, Malay Acharya, my mother, Geeta Acharya, and my older brother, Ishaan Acharya – for being the best role models one could ask for. I'm so grateful that all three will attend my defense, and I hope I can make them proud.

Biology is the study of complicated things that have the appearance of having been designed with a purpose.
Richard Dawkins

ABSTRACT

Gene circuits are complex biological networks composed of numerous regulatory elements, including transcription factors, mRNAs, and microRNAs. Fluorescent *in situ* hybridization (FISH) is a powerful method for spatially mapping expression levels of RNA elements within an intact organism, but traditional methods exhibit at least one of the following drawbacks: low signal-to-background, arduous and/or destructive multiplexing, and non-quantitative signal. These issues are all overcome using *in situ* amplification based on the mechanism of hybridization chain reaction (HCR). With this approach, nucleic acid probes complementary to RNA targets trigger the self-assembly of fluorophore-labeled nucleic acid hairpins into tethered fluorescent amplification polymers. *In situ* HCR enables straightforward multiplexing, high signal-to-background, and quantitative signal. Here, we address three key scenarios in which HCR enables novel applications for *in situ* hybridization. First, we address the challenge of sorting cell subpopulations based on mRNA abundance using flow cytometry to enable high-throughput measurement of the signal intensity from individual cells. High signal is required to overcome the background autofluorescence integrated over the volume of each cell. Quantitative HCR signal amplification enables multi-dimensional sorting of mammalian cell lines based on expression levels of multiple target mRNAs. Second, we address the challenge of mapping multiple microRNA and mRNA targets simultaneously. Traditional methods enable mapping of single microRNA targets in isolation and use costly LNA probes with proprietary compositions that differ for each target. Here we develop *in situ* HCR for multiplexed mapping not only of microRNAs, but of microRNAs and mRNAs together, using non-proprietary 2'OMe-RNA probes for miRNA targets and DNA probes for mRNA targets. Third, to enable studies of gut flora, we address the challenge of mapping spatial relationships between different bacterial species within the intact mouse colon. *In situ* HCR enables multiplexed discrimination of multiple closely-related Bacteroides species with rRNAs that differ by only a few nucleotides. In summary, this thesis presents *in situ* HCR as a tool for multiplexed analysis of diverse RNA classes and expands the range of gene circuit regulatory elements that can be spatially and quantitatively mapped.

TABLE OF CONTENTS

LIST OF ILLUSTRATIONS

LIST OF TABLES

Chapter 1

INTRODUCTION

Throughout human history, progress in our collective understanding of the pure sciences has led to the rise of complementary engineering disciplines. These disciplines set out to distill our knowledge of natural systems into a concise set of design principles for rationally designing artificial ones. Consequently, biological engineering aims to apply engineering principles to biological systems. Perhaps the most elusive, yet impactful goal of biological engineering is to enable rational design of biological gene circuits and gene circuit components [1–4].

It is important to recognize two complementary fields of study: systems and synthetic biology. Together they are locked in a mutualistic cycle; systems biologists approach existing biological systems with a top-down approach [5–7], and they often discover design principles that synthetic biologists can adopt in their bottom-up approach to building gene circuits *de novo* [8]. Long heralded as a new frontier in biological engineering, synthetic biology promises to revolutionize mankind's long-standing, systemic problems, ranging from waste management [9], clean fuel production [10], cancer treatment [11], and many more [4, 12, 13].

Future implications aside, it is becoming clearer that gene circuits, unlike electronic circuits, are not quite predictable [14]. To name just two differences, gene circuits are composed of a far wider set of elements than their electronic counterparts, and stochastic fluctuations in expression are a crucial feature, rather than an unwanted side effect [15–17]. The sheer number and diversity of regulatory elements in gene circuits, such as messenger RNA (mRNA), microRNA (miRNA), ribosomal RNA (rRNA), and many more, add layers to their complexity. As a result, the systems biology approach is crucial to build our design principles by studying naturally-occurring circuits. In order to enable biologists to learn these design principles, a new generation of tools is required to allow for detailed study of naturally-occurring gene circuits.

Simultaneous to efforts in synthetic and systems biology, the field of molecular

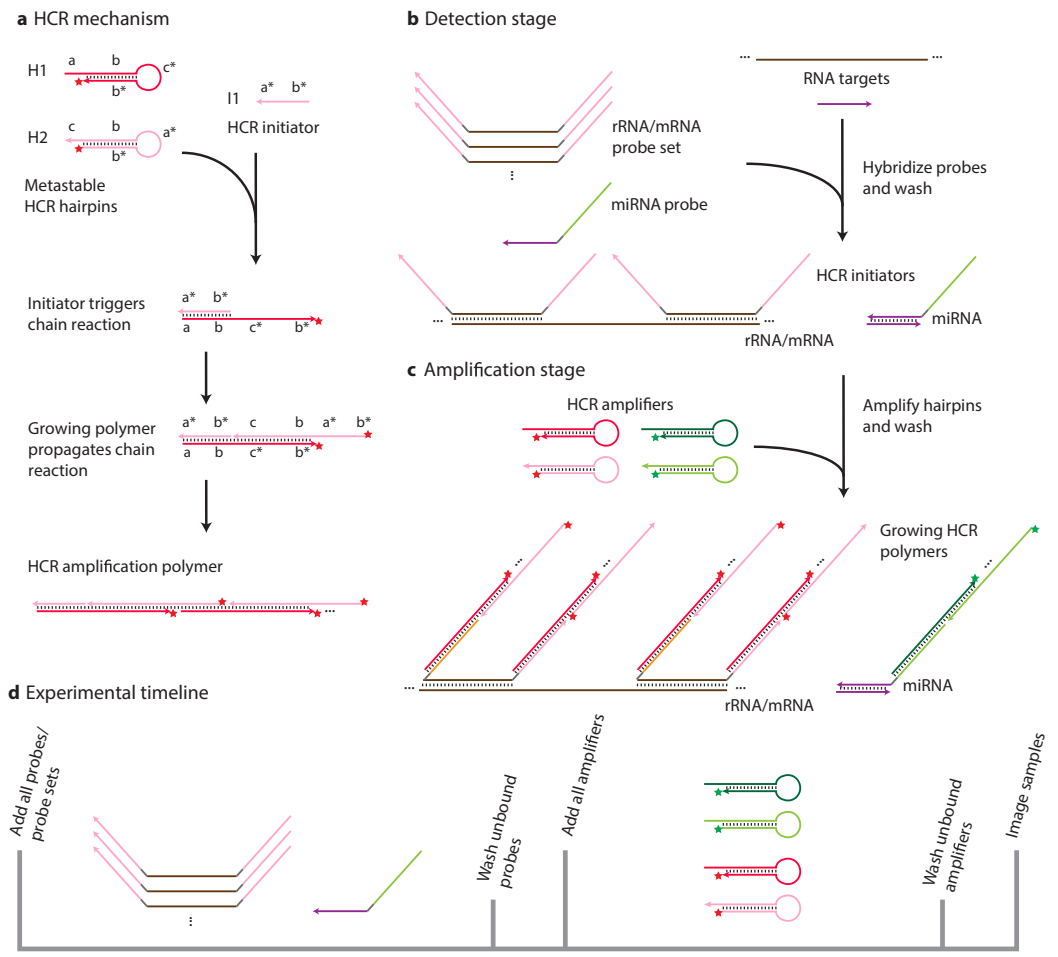

Figure 1.1: **Multiplexed in situ amplification via hybridization chain reaction (HCR). a.** HCR mechanism. Metastable fluorescent hairpins self-assemble into fluorescent amplification polymers upon detection of a cognate initiator. Initiator I1 nucleates with hairpin H1 via base-pairing to single-stranded toehold "a," mediating a branch migration that opens the hairpin to form complex I1H1 containing single-stranded segment "c*-b." This complex nucleates with hairpin H2 via base-pairing to toehold "c," mediating a branch migration that opens the hairpin to form complex I1H1H2 containing single-stranded segment "b*-a*." Thus, the initiator sequence is regenerated, providing the bases for a chain reaction of alternating H1 and H2 addition steps. Stars denote fluorophores. **b.** Detection stage. Probe sets are hybridized to RNA targets and then unused probes are washed from the sample. **c.** Amplification stage. Initiators trigger self-assembly of tethered HCR polymers and then unused hairpins are washed from the sample. **d.** Experimental timeline. The same two-stage protocol is used regardless of number of targets. For multiplexed experiments (two-color example depicted), probe sets for different target RNAs carry orthogonal initiators that trigger orthogonal HCR amplification cascades labeled by spectrally distinct fluorophores.

programming has created design principles and tools for building programmable nucleic acid mechanisms with tangible functionality [18–21]. Hybridization chain reaction (HCR, Figure 1.1) [18] is a crucial nucleic acid mechanism that has enabled diverse applications. Specifically, HCR is a mechanism by which two kinetically trapped nucleic acid hairpin molecules (H1 and H2 in 1.1a) coexist metastably, but in the presence of a cognate initiator (I1), react to assemble a long, double-stranded amplification polymer. Figure 1.1 is a schematic representation of HCR (1.1a) and the generalized *in situ* HCR protocol (1.1b-d). This technology has been harnessed to allow for parallel *in situ* amplification of up to five target mRNA molecules within whole-mount zebrafish embryos[22, 23], an advancement that will revolutionize the use cases for *in situ* hybridization in years to come [24, 25].

In situ HCR represents a fundamental addition to the current toolkit for studying gene circuits. Yet gene circuits are composed of many different components in many different settings and organisms. Thus, it is critical to extend *in situ* HCR to allow for the sampling of a variety of gene circuit elements beyond mRNAs, as well as new settings to enable profoundly new applications. Here, we extend *in situ* HCR to cover new applications and a new class of short RNA targets.

In Chapter II, it is demonstrated that *in situ* HCR can be applied to profiling heterogeneous mammalian cell populations and subpopulations can be isolated based upon expression of an mRNA transcript.

In Chapter III, modified short probes are engineered to enable simultaneous detection of microRNA and longer RNA targets within an intact zebrafish embryo.

In Chapter IV, short probes are coupled with optimized experimental conditions and HCR amplification to enable species-specific identification and spatial localization within mouse colon tissue sections.

Appendices A, B, and C provide supplementary information for Chapters II, III, and IV, respectively.

References

1. Church, G. M., Elowitz, M. B., Smolke, C. D., Voigt, C. A. & Weiss, R. Realizing the potential of synthetic biology. *Nature reviews. Molecular cell biology* **15,** 289–294 (Mar. 2014).
2. Andrianantoandro, E., Basu, S., Karig, D. K. & Weiss, R. Synthetic biology: new engineering rules for an emerging discipline. *Molecular systems biology* **2,** 2006.0028 (May 2006).
3. Heinemann, M. & Panke, S. Synthetic biology–putting engineering into biology. *Bioinformatics (Oxford, England)* **22,** 2790–2799 (Sept. 2006).
4. Khalil, A. S., Khalil, A. S., Collins, J. J. & Collins, J. J. Synthetic biology: applications come of age. *Nature reviews. Genetics* **11,** 367–379 (Apr. 2010).
5. Lin, Y., Sohn, C. H., Dalal, C. K., Cai, L. & Elowitz, M. B. Combinatorial gene regulation by modulation of relative pulse timing. *Nature* **527,** 54–58 (Oct. 2015).
6. Young, J. W. *et al.* Measuring single-cell gene expression dynamics in bacteria using fluorescence time-lapse microscopy. *Nature protocols* **7,** 80–88 (Dec. 2011).
7. Sprinzak, D. *et al.* Cis-interactions between Notch and Delta generate mutually exclusive signalling states. *Nature* **465,** 86–90 (Apr. 2010).
8. Morsut, L. *et al.* Engineering Customized Cell Sensing and Response Behaviors Using Synthetic Notch Receptors. *Cell* **164,** 780–791 (Jan. 2016).
9. Cases, I. & de Lorenzo, V. Genetically modified organisms for the environment: stories of success and failure and what we have learned from them. *International microbiology : the official journal of the Spanish Society for Microbiology* **8,** 213–222 (Oct. 2005).
10. Savage, D. F., Way, J. & Silver, P. A. Defossiling fuel: how synthetic biology can transform biofuel production. *ACS chemical biology* **3,** 13–16 (Jan. 2008).
11. Anderson, J. C., Clarke, E. J., Arkin, A. P. & Voigt, C. A. Environmentally controlled invasion of cancer cells by engineered bacteria. *Journal of molecular biology* **355,** 619–627 (Nov. 2005).
12. Antunes, M. S. *et al.* A synthetic de-greening gene circuit provides a reporting system that is remotely detectable and has a re-set capacity. *Plant biotechnology journal* **4,** 605–622 (Feb. 2007).
13. Bowen, T. A., Zdunek, J. K. & Medford, J. I. Cultivating plant synthetic biology from systems biology. *The New phytologist* **179,** 583–587 (Mar. 2008).

14. Purnick, P. E. M. & Weiss, R. The second wave of synthetic biology: from modules to systems. *Nature reviews. Molecular cell biology* **10,** 410–422 (May 2009).

15. Raj, A. & van Oudenaarden, A. Nature, nurture, or chance: stochastic gene expression and its consequences. *Cell* **135,** 216–226 (Oct. 2008).

16. Weinberger, L. S., Burnett, J. C., Toettcher, J. E., Arkin, A. P. & Schaffer, D. V. Stochastic gene expression in a lentiviral positive-feedback loop: HIV-1 Tat fluctuations drive phenotypic diversity. *Cell* **122,** 169–182 (July 2005).

17. Elowitz, M. B. Stochastic Gene Expression in a Single Cell. *Science* **297,** 1183 (2002).

18. Dirks, R. M. & Pierce, N. A. Triggered amplification by hybridization chain reaction. *Proceedings of the National Academy of Sciences of the United States of America* **101,** 15275–15278 (Oct. 2004).

19. Breaker, R. R. Natural and engineered nucleic acids as tools to explore biology. *Nature* **432,** 838–845 (Dec. 2004).

20. Sternberg, J. B. & Pierce, N. A. Exquisite sequence selectivity with small conditional RNAs. *Nano letters* **14,** 4568–4572 (June 2014).

21. Zhang, F., Nangreave, J., Liu, Y. & Yan, H. Structural DNA nanotechnology: state of the art and future perspective. *Journal of the American Chemical Society* **136,** 11198–11211 (July 2014).

22. Choi, H. M. T. *et al.* Programmable in situ amplification for multiplexed imaging of mRNA expression. *Nature Biotechnology* **28,** 1208–1212 (Oct. 2010).

23. Choi, H. M. T., Beck, V. A. & Pierce, N. A. Next-Generation in SituHybridization Chain Reaction: Higher Gain, Lower Cost, Greater Durability. *ACS Nano* **8,** 4284–4294 (May 2014).

24. Rosenthal, A. Z. *et al.* Localizing transcripts to single cells suggests an important role of uncultured deltaproteobacteria in the termite gut hydrogen economy. *Proceedings of the National Academy of Sciences of the United States of America* **110,** 16163–16168 (Sept. 2013).

25. Huss, D. *et al.* Combinatorial analysis of mRNA expression patterns in mouse embryos using hybridization chain reaction. *Cold Spring Harbor protocols* **2015,** 259–268 (Mar. 2015).

Chapter 2

MULTIPLEXED QUANTITATIVE CELL SORTING BASED ON RNA ABUNDANCE

2.1 Introduction

Flow cytometry is a crucial data acquisition tool used in research and clinical settings for many applications, including cell counting, sorting, and biomarker detection [1–5]. Cytometry allows for simultaneous multi-parametric analysis of the physical properties of thousands of cells per second. Fluorescence-activated cell sorting (FACS) is a specialized form of flow cytometry; using FACS, it is possible to sort a heterogeneous mixture of cells on a cell-by-cell basis, based upon any logical combination of the measured parameters. FACS is used frequently in biological research labs because it provides a fast and high-throughput measurement of fluorescent signals from individual cells, as well as physical separation of cells of interest [6–8].

Coupling flow cytometry with fluorescent *in situ* hybridization (flow-FISH) is a technique that is growing in popularity [9–16]. The specificity of probe base-pairing of FISH combined with the many advantages of flow cytometry make this an enticing tool for a variety of applications, including telomere length determination [9, 10], cellular identification and gene expression [11], monitoring viral multiplication in infected cells [12], and bacterial community analysis and enumeration [13].

In order for staining to be useful in cytometry and cell sorting, sufficient amplification of the fluorescent signal is required to separate heterogeneous populations. When measuring fluorescent signal with cytometry, an entire cell represents the smallest physical unit that can be measured, or voxel. Since most cells do not contain many copies of any single transcript, measured intensities from cytometry include a large component of integrated background. This represents a significant challenge for current methods of flow-FISH, which suffer from drawbacks, such as poor separation of heterogeneous mixtures due to low signal-to-background [13, 17]. Additionally, given that mRNAs represent just one type of element in natural gene circuits, stronger signal amplification

is necessary in order to detect smaller or sequence constrained targets, such as microRNAs or mRNA transcript variants.

Hybridization chain reaction (HCR) is a technology developed by the Pierce Lab in 2004 [18], and it has been demonstrated as a superior amplification method for the *in situ* detection of mRNA in whole-mount zebrafish embryos [19]. Here we propose a protocol for adapting this *in situ* amplification technique for use with cell suspension. In doing so, we preserve the advantages conferred by HCR, including high signal-to-background, multiplexed target detection, relatively quantitative measurements, and the potential for short target detection. Additionally, the work presented here utilizes RNA HCR; the planned switch to DNA HCR will offer greater signal-to-background when dealing with low-copy or short RNA targets.

HCR amplification for *in situ* hybridization occurs in two stages independent of the number of target mRNAs (Figure 2.1). In the detection stage, all target mRNAs are detected simultaneously via *in situ* hybridization of complementary RNA probes; unused probes are washed from the sample. Each target mRNA is addressed by a probe set containing one or more RNA probe species; different targets are addressed by probe sets carrying orthogonal initiators. Each RNA probe carries four identical initiators, thus each supports formation of four RNA HCR polymers. In the amplification stage, fluorescent signals are generated for all target mRNAs simultaneously using RNA HCR. Orthogonal initiators trigger formation of orthogonal HCR polymers, labeled with spectrally distinct fluorophores; unused hairpins are washed from the sample prior to flow cytometry.

To characterize the performance of HCR as a method for isolating cells based on mRNA expression, we designed a battery of experiments to rigorously test *in situ* HCR's signal-to-background, target specificity, and ability to quantify target expression. Samples are analyzed using flow cytometry and cell sorting. Additional data for all figures can be found in Appendix A.

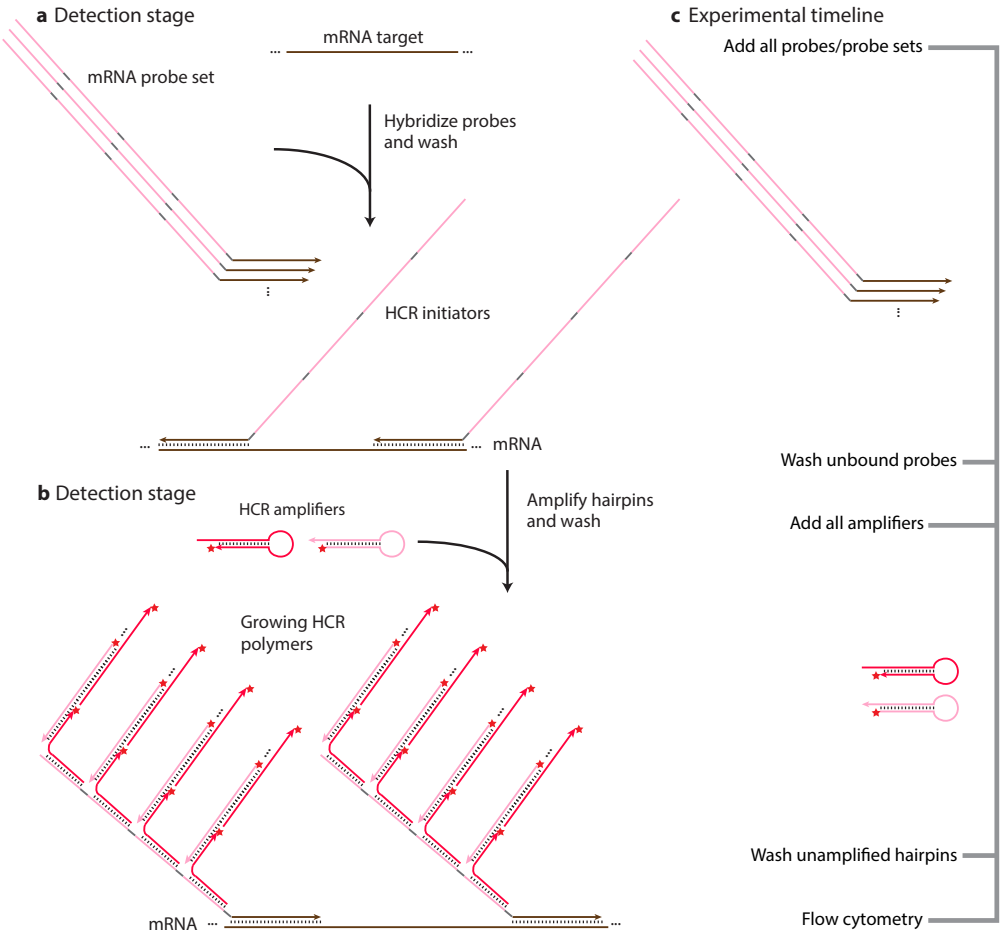

Figure 2.1: **Multiplexed in situ amplification via hybridization chain reaction (HCR). a.** Detection stage. Probe sets are hybridized to mRNA targets and then unused probes are washed from the sample. **b.** Amplification stage. Initiators trigger self-assembly of tethered HCR polymers and then unused hairpins are washed from the sample. **c.** Experimental timeline. The same two-stage protocol is used regardless of number of target mRNAs. For multiplexed experiments (single color example depicted), probe sets for different target mRNAs carry orthogonal initiators that trigger orthogonal HCR amplification cascades labeled by spectrally distinct fluorophores (denoted by red stars).

2.2 Probe Set Optimization

Signal observed from samples that have undergone *in situ* HCR can be componentized into four categories: autofluorescence (AF), non-specific amplification of hairpins without a present probe containing a cognate initiator (NSA), non-specific binding of the probe to an off-target (NSD), or true signal (SIG). This section highlights how HCR probe sets against transgenic targets are optimized and proposes a method for optimizing those against endogenous targets. Note that probe set optimization is not always necessary, but is a useful tool when required.

2.2.1 Transgenic Targets

In order to characterize the performance of a given HCR probe set, signal-to-background can be calculated from samples that feature each of the aforementioned categories. All samples are subject to experimental conditions of *in situ* HCR, but lack key components. Table 2.1 depicts these control samples. A crucial aspect of this type of analysis is that each form of background can only be measured in its native summation. For example, it is impossible to study NSA in isolation, but rather the sum of AF and NSA can be measured directly.

Cell Line	Sample Type	HCR Probe	HCR Amplifier
Either	AF	✗	✗
Either	AF + NSA	✗	✓
Wild-Type	AF + NSA + NSD	✓	✓
Transgenic	AF + NSA + NSD + SIG	✓	✓

Table 2.1: Description of how negative and positive control samples can be created for *in situ* HCR.

Figure 2.2 demonstrates proof-of-concept for this type of validation for a probe set designed against *d2egfp*. Transgenic and wild-type cell lines were used for determining "AF + NSA + NSD + SIG" and "AF + NSA + NSD," respectively. Typical performance of good (2.2a) and bad (2.2b) probes are shown. Additionally, 2.2c,d showcase performance of unoptimized and optimized probe sets. Qualitatively, background and signal histograms become entirely separable using an optimized probe set. 2.2e,f demonstrate the data shown in 2.2c,d, respectively, with linear scaling.

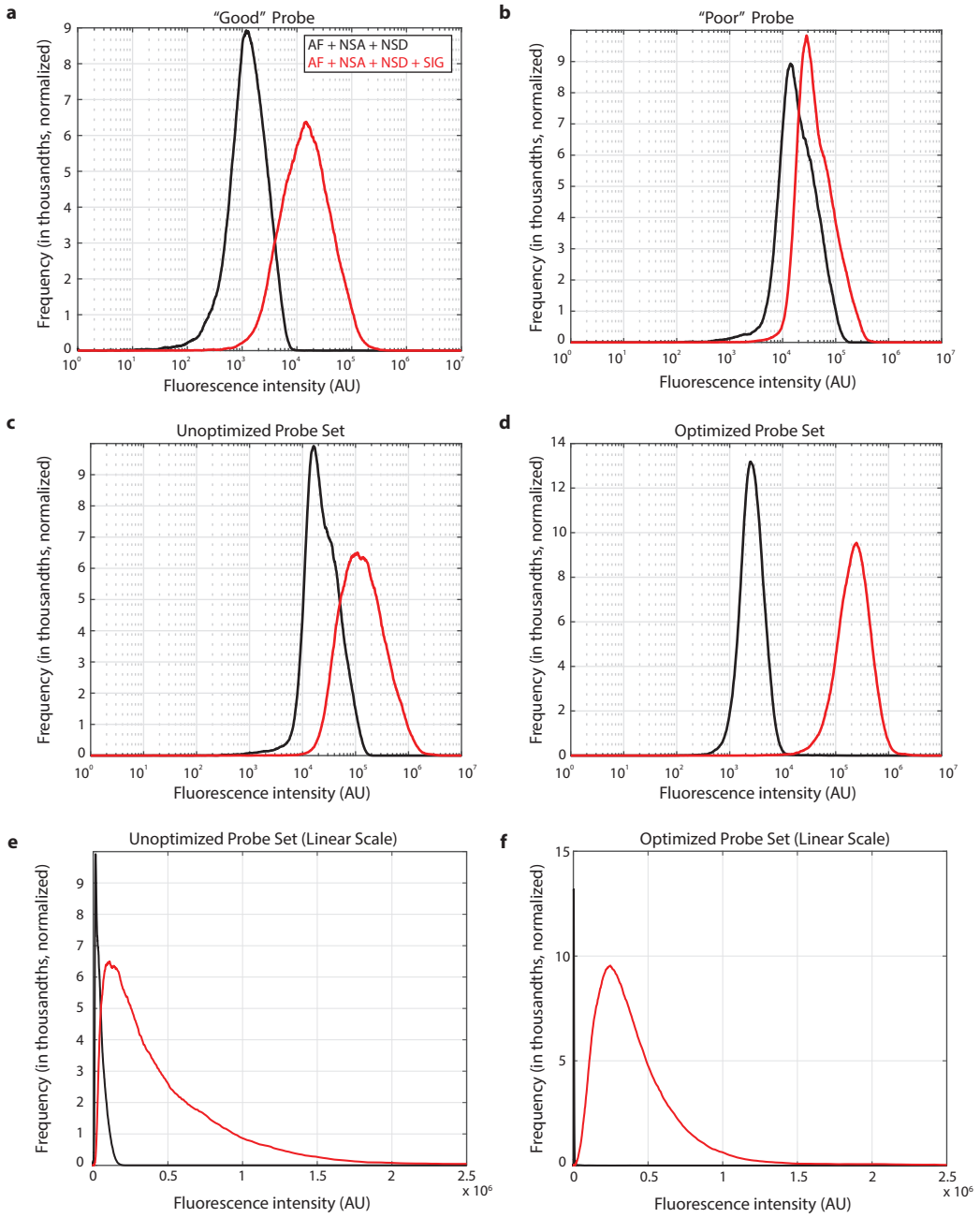

Figure 2.2: **Sample probe optimization results.** Cell lines are HEK293T (black) and HEK293 + *d2egfp* (red). Probe sets target *d2egfp* transcript. Each histogram is composed of 50,000 cell counts. **a.** Typical performance of a single good probe. **b.** Typical performance of a single poor probe. **c.** Performance of entire probe set including poor probes. Linear plot shown in (e). **d.** Resultant performance of optimized probe set excluding poor probes. Linear plot shown in (f). **e.** Linear-scaled axis for data shown in (c). **f.** Linear-scaled axis for data shown in (d). Samples: HEK293T, HEK293 + *d2egfp*. Target: transgenic mRNA *Tg(d2egfp)*.

2.2.2 Endogenous Targets

Optimizing probe sets against endogenous targets presents an entirely different challenge. Although a scramble probe, designed to have no sequence specificity to any transcript present, is often used, this method does not measure sequence specific NSD. Here, we present a novel method for probe optimization using pairwise combinations of probes.

To perform pairwise probe optimization, probes within a probe set are applied combinatorially containing initiators for orthogonal HCR amplification systems to expose poor performing probes. Two caveats are that this method requires a single probe to produce sufficient signal to overcome AF + NSA + NSD, and the probe set being tested must contain at least two good probes. If these conditions are met, then it follows that pairs of good probes will produce high correlation, while probe pairs containing one or more bad probes will not produce high correlation. For a probe set containing n probes, $\frac{n \cdot (n-1)}{2}$ experiments are required to complete the optimization.

Table 2.2 outlines the results of experiments performed to optimize a probe set consisting of five probes targeting beta-actin (*actb*). Probes listed in rows of the table were amplified with Alexa488-labeled HCR, and probes listed in columns were amplified with Alexa647-labeled HCR. Entries in the table refer to Pearson correlation coefficients calculated on a cell-by-cell basis between the two fluorescent channels.

Probe #	1	2	3	4	5
1	✗	0.03	0.02	0.02	0.02
2	✗	✗	0.77	0.73	0.75
3	✗	✗	✗	0.50	0.75
4	✗	✗	✗	✗	0.73
5	✗	✗	✗	✗	✗

Table 2.2: **Overview of experiments required to complete pairwise optimization of actb probe set.** Entries refer to Pearson correlation coefficient calculated on a cell-by-cell basis between signal collected in orthogonal HCR amplified channels. High correlation indicates both probes in a pair bind correct target sufficiently to overcome background (AF + NSA + NSD). Low correlation implies one or both probes in the pair is poorly performing.

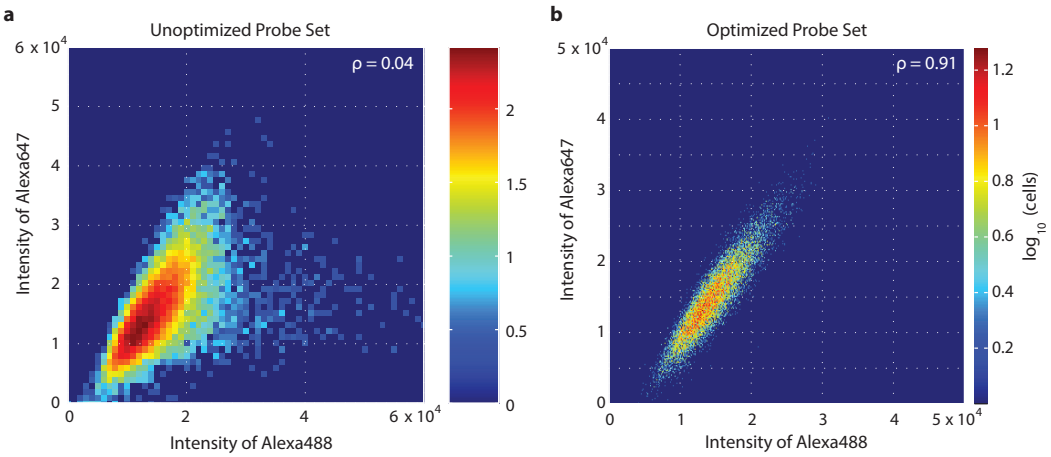

Figure 2.3: **Sample probe optimization results for targeting endogenous transcript actb. a.** Density histogram depicting correlation between two channels when unoptimized probe set is split into two orthogonally-amplified sets. **b.** Density histogram depicting correlation between two channels when optimized probe set is split into two orthogonally-amplified sets. Sample: HEK293T. Target: endogenous mRNA *actb*. Each panel depicts 50,000 cell counts.

From Table 2.2, it is clear that probe 1 performs poorly when paired with any of the other four probes. Figure 2.3 demonstrates redundant detection of *actb* using both unoptimized 2.3a and optimized 2.3b probe sets. Removal of the bad probe improves the Pearson correlation coefficient from 0.04 to 0.91. This successful optimization is a strong proof-of-concept demonstration of pairwise probe optimization, and could potentially be used for probe sets against transgenic targets in cases in which obtaining a wild-type sample is prohibitive.

2.3 Comparison of Single vs. Quad Initiator HCR Probes

Validation of probes with four HCR initiators has been completed for cell suspension experiments. By potentially increasing the signal by a factor of four by switching to HCR probes with four initiators instead of one, NSD should also increase by a factor of at least four. Autofluorescence and nonspecific HCR amplification should remain constant, since they occur independent of the initiator. For regimes in which AF dominates relative to NSD, adding initiators or probes is beneficial to signal-to-background.

Figure 2.4 shows this comparison between HCR probes with one and four initiators. This experiment involved using the HEK293T line as wild-type and the HEK293 + *d2egfp* as a transgenic line and data acquisition with flow cytometry. For both types of HCR probes, the same cell lines, target mRNA, probe recognition sequence, and HCR amplifiers were used. The only variable was the number of HCR initiators attached to the probe recognition sequence.

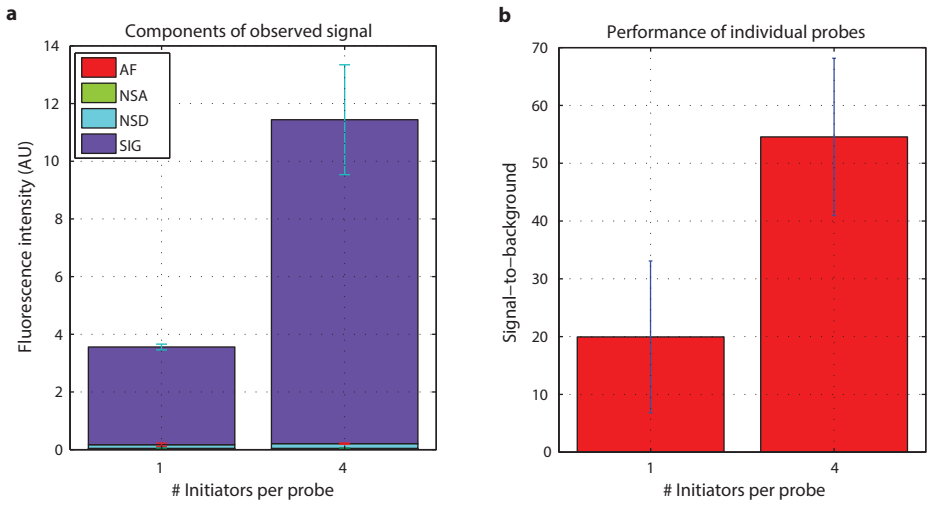

Figure 2.4: **Quantitative analysis of one versus four initiators per HCR probe. a.** Component depiction of signal and all sources of background. Background signals are very small relative to true signal. **b.** Signal-to-background ratio calculation for each probe type. The probe set with four initiators yields a signal-to-background ratio 2.7 fold over the single initiator probes. Sample: HEK293T, HEK293 + *d2egfp*. Target: transgenic mRNA Tg(*d2egfp*). Each panel represents 50,000 cell counts. Error bars are drawn as standard error over three samples. n = 3.

2.4 Troubleshooting in situ HCR with Heterogeneous Cell Populations

A significant engineering challenge was posed when optimizing the *in situ* HCR protocol for detection of cells within heterogeneous cell mixtures. Cells in mixtures corresponding to the background peak showed higher fluorescence than those from the same cell line in isolation (NSD). Crucially, the average signal did not appear to change between homogeneous and heterogeneous samples. Figure 2.5a demonstrates this increased NSD.

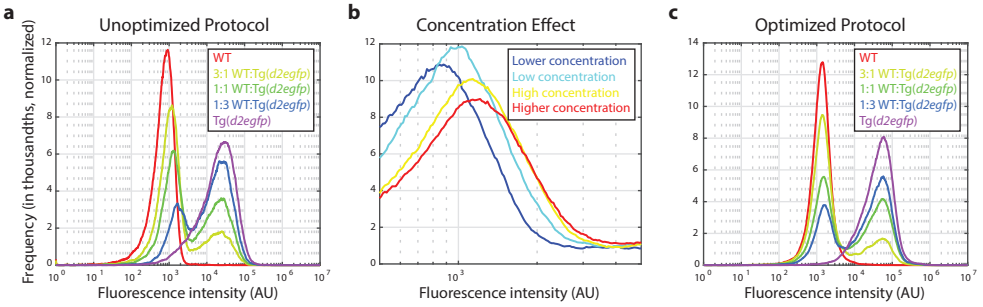

Figure 2.5: **Troubleshooting HCR with heterogeneous cell populations. a.** *In situ* HCR with heterogeneous cell mixtures using unoptimized conditions for cell concentrations. **b.** Examining the effect of cell concentration upon NSD peak. **c.** *In situ* HCR with heterogeneous cell mixtures using optimized conditions for cell concentrations. Sample: mixtures of HEK293T, HEK293 + *d2egfp*. Target: transgenic mRNA Tg(*d2egfp*). Each panel represents 50,000 cell counts.

It was determined that the root cause of the increased NSD in heterogeneous cell mixtures was cell concentration of the *in situ* reaction. 2.5b shows a zoomed version of the NSD peak within a heterogeneous mixture. The trend indicates that as concentration of cells in the sample tube increases, so does the fluorescence of the NSD peak. Furthermore, the issue can be traced directly to the concentration of transgenic cells. Note that in 2.5a as the fraction of transgenic cells increases, the size of the NSD shift also increases.

To mitigate this effect, we optimized hybridization volumes and cell counts per reaction. 2.5c demonstrates the identical experiment in 2.5a but with the optimized protocol. Note the shift has virtually disappeared. The data are consistent with the hypothesis that if transgenic cells produce large numbers of the transgene's transcript, combined with imperfect retention of transcripts after 4 % FA fixation, it is possible that transcripts are in a state of flux

entering and leaving cells on an individual basis. Thus, as the concentration of cells increases, it becomes more likely that the transgene will be detected in wild-type cells. Further evidence to support this is given by Figure **??**, in which it is proven that the probe set used is highly specific. It is likely that probes are detecting the correct target present in the incorrect cell type.

2.5 Single Color Validation of in situ HCR

Figure 2.6 demonstrates the ability of HCR to discriminate two homogeneous populations based on expression of a target transgenic mRNA. Additionally, Figure 2.7 demonstrates the same data on a linear axis. HCR generated signal in target cells that was fully separable from the background in cells that lacked the target. This was demonstrated in the cases of two independent target transgenic mRNAs: *d2egfp* (2.6a) and *dsRed2* (2.6b). The results confirm strong HCR amplification with high target specificity.

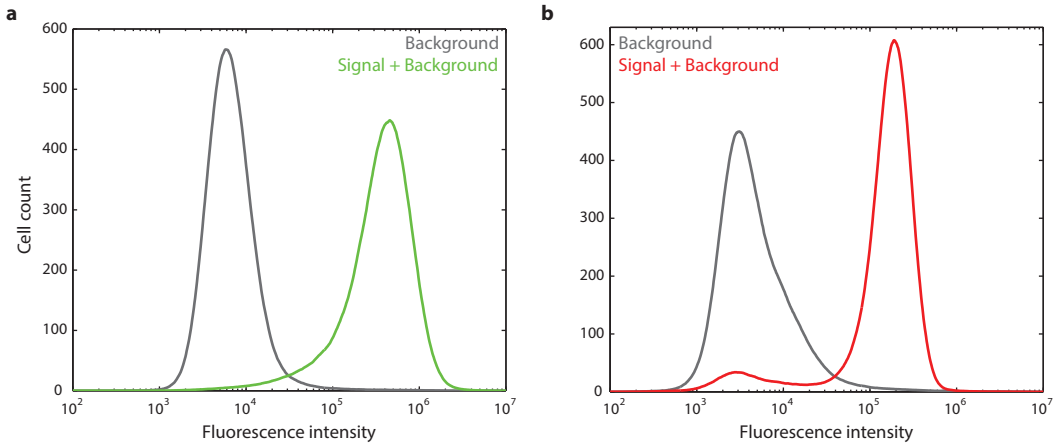

Figure 2.6: **Validation of fluorescent HCR in situ amplification with flow cytometry.** Fluorescence intensity histograms for background (wild-type cells) and signal plus background (transgenic cells). Protein fluorescence is quenched by heat and chemical treatment during the HCR protocol. Excellent discrimination is indicated by the minimal overlap between background (gray) and background plus signal (colored) histograms. Samples: HEK293T, HEK293 + *d2egfp*, HEK293 + *dsRed2*. Targets: transgenic mRNAs: (a) *Tg(d2egfp)* and (b) *Tg(dsRed2)*. Probe sets: single HCR probe per target. Due to impurities in the vector integration process, a small population of wild-type cells are observed in the *Tg(dsRed2)* cell line. Each histogram is composed of 50,000 cells. n = 3 (See Figure A.1).

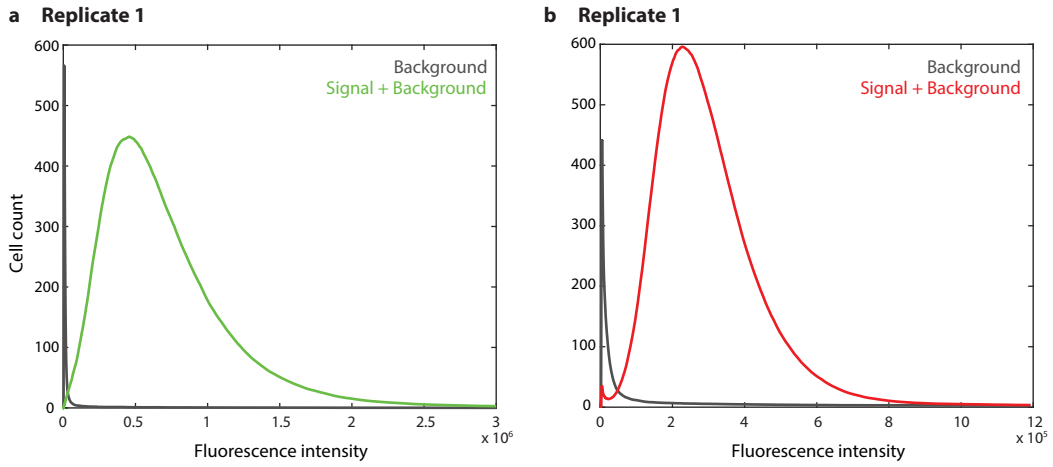

Figure 2.7: **Validation of fluorescent HCR in situ amplification with flow cytometry (linear axis).** Data shown is identical to Figures 2.6 and A.1 but with linear scaling along the fluorescence intensity axis. Samples: HEK293T, HEK293 + *d2egfp*, HEK293 + *dsRed2*. Targets: transgenic mRNAs: (a) *Tg(d2egfp)* and (b) *Tg(dsRed2)*. Probe sets: single HCR probe per target. Due to impurities in the vector integration process, a small population of wild-type cells are observed in the *Tg(dsRed2)* cell line. Each histogram is composed of 50,000 cells. n = 3 (See Figure A.2).

2.6 Single Color Validation of in situ HCR with Heterogeneous Mixtures

Figure 2.8 demonstrates *in situ* HCR's consistent ability to maintain high discrimination between cell types in mixtures of cell lines. Additionally, Figure 2.9 demonstrates the same data on a linear axis. Artificial mixtures of cell types were created in varying ratios prior to HCR. Regardless of the composition of the mixture, HCR allows clear separation of cell types on histograms. Further, Figure 2.10 demonstrates identification and quantitation of the subpopulations of cells within the heterogeneous mixtures.

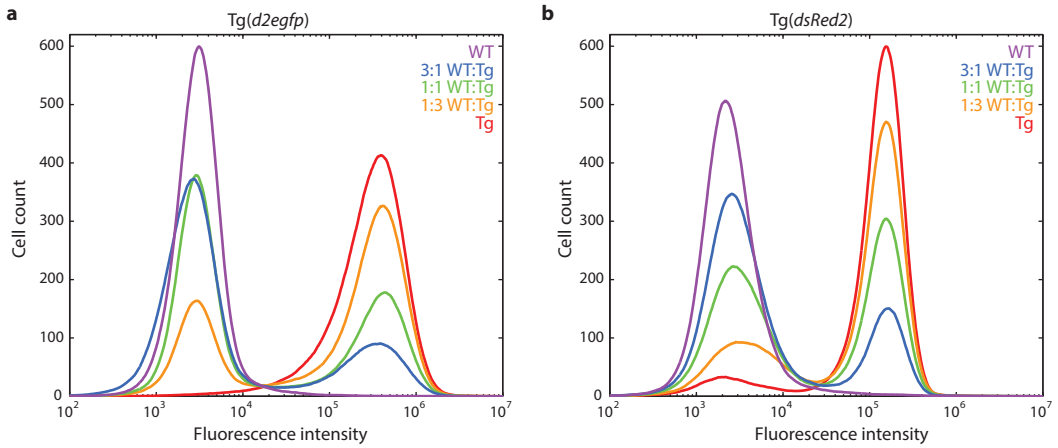

Figure 2.8: **Detection of transgenic cells in artificial mixtures of varying composition.** Fluorescence intensity histograms for varying ratios of wild-type and transgenic cell mixtures. Excellent discrimination indicates that HCR produces high signal-to-background regardless of composition of cell mixture. Cell lines: HEK293T, HEK293 + *d2egfp*, HEK293 + *dsRed2*. Targets: transgenic mRNAs: (a) *Tg(d2egfp)* and (b) *Tg(dsRed2)*. Probe sets: single HCR probe per target. Due to impurities in the vector integration process, a small population of wild-type cells are observable in the 100% *Tg(dsRed2)* sample and contribute to all mixtures of wild-type and *Tg(dsRed2)* cells. Each histogram is composed of 50,000 cells. n = 3 (See Figure A.3).

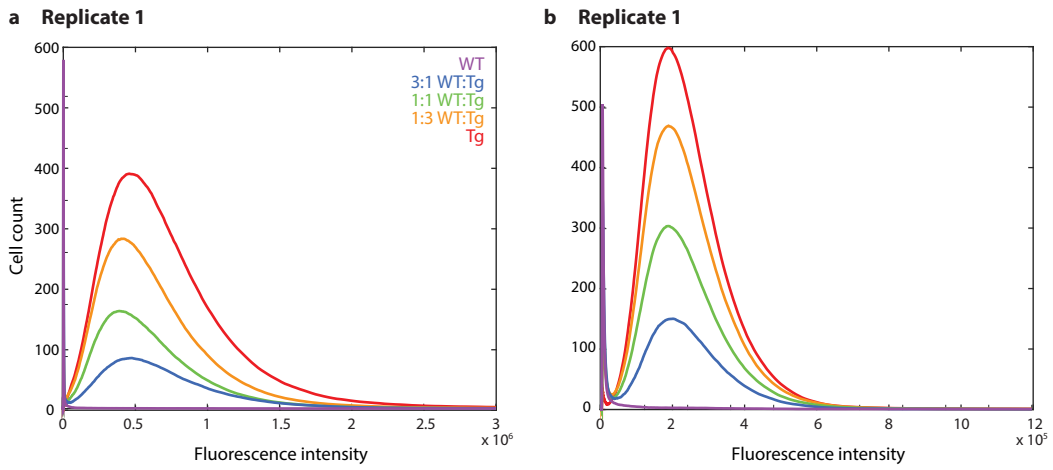

Figure 2.9: **Detection of transgenic cells in artificial mixtures of varying composition (linear axis).** Data shown is identical to Figures 2.8 and A.3 but with linear scaling along the fluorescence intensity axis. Cell lines: HEK293T, HEK293 + *d2egfp*, HEK293 + *dsRed2*. Targets: transgenic mRNAs: (a) *Tg(d2egfp)* and (b) *Tg(dsRed2)*. Probe sets: single HCR probe per target. Due to impurities in the vector integration process, a small population of wild-type cells are observable in the 100% *Tg(dsRed2)* sample and contribute to all mixtures of wild-type and *Tg(dsRed2)* cells. Each histogram is composed of 50,000 cells.

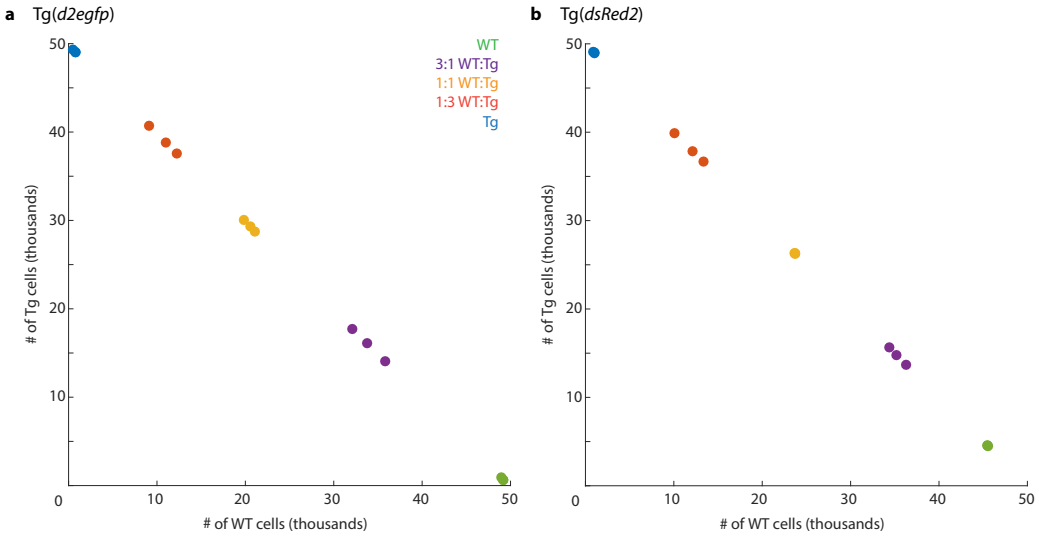

Figure 2.10: **Quantitation of artificial mixtures of varying composition.** Using data from Figures 2.8 and A.3, cell subpopulations are quantified and plotted on scatter plots. Each point refers to a single heterogeneous mixture. Data falls on a line because every sample includes 50,000 cells. Cell lines: HEK293T, HEK293 + *d2egfp*, HEK293 + *dsRed2*. Targets: transgenic mRNAs: (a) *Tg(d2egfp)* and (b) *Tg(dsRed2)*. Probe sets: single HCR probe per target. Due to impurities in the vector integration process, a small population of wild-type cells are observable in the 100% *Tg(dsRed2)* sample and contribute to all mixtures of wild-type and *Tg(dsRed2)* cells.

2.7 Relative Quantitation of mRNA Abundance by Redundant Detection

Figures 2.11 (linear axes) and 2.12 (logarithmic axes) demonstrate the relative quantitation of mRNA abundance HCR provides. Additionally the 1-dimensional histograms are overlaid to show consistency to Figures 2.6 and 2.7. To show this, redundant detection of a single mRNA target was performed using two probe sets, each targeting unique regions of the mRNA, and each triggering one of two orthogonal HCR amplifiers labeled with spectrally distinct fluorophores. Redundant detection should therefore result in correlated signal intensities if signal generated by HCR scales with target abundance. The highly-correlated relationship between the two measurements for each target (Pearson correlation coefficient $r = 0.98$ and $r = 0.91$ for *Tg(d2egfp)* and *Tg(dsRed2)*, respectively) indicates that HCR signal scales approximately linearly with the number of target mRNAs per cell. Additionally, the strong correlation also implies the variability in the average HCR polymer length per voxel (cell) is small relative to the variability of target mRNA abundance within a population of cells. Thus, HCR signal generated for an mRNA target can be used to quantify its relative abundance within a population of cells.

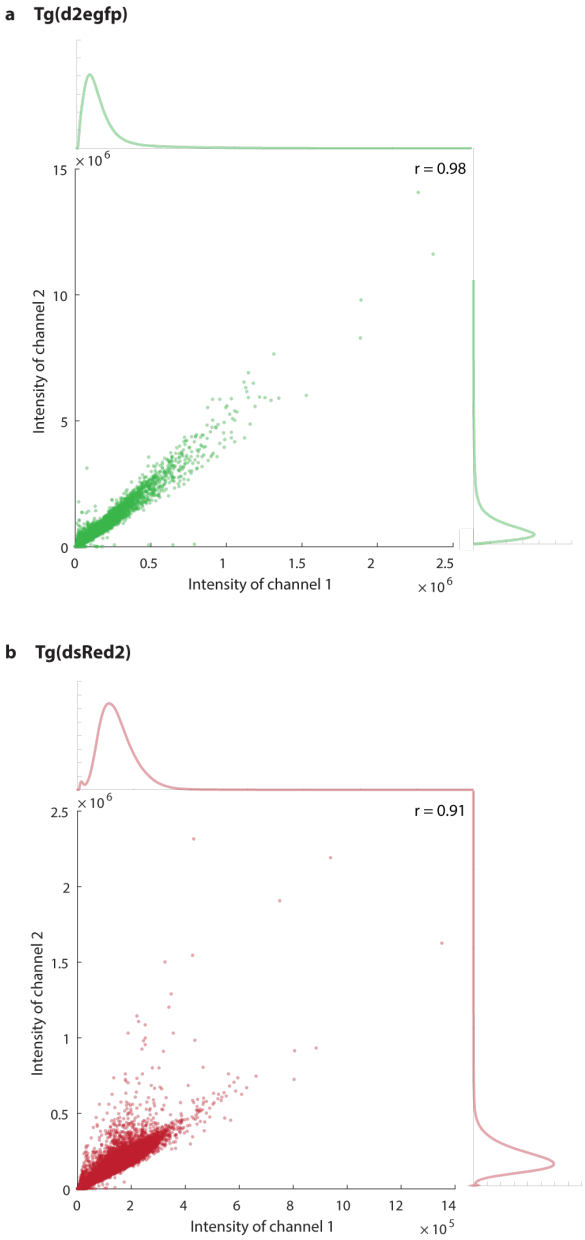

Figure 2.11: **Relative quantitation of mRNA abundance with flow cytometry (linear axes).** Two-color redundant detection of target mRNAs using orthogonal probe sets that initiate spectrally distinct HCR amplifiers. Quantitative ability is inferred from high Pearson correlation coeffcients. Samples: HEK293 + *d2egfp*, HEK293 + *dsRed2*. Targets: transgenic mRNAs: (a) *Tg(d2egfp)* and (b) *Tg(dsRed2)*. Probe sets: (a) three HCR probes for channel 1, single HCR probe for channel 2 and (b) two HCR probes for channel 1, three HCR probes for channel 2. Due to impurities in the vector integration process, a small population of wild-type cells are observable in the *Tg(dsRed2)* cell line (cluster near origin in (b)). n = 3 (See Figure A.5).

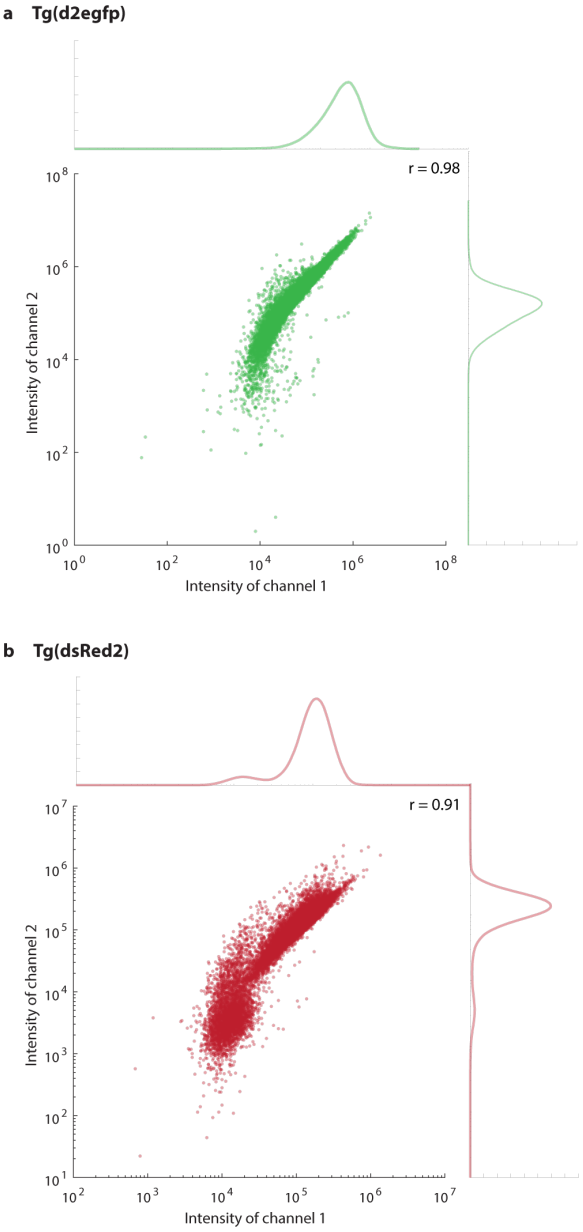

Figure 2.12: **Relative quantitation of mRNA abundance with flow cytometry (logarithmic axes).** Two-color redundant detection of target mRNAs using orthogonal probe sets that initiate spectrally distinct HCR amplifiers. Quantitative ability is inferred from high Pearson correlation coeffcients. Samples: HEK293 + *d2egfp*, HEK293 + *dsRed2*. Targets: transgenic mRNAs: (a) *Tg(d2egfp)* and (b) *Tg(dsRed2)*. Probe sets: (a) three HCR probes for channel 1, single HCR probe for channel 2 and (b) two HCR probes for channel 1, three HCR probes for channel 2. Due to impurities in the vector integration process, a small population of wild-type cells are observable in the *Tg(dsRed2)* cell line (cluster near origin in (b)). n = 3 (See Figure A.6).

2.8 Multiplexed Cell Sorting Based on the Abundance of mRNA Targets

Figure 2.13 is a demonstration of multiplexed HCR being used to discriminate and sort three cell populations within one mixture. Cell lines were examined individually (Figure 2.13a) and then compared to the scatter plot obtained when all three lines were mixed prior to HCR (Figure 2.13b). After sorting, populations were analyzed once more to confirm homogeneous populations were isolated (Figure 2.13c). The high degree of separation verifies HCR amplification is sufficiently strong enough to provide multi-dimensional sorting of cell populations based on mRNA abundance.

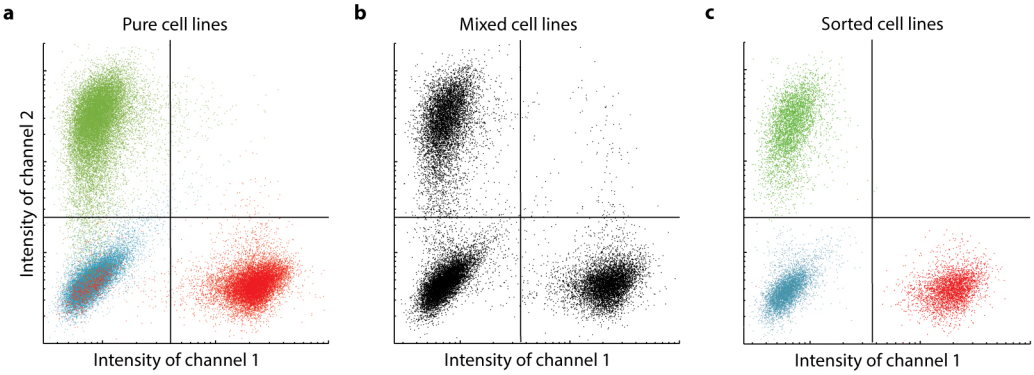

Figure 2.13: **Multiplexed cell sorting based on mRNA abundance. a.** Simultaneous detection of *Tg(d2egfp)* and *Tg(dsRed2)* in three pure cell lines: HEK293 + *dsRed2* (red), HEK293 + *d2egfp* (green), and HEK293T (cyan). **b.** Characterization of cell type within an artificial mixture of cell lines from (a) based on the presence or absence of mRNA targets. **c.** Fluorescence-activated cell sorting (FACS) performed on the cell mixture from (b). Sorted cell populations were analyzed to demonstrate the ability of HCR to be used for the isolation of heterogeneous populations. Cell lines: HEK293T, HEK293 + *d2egfp*, HEK293 + *dsRed2*. Targets: transgenic mRNAs *Tg(d2egfp)* and *Tg(dsRed2)*. Probe sets: three HCR probes per target. Due to impurities in the HEK293 + *dsRed2* line, a small number of cells are indistinguishable from the wild-type.

2.9 Conclusion

Coupling HCR amplification with flow cytometry enables a powerful new tool for studying, quantifying, and profiling heterogeneous cell populations based on mRNA abundance. HCR amplification confers high signal-to-background, multiplexed target detection, relative quantitation of mRNA abundance, and the potential for short target detection to the high-throughput analysis and isolation tool that FACS provides. Existing techniques exhibit limitations in at least one of these four areas, thus creating a need for this new tool.

In situ HCR can be used to quantify relative mRNA abundance between cells in a sample. We demonstrate that HCR signal scales linearly, with high correlation, as a function of target abundance. The variability of the average HCR polymer length per voxel (cell) is small relative to the variability of mRNA abundance within a population of cells with the targets we studied (Figure **??**). The combination of relative quantitation and high-throughput sampling offered by FACS is an exciting development for *in situ* hybridization techniques.

We have presented validated properties of HCR amplification that allow for multiplexed profiling of mRNA abundance. These properties can be used for isolation of cells that exhibit combinations of mRNA abundance or scarcity across multiple targets or biomarkers. With multiplexed target detection of mRNA targets exhibiting bimodal expression (high versus low), *in situ* HCR enables FACS of 2^n distinct cell types, where n is the number of mRNA targets (here we present n = 2 used to sort 3 distinct cell types). We show that in a sample with three cell types (two of which each expressing a unique mRNA transcript), all three populations can be successfully identified with high fidelity using *in situ* HCR and FACS. Additionally, we propose that these properties can be extended to any sufficiently highly-expressed mRNA target, including endogenous transcripts, for performing logic-based cell population sorting based on mRNA abundance.

2.10 Future Directions

Future directions of this technology should capitalize upon HCR's unique strengths. One such key feature is the probe agnostic nature of HCR amplification. This allows for switching probe designs without impacting amplification *in situ*. For example, this can allow for HCR-amplified detection of short regulatory elements, such as microRNAs (detailed in Chapter 3) or other noncoding RNA molecules.

Two immediate goals are to extend *in situ* HCR to include endogenous mRNA and microRNA targets (inspired by efforts in Chapter 3). Second is to build on the core application presented here: isolation of cell subpopulations. For example, HCR detection of mRNA marker transcripts could be used to identify and isolate subpopulations based on cell states in heterogeneous mixtures. The ability to use HCR for transcriptome-level profiling of cell subpopulations based on endogenous target would represent a powerful tool for cell biologists.

An emerging technology is mass cytometry, a technology that enables high-throughput mass spectrometry-based analysis and sorting of cells [20–22]. Recent developments have shown multiplexing of up to 40 different mRNA and protein targets [22]. Given the modularity of HCR amplification, it is possible to label HCR amplifiers with mass cytometry-compliant isotopes (mass cytometry's complement to fluorophores). This combination could enable hyper-multiplexed detection of short regulatory elements in addition to mRNA and proteins, enabling the mapping of entire gene circuits.

Another exciting application of the technology presented here is profiling of bacteria found in environmental or clinical samples. Current methods for conducting flow-FISH with bacterial samples are limited by techniques that do not provide quantitative signal amplification [11, 13, 23–25] or cannot support multiplexed target detection [13, 23]. HCR amplification can potentially solve these issues by bringing programmable logic to signal generation. Further, *in situ* HCR's ability to quantify mRNA abundance permits sub-profiling of a cell population exhibiting a broad range of expression for a given mRNA.

Additionally, this technique could be combined with RNA-Seq for profiling and quantifying mRNA abundance in great detail [26, 27]. Current methods for RNA-Seq depend on bulk measurements of many cells [27–30]. More recently,

single cell RNA-Seq has emerged as a useful tool for developing mRNA transcriptomes for single cells [31–34] . However, this technique can be prohibitively expensive [33] and require relatively long times for completion [32], and data obtained can be extremely difficult to interpret due to large variation from cell-to-cell and low total cell count [35].

HCR amplification and FACS can provide relevant, high-throughput measurements by isolating cell populations and analyzing their individual transcriptomes with traditional RNA-Seq. This method significantly lowers the barrier-to-entry to obtaining highly detailed RNA expression information offered by single cell RNA-Seq.

Combining HCR amplification with high-throughput imaging, such as flow or mass cytometry, is an application rich with potential. In Chapter 2, we presented a platform for building these techniques. Looking forward, it is crucial to continue building on the strengths of HCR amplification by optimizing for short or low-expression targets, as well as coupling to the latest advances elsewhere to create compelling solutions for biologists.

References

1. Laerum, O. D. & Farsund, T. Clinical application of flow cytometry: a review. *Cytometry* **2,** 1–13 (July 1981).

2. Tracy, B. P., Gaida, S. M. & Papoutsakis, E. T. Flow cytometry for bacteria: enabling metabolic engineering, synthetic biology and the elucidation of complex phenotypes. *Current opinion in biotechnology* **21,** 85–99 (Feb. 2010).

3. Jaye, D. L., Bray, R. A., Gebel, H. M., Harris, W. A. C. & Waller, E. K. Translational applications of flow cytometry in clinical practice. *Journal of immunology (Baltimore, Md. : 1950)* **188,** 4715–4719 (May 2012).

4. Gallaher, B. L. & Stamatatos, L. Detection of HIV Env-mediated B cell receptor aggregation on engineered B cells by flow cytometry. *The Journal of Immunology* **196,** 146–15 (2016).

5. Papanikolaou, X. *et al.* Flow cytometry defined cytoplasmic immunoglobulin index is a major prognostic factor for progression of asymptomatic monoclonal gammopathies to multiple myeloma (subset analysis of SWOG S0120). *Blood cancer journal* **6,** e410 (2016).

6. Mattanovich, D. & Borth, N. Applications of cell sorting in biotechnology. *Microbial cell factories* **5,** 12 (2006).

7. Terashima, M., Freeman, E. S., Jinkerson, R. E. & Jonikas, M. C. A fluorescence-activated cell sorting-based strategy for rapid isolation of high-lipid Chlamydomonas mutants. *The Plant Journal* **81,** 147–159 (2015).

8. Wallberg, F., Tenev, T. & Meier, P. Analysis of apoptosis and necroptosis by fluorescence-activated cell sorting. *Cold Spring Harbor Protocols* **2016,** pdb–prot087387 (2016).

9. Rufer, N., Dragowska, W., Thornbury, G., Roosnek, E. & Lansdorp, P. M. Telomere length dynamics in human lymphocyte subpopulations measured by flow cytometry. *Nature Biotechnology* **16,** 743–747 (Aug. 1998).

10. Baerlocher, G. M., Vulto, I., de Jong, G. & Lansdorp, P. M. Flow cytometry and FISH to measure the average length of telomeres (flow FISH). *Nature protocols* **1,** 2365–2376 (2006).

11. Pernthaler, A. & Amann, R. Simultaneous fluorescence in situ hybridization of mRNA and rRNA in environmental bacteria. *Applied and environmental microbiology* **70,** 5426–5433 (Sept. 2004).

12. Robertson, K. L., Verhoeven, A. B., Thach, D. C. & Chang, E. L. Monitoring viral RNA in infected cells with LNA flow-FISH. *RNA (New York, N.Y.)* **16,** 1679–1685 (Aug. 2010).

13. Robertson, K. L., Soto, C. M., Archer, M. J., Odoemene, O. & Liu, J. L. Engineered T4 viral nanoparticles for cellular imaging and flow cytometry. *Bioconjugate chemistry* **22,** 595–604 (Apr. 2011).

14. Hanley, M. B., Lomas, W., Mittar, D., Maino, V. & Park, E. Detection of low abundance RNA molecules in individual cells by flow cytometry. *PloS one* **8,** e57002 (Feb. 2013).

15. Maiti, S. N. Measurement of Average Telomere Length in Ex Vivo Expanded Natural Killer Cells by Fluorescence In Situ Hybridization (FISH) and Flow Cytometry. *Natural Killer Cells: Methods and Protocols,* 57–63 (2016).

16. Meagher, R. J. & Wu, M. Microfluidic Approaches to Fluorescence In Situ Hybridization (FISH) for Detecting RNA Targets in Single Cells, 95–112 (2016).

17. Yamada, H. *et al.* Messenger RNA quantification after fluorescence-activated cell sorting using in situ hybridization. *Cytometry. Part A : the journal of the International Society for Analytical Cytology* **77,** 1032–1037 (Nov. 2010).

18. Dirks, R. M. & Pierce, N. A. Triggered amplification by hybridization chain reaction. *Proceedings of the National Academy of Sciences of the United States of America* **101,** 15275–15278 (Oct. 2004).

19. Choi, H. M. T. *et al.* Programmable in situ amplification for multiplexed imaging of mRNA expression. *Nature Biotechnology* **28,** 1208–1212 (Oct. 2010).

20. Giesen, C. *et al.* Highly multiplexed imaging of tumor tissues with subcellular resolution by mass cytometry. *Nature Methods* **11,** 417–422 (Mar. 2014).

21. Bodenmiller, B. *et al.* Multiplexed mass cytometry profiling of cellular states perturbed by small-molecule regulators. *Nature Biotechnology* **30,** 858–867 (Aug. 2012).

22. Frei, A. P. *et al.* Highly multiplexed simultaneous detection of RNAs and proteins in single cells. *Nature Methods* **13,** 269–275 (Jan. 2016).

23. Kalyuzhnaya, M. G. *et al.* Fluorescence in situ hybridization-flow cytometry-cell sorting-based method for separation and enrichment of type I and type II methanotroph populations. *Applied and environmental microbiology* **72,** 4293–4301 (June 2006).

24. Yilmaz, S., Haroon, M. F., Rabkin, B. A., Tyson, G. W. & Hugenholtz, P. Fixation-free fluorescence in situ hybridization for targeted enrichment of microbial populations. *The ISME Journal* **4,** 1352–1356 (Oct. 2010).

25. Hoshino, T. & Schramm, A. Detection of denitrification genes by in situ rolling circle amplification-fluorescence in situ hybridization to link metabolic potential with identity inside bacterial cells. *Environmental microbiology* **12,** 2508–2517 (Sept. 2010).

26. Wang, Z., Gerstein, M. & Snyder, M. RNA-Seq: a revolutionary tool for transcriptomics. *Nature Reviews Genetics* **10,** 57–63 (Jan. 2009).

27. Papenfort, K., Förstner, K. U., Cong, J.-P., Sharma, C. M. & Bassler, B. L. Differential RNA-seq of Vibrio cholerae identifies the VqmR small RNA as a regulator of biofilm formation. *Proceedings of the National Academy of Sciences* **112,** E766–E775 (2015).

28. Mortazavi, A., Williams, B. A., McCue, K., Schaeffer, L. & Wold, B. Mapping and quantifying mammalian transcriptomes by RNA-Seq. *Nature Methods* **5,** 621–628 (July 2008).

29. Nagalakshmi, U. *et al.* The Transcriptional Landscape of the Yeast Genome Defined by RNA Sequencing. *Science* **320,** 1344–1349 (June 2008).

30. Severin, A. J. *et al.* RNA-Seq Atlas of Glycine max : A guide to the soybean transcriptome. *BMC Plant Biology* **10,** 1 (Aug. 2010).

31. Tang, F. *et al.* mRNA-Seq whole-transcriptome analysis of a single cell. *Nature Methods* **6,** 377–382 (May 2009).

32. Tang, F. *et al.* RNA-Seq analysis to capture the transcriptome landscape of a single cell. *Nature protocols* **5,** 516–535 (Mar. 2010).

33. Islam, S. *et al.* Characterization of the single-cell transcriptional landscape by highly multiplex RNA-seq. *Genome research* **21,** 1160–1167 (July 2011).

34. Zeisel, A. *et al.* Cell types in the mouse cortex and hippocampus revealed by single-cell RNA-seq. *Science* **347,** 1138–1142 (2015).

35. Bengtsson, M., Ståhlberg, A., Rorsman, P. & Kubista, M. Gene expression profiling in single cells from the pancreatic islets of Langerhans reveals lognormal distribution of mRNA levels. *Genome research* **15,** 1388–1392 (Oct. 2005).

Chapter 3

MULTIPLEXED MAPPING OF MICRORNA AND MRNA EXPRESSION IN VERTEBRATE EMBRYOS

3.1 Introduction

Ever since their initial discovery more than 20 years ago in *Caenorhabditis elegans*, microRNAs (miRNAs) have risen in importance within gene regulation circuits [1–8], and much effort has been dedicated to unearthing details of miRNA biogenesis and their role in post-transcriptional gene regulation in both plants and animals. As our collective knowledge regarding the role of miRNAs in gene regulation has grown, recent studies have applied this understanding towards creating novel principles. These innovations range from predicting miRNA target sites [9, 10], identifying miRNAs key to disease pathways [6, 8, 11, 12], and designing novel miRNA genes [13].

For decades biologists have relied upon *in situ* hybridization to obtain spatial and cell type-specific information regarding mRNA expression. Current techniques for detecting miRNA targets offer robust detection of a single target in a range of sample types [14–23]. While these methods for improving miRNA retention within samples [19, 24] and LNA-based oligonucleotide probes [14] have allowed for the detection of miRNA targets using traditional *in situ* hybridization protocols, several crucial hurdles remain. These include multiplexed miRNA detection, co-detection of miRNAs with mRNAs, and easier probe synthesis and use. Solving these problems would enable biologists to study miRNA expression in relation to both expression of other microRNAs and key mRNAs and significantly reduce the cost per experiment.

In order to create a fundamentally new platform for studying how miRNAs and mRNAs are related within intact samples, two critical technical challenges must be addressed. First, current probes targeting miRNAs tend to incorporate LNA bases, which are proprietary, expensive, and difficult to design *de novo*. Second, current signal amplification techniques are either incompatible with short target detection [25], too weak to be useful within intact vertebrate embryos [26], or cannot be used for multiplexing [14–23]. Here, we couple 2'-O-methylated

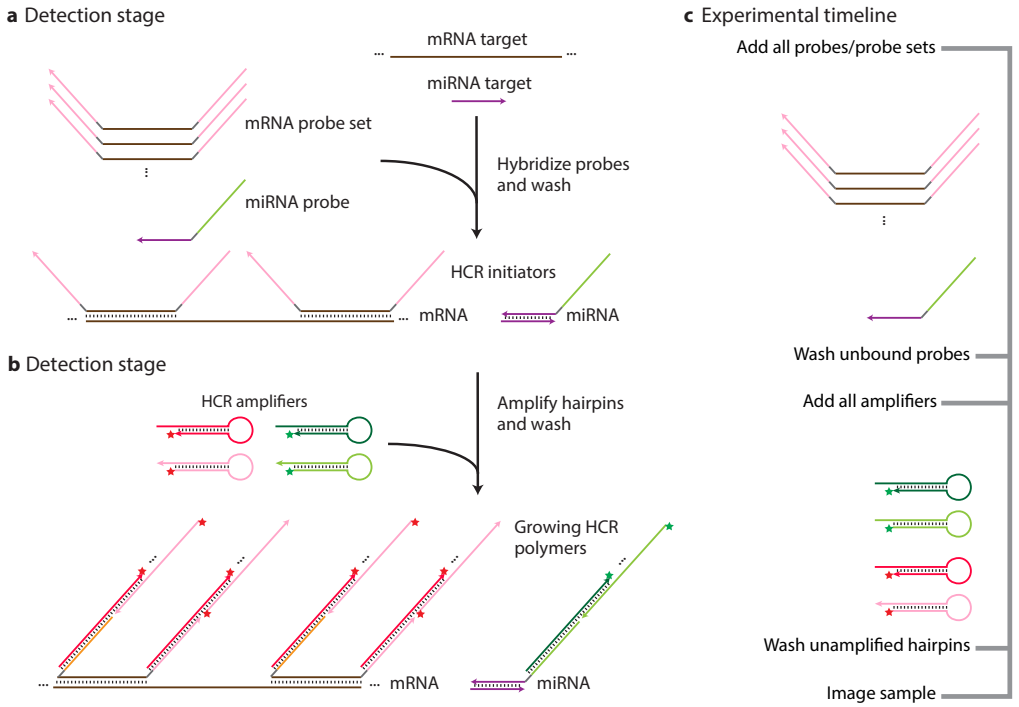

Figure 3.1: **Multiplexed in situ amplification via hybridization chain reaction (HCR). a.** Detection stage. Probe sets are hybridized to miRNA/mRNA targets and then unused probes are washed from the sample. **b.** Amplification stage. Initiators trigger self-assembly of tethered HCR polymers and then unused hairpins are washed from the sample. **c.** Experimental timeline. The same two-stage protocol is used regardless of number of target miRNA/mRNA targets. For multiplexed experiments (two-color example depicted), probe sets for different target RNAs carry orthogonal initiators that trigger orthogonal HCR amplification cascades labeled by spectrally distinct fluorophores.

RNA probes with signal amplification via hybridization chain reaction (HCR) [27–29] in order to reduce the per experiment cost by up to 10 times and enable true target multiplexing in whole-mount zebrafish embryos. As a proof-of-concept, we demonstrate four-color multiplexed *in situ* HCR involving the co-detection of miRNA and mRNA targets.

HCR-based amplification for *in situ* hybridization has been engineered and demonstrated to enable parallel multiplexing of up to five target mRNAs within whole-mount zebrafish embryos [28, 29]. An HCR amplifier is composed of two kinetically trapped fluorescent nucleic acid hairpin species (H1 and H2 in Figure 1.1a) that, in the absence of a cognate initiator strand (I1), coexist metastably. Presence of the initiator triggers a chain reaction in which H1 and

H2 hairpins sequentially nucleate and open to assemble a long nicked double-stranded fluorescent amplification polymer. Due to the large sequence space available to the HCR amplifiers, orthogonal amplifiers have been designed for the simultaneous amplification of multiple targets. As a result, the bottleneck to the number of concurrent targets that can be detected is the number of spectrally distinct fluorophores available, rather than the number of orthogonal HCR amplifiers [28, 29].

In situ HCR offers four distinct advantages over traditional *in situ* hybridization techniques. First, HCR is programmable, allowing for straightforward multiplexing of target detection and signal amplification within the same sample. The same two-stage protocol was used independent of the number of target mRNAs or miRNAs (Figure 3.1). Second, while HCR polymerization is based upon a catalytic reaction, it reaches equilibrium within a reasonable timeframe – this means amplification time does not need to be tuned on a per-target basis to maximize signal-to-background. Third, HCR amplification polymers are designed to remain attached to their initiators, preventing their diffusion throughout the sample and ensuring sharp signal localization. Fourth, HCR self-assembly occurs only in the presence of the initiator, thereby allowing for hairpins to penetrate the sample before forming long polymers. These properties have been demonstrated in an *in situ* setting [28, 29].

These properties make HCR amplification an ideal fit for detection of miRNAs *in situ*. In order to allow for simultaneous detection of miRNA and mRNA targets, we defined two engineering challenges: straightforward probe design and synthesis and protocol compatibility with *in situ* HCR detection of mRNAs. Although HCR amplification is modular by design and is compatible with any probe type, we found 2'-O-methylated RNA probes offered a few key advantages over the more commonly used locked nucleic acid-based (LNA) probes. While LNA probes have been successfully used to detect miRNA targets *in situ* [14, 16–24, 30–35], we found key drawbacks to their use: design and synthesis are relatively costly and strands are available only from a single vendor (Exiqon, Inc.).

Short probes, like ones targeting miRNAs, have tended to incorporate LNA bases due to the large increase in melting temperature their incorporation offers (3-8 °C per base) [36]. Because of this large increase, short probes cannot

be composed entirely of LNA bases and remain compatible with optimal *in situ* hybridization conditions. Therefore, it is necessary to use some fraction of LNA bases along with RNA or DNA bases, thus necessitating design and testing. 2'-O-methylated RNA bases also grant increased melting temperature per substituted base, albeit smaller gains (1-3 °C per base)[37]. We found this to work in our favor – instead of being tasked with discovering the best ratio of modified base to traditional base, we synthesize miRNA probes solely using 2'-O-methylated RNA. Compared to their LNA counterparts, these probes are cheaper (∼10x) on a per-experiment basis (see Chapter 3.2 for calculation), and the nucleotides are not proprietary. Crucially, we show the use of these probes to detect miRNA targets simultaneously with standard DNA *in situ* HCR probes to detect mRNA targets.

3.2 Comparison of Cost of LNA versus 2'-O-Methylated RNA Probes

Table 3.1 depicts the difference in costs between single DIG-labeled LNA probes, the more commonly used dual DIG-labeled LNA probes, and the 2'-O-methylated RNA probes used in our studies.

	Single DIG-labeled LNA	Dual DIG-labeled LNA	2'-O-Methlyated RNA
Purchase Price	$508.66	$674.13	$271.00
Amount (# Reactions)	250	250	800
Cost per Reaction	$2.04	$2.70	$0.27

Table 3.1: **Cost comparison between LNA versus 2'-O-methylated RNA probes.** 2'-O-methylated RNA probe cost is based upon 250 nmol synthesis from IDT with PAGE or HPLC purification.

3.3 Linear Unmixing for Decreased Autofluorescence

Spectral imaging and linear unmixing were employed in order to mitigate the effect of autofluorescence in the samples using the ZEISS Zen Black software with the Linear Unmixing module. This combination of pre- and post-processing was used to characterize a fluorescent molecule's emission fingerprint, rather than attempting to distinguish them based solely upon bandpass filtering. Reference spectra for sample autofluorescence and Alexa Fluor dyes were collected using identical imaging conditions to the *in situ* HCR data. For the multi-channel samples, spectra were collected for each laser source: 488 nm, 514 nm, 561 nm, and 633 nm. All spectra were measured using 9.7 nm intervals (Figure B.3). Further information can be found in Chapter 3.3.1 and Appendix B.4.

3.3.1 Comparison of Spectral Imaging and Linear Unmixing to Standard Imaging

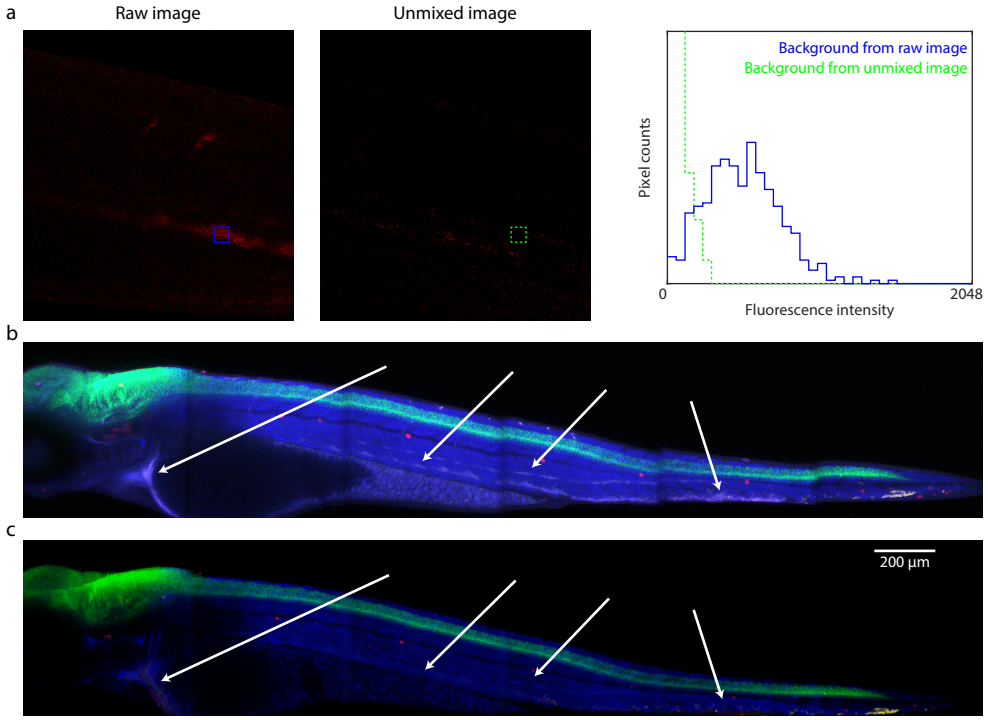

Figure 3.2: **Impact of linear unmixing on autofluorescence. a.** Images comparing a single channel when imaged normally and spectrally. Boxes indicate sample autofluorescence plotted in histogram. **b.** Maximum intensity z-projection of standard confocal microscopy images of multiplexed mRNA/miRNA detection. **c.** Maximum intensity z=projection of spectral confocal microscopy and linear unmixed images of multiplexed mRNA/miRNA detection. Note the subtraction of blood vessel-specific autofluorescence present in (b) and absent in (c) (indicated by white arrows). Sample: Casper zebrafish fixed at 72 hpf. Probes: one single-initiator DNA probe per target. Amplifiers: four orthogonal HCR amplifiers carrying spectrally distinct fluorophores.

Laser (nm)	Standard Imaging (AU)	Spectral Imaging (AU)	Background Reduction (%)
488	600	200	67
514	2000	400	80
561	500	5	99

Table 3.2: **Reduction of autofluorescence by spectral imaging and linear unmixing.** Values presented are mean intensities of boxes placed to extract blood vessel-specific autofluorescence.

3.4 Multiplexed Detection of microRNA and mRNA Targets

In order to best demonstrate *in situ* HCR as a technique for the co-detection of miRNA and mRNA targets within whole-mount zebrafish embryos, we designed a proof-of-concept experiment detecting targets that are spatially distinct. Reference data from ZFIN is shown in Appendix B. Figure 3.3 shows simultaneous mapping of three target miRNAs and one target mRNA with high signal-to-background. Each miRNA target is detected using a single 2'-O-methlyated RNA probe carrying a single HCR initiator, and the mRNA target is detected using a probe set containing seven two-initiator DNA probes. The same two-stage protocol is used, regardless of probe and target type using orthogonal HCR amplifiers carrying spectrally distinct fluorophores. See Chapter 3.5 for histogram and signal-to-background analysis for all targets.

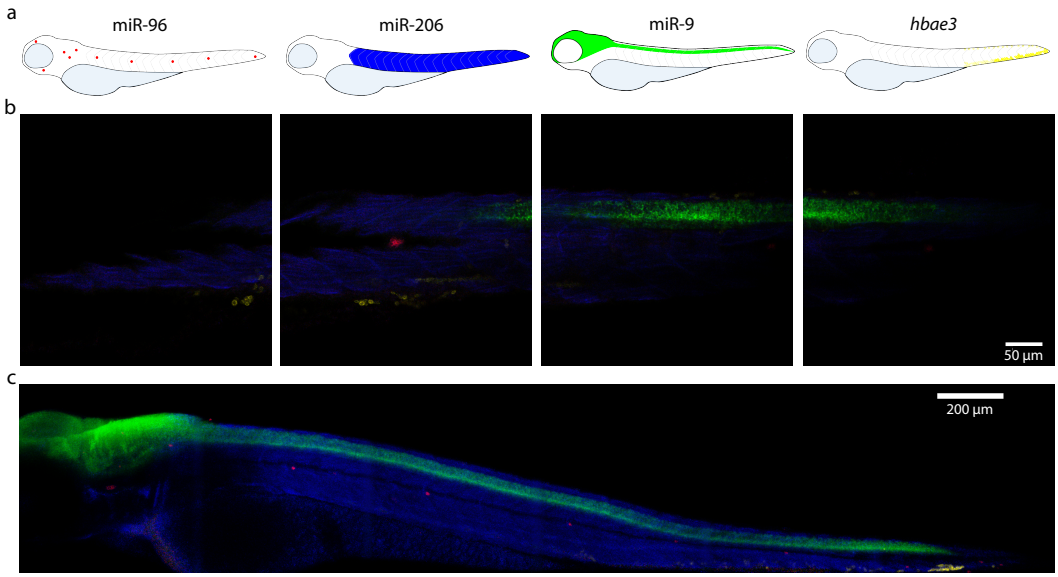

Figure 3.3: **Multiplexed mapping of microRNA and mRNA targets in fixed whole-mount zebrafish embryos. a.** Expression atlas for three microRNAs (miR-9, miR-206, miR-96) and one mRNA (*hbae3*). **b.** miRNA/mRNA expression of targets imaged via confocal microscopy at four planes within an embryo. **c.** Full lateral view of expression of targets. Maximum intensity projection composite image of the four channels. Sample: Casper zebrafish embryos fixed at 72 hpf. Probe set: single 1-initiator 2'O-Me probe for microRNA and seven 2-initiator DNA probes for mRNA. Scale bars indicated on images. All images were acquired spectrally and processed via linear unmixing to subtract channel cross-talk and autofluorescence. See Appendix B for details.

3.5 Histogram Analysis of microRNA and mRNA Mapping

Figure 3.4 shows histogram-based analysis of signal-to-background for each target. Boxes were extracted from each replicate for each target to represent the sum of signal + background and background. Box size was different across targets, but consistent across replicates in order to account for the varying spatial expression for each. Histograms demonstrate near complete separation of signal + background and background intensities for all targets and replicates.

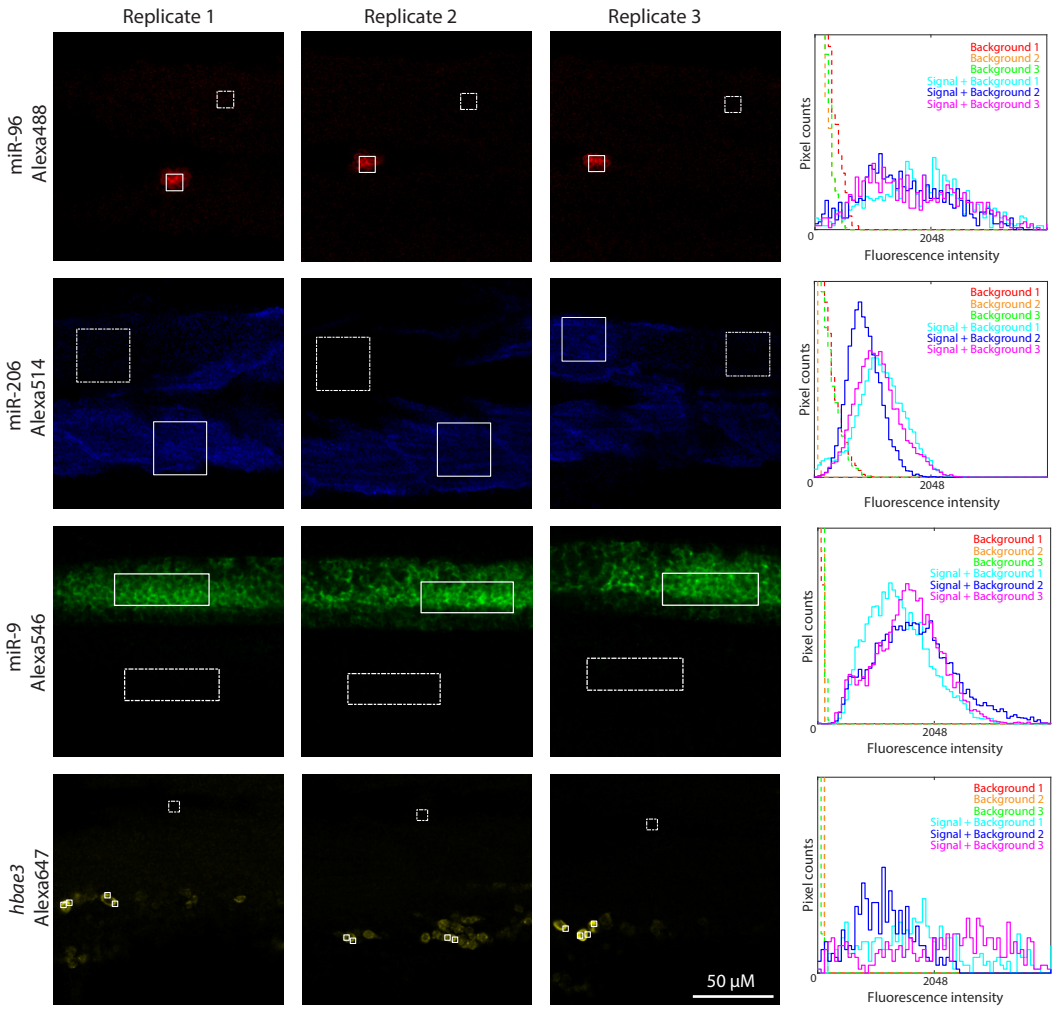

Figure 3.4: **Histogram analysis of signal-to-background.** Columns 1-3 are technical replicates of *in situ* HCR. Column 4 shows histograms extracted from boxes overlaid on images columns 1-3. Rows correspond to different target miRNA/mRNA. Solid boxes represent regions of signal + background, and dotted boxes represent regions of background. All images were acquired spectrally and processed via linear unmixing to subtract channel cross-talk and autofluorescence.

Target	Signal	Background	Signal-to-Background
miR-96	2,000 ± 100	100 ± 50	20 ± 7
miR-206	900 ± 200	90 ± 80	10 ± 9
miR-9	2,000 ± 100	20 ± 7	100 ± 40
hbae3	2,000 ± 500	20 ± 20	90 ± 90

Table 3.3: **Signal-to-background calculation for individual targets.** Calculations made using data extracted from boxes depicted in Figure 3.4. See Appendix B for calculation details.

3.6 Conclusion

Coupling *in situ* HCR amplification technology with straightforward, low cost probe design and synthesis results in key improvements to dramatically increase the functionality and robustness of *in situ* hybridization to detect miRNA targets. The 2'-O-methylated RNA probes used here are free of any design requirements since they are composed of only 2'-O-methylated RNA nucleotides and are significantly cheaper than LNA-based alternatives. Additionally, we enable simultaneous detection of multiple miRNA targets, as well as co-detection of both miRNA and mRNA targets. To decrease sample autofluorescence and increase the number of dyes available for use, we also employed spectral imaging and linear unmixing. We believe this protocol enables fundamentally new studies regarding the role of miRNAs within gene circuits in complex samples.

3.7 Future Directions

This technology enables significant applications. Keys to enabling microRNA detection *in situ* were advances in probe design as well as harnessing HCR amplification.

Within the scope of this thesis, it may be possible to analyze and isolate cell subpopulations based upon microRNA expression (see Chapter 2). Additionally, while we focus here on microRNA targets, the technology proposed could be adapted for detection of other kinds of short targets, including mRNA splice variants.

Additionally, the spectral imaging methods used in this chapter can be extended to expand our multiplexing ability, rather than being primarily used for background correction. Moving forward, it may be possible to increase the number of simultaneous targets from four[38, 39]. Further *in situ* HCR is currently being developed for detection of protein via antibody binding[40, 41].

In situ HCR can be a powerful tool for mapping diverse RNA target classes while retaining spatial information. Here, we present the ability to detect both long and short targets, specifically mRNA and microRNA targets. Looking forward, we hope to expand the range of gene circuit components that can be mapped, including proteins and other types of non-RNA targets.

References

1. Ruvkun, G., Wightman, B. & Ha, I. The 20 years it took to recognize the importance of tiny RNAs. *Cell* **116,** S93–S98 (Jan. 2004).

2. Alvarez-Garcia, I. & Miska, E. A. MicroRNA functions in animal development and human disease. *Development* **132,** 4653–4662 (Nov. 2005).

3. Winter, J., Jung, S., Keller, S., Gregory, R. I. & Diederichs, S. Many roads to maturity: microRNA biogenesis pathways and their regulation. *Nature Cell Biology* **11,** 228–234 (Mar. 2009).

4. Kozomara, A. & Griffiths-Jones, S. miRBase: integrating microRNA annotation and deep-sequencing data. *Nucleic acids research* **39,** D152–7 (Jan. 2011).

5. Krol, J., Loedige, I. & Filipowicz, W. The widespread regulation of microRNA biogenesis, function and decay. *Nature Reviews Genetics* (2010).

6. Iorio, M. V. & Croce, C. M. MicroRNA dysregulation in cancer: diagnostics, monitoring and therapeutics. A comprehensive review. *EMBO Molecular Medicine* **4,** 143–159 (Feb. 2012).

7. Ha, M. & Kim, V. N. Regulation of microRNA biogenesis. *Nature reviews Molecular cell biology* **15,** 509–524 (Aug. 2014).

8. Lin, Y., Sohn, C. H., Dalal, C. K., Cai, L. & Elowitz, M. B. Combinatorial gene regulation by modulation of relative pulse timing. *Nature* **527,** 54–58 (Oct. 2015).

9. Chi, S. W., Hannon, G. J. & Darnell, R. B. An alternative mode of microRNA target recognition. *Nature structural & molecular biology* **19,** 321–327 (Mar. 2012).

10. Agarwal, V., Bell, G. W., Nam, J. W. & Bartel, D. P. Predicting effective microRNA target sites in mammalian mRNAs. *Elife* (2015).

11. Png, K. J., Halberg, N., Yoshida, M. & Tavazoie, S. F. A microRNA regulon that mediates endothelial recruitment and metastasis by cancer cells. *Nature . . .* **481,** 190–194 (Jan. 2012).

12. Janssen, H. L. A. *et al.* Treatment of HCV Infection by Targeting MicroRNA. *New England Journal of Medicine* **368,** 1685–1694 (May 2013).

13. Fang, W. & Bartel, D. P. The Menu of Features that Define Primary MicroRNAs and Enable De Novo Design of MicroRNA Genes. *Molecular cell* **60,** 131–145 (Oct. 2015).

14. Wienholds, E., Kloosterman, W. P. & Miska, E. MicroRNA expression in zebrafish embryonic development. *Science* **309,** 307–310 (2005).

15. Deo, M., Yu, J.-Y., Chung, K.-H., Tippens, M. & Turner, D. L. Detection of mammalian microRNA expression by in situ hybridization with RNA oligonucleotides. *Developmental . . .* **235,** 2538–2548 (2006).

16. Kloosterman, W. P., Wienholds, E., de Bruijn, E., Kauppinen, S. & Plasterk, R. H. A. In situ detection of miRNAs in animal embryos using LNA-modified oligonucleotide probes. *Nature Methods* **3,** 27–29 (Jan. 2006).

17. Silahtaroglu, A. N., Nolting, D., Dyrskjøt, L. & Berezikov, E. Detection of microRNAs in frozen tissue sections by fluorescence in situ hybridization using locked nucleic acid probes and tyramide signal amplification. *Nature protocols* **2,** 2520–2528 (2007).

18. Obernosterer, G., Martinez, J. & Alenius, M. Locked nucleic acid-based in situ detection of microRNAs in mouse tissue sections. *Nature protocols* **2,** 1508–1514 (June 2007).

19. Pena, J. T. G. *et al.* miRNA in situ hybridization in formaldehyde and EDC–fixed tissues. *Nature Methods* **6,** 139–141 (Jan. 2009).

20. Jørgensen, S., Baker, A., Møller, S. & Nielsen, B. S. Robust one-day in situ hybridization protocol for detection of microRNAs in paraffin samples using LNA probes. *Methods* **52,** 375–381 (Dec. 2010).

21. Soe, M. J., Moller, T., Dufva, M. & Holmstrom, K. A Sensitive Alternative for MicroRNA In Situ Hybridizations Using Probes of 2'-O-Methyl RNA + LNA. *Journal of Histochemistry & Cytochemistry* **59,** 661–672 (June 2011).

22. Lagendijk, A. K., Moulton, J. D. & Bakkers, J. Revealing details: whole mount microRNA in situ hybridization protocol for zebrafish embryos and adult tissues. *Biology Open* **1,** 566–569 (June 2012).

23. Carbone, A., Gualeni, A., Volpi, C. & Gloghini, A. MicroRNA detection in tumor tissue by in situ hybridization. *Issues* **1,** 28 (2015).

24. Renwick, N. *et al.* Multicolor microRNA FISH effectively differentiates tumor types. *The Journal of clinical investigation* **123,** 2694–2702 (June 2013).

25. Wang, F. *et al.* RNAscope: a novel in situ RNA analysis platform for formalin-fixed, paraffin-embedded tissues. *The Journal of molecular diagnostics : JMD* **14,** 22–29 (Jan. 2012).

26. Raj, A. & van Oudenaarden, A. Single-Molecule Approaches to Stochastic Gene Expression. *Annual Review of Biophysics* **38,** 255–270 (June 2009).

27. Dirks, R. M. & Pierce, N. A. Triggered amplification by hybridization chain reaction. *Proceedings of the National Academy of Sciences of the United States of America* **101,** 15275–15278 (Oct. 2004).

28. Choi, H. M. T. *et al.* Programmable in situ amplification for multiplexed imaging of mRNA expression. *Nature Biotechnology* **28,** 1208–1212 (Oct. 2010).

29. Choi, H. M. T., Beck, V. A. & Pierce, N. A. Next-Generation in SituHybridization Chain Reaction: Higher Gain, Lower Cost, Greater Durability. *ACS Nano* **8,** 4284–4294 (May 2014).

30. Nuovo, G. J. In situ detection of precursor and mature microRNAs in paraffin embedded, formalin fixed tissues and cell preparations. *Methods* **44,** 39–46 (Jan. 2008).

31. Yamamichi, N. *et al.* Locked nucleic acid in situ hybridization analysis of miR-21 expression during colorectal cancer development. *Clinical Cancer Research* **15,** 4009–4016 (June 2009).

32. Nelson, P. T. & Wilfred, B. R. In situ hybridization is a necessary experimental complement to microRNA (miRNA) expression profiling in the human brain. *Neuroscience letters* **466,** 69–72 (Dec. 2009).

33. Lu, J. & Tsourkas, A. Imaging individual microRNAs in single mammalian cells in situ. *Nucleic acids research* **37,** e100–e100 (Aug. 2009).

34. Hanna, J. *et al.* Quantitative analysis of microRNAs in tissue microarrays by in situ hybridization. *BioTechniques* **52,** 1–15 (Apr. 2012).

35. Yelamanchili, S. V., Chaudhuri, A. D., Yelamanchili, S. V., Fox, H. S. & Fox, H. S. Combined fluorescent in situ hybridization for detection of microRNAs and immunofluorescent labeling for cell-type markers. *Frontiers in cellular neuroscience* **7,** 160 (2013).

36. Koshkin, A. A. *et al.* LNA (Locked Nucleic Acids): Synthesis of the adenine, cytosine, guanine, 5-methylcytosine, thymine and uracil bicyclonucleoside monomers, oligomerisation, and unprecedented nucleic acid recognition. *Tetrahedron* **54,** 3607–3630 (Apr. 1998).

37. Majlessi, M., Nelson, N. C. & Becker, M. M. Advantages of 2'-O-methyl oligoribonucleotide probes for detecting RNA targets. *Nucleic acids research* **26,** 2224–2229 (May 1998).

38. Valm, A. M., Welch, J. L. M. & Borisy, G. G. CLASI-FISH: principles of combinatorial labeling and spectral imaging. *Systematic and applied microbiology* **35,** 496–502 (2012).

39. Zimmermann, T., Marrison, J., Hogg, K. & O'Toole, P. Clearing up the signal: spectral imaging and linear unmixing in fluorescence microscopy. *Confocal Microscopy: Methods and Protocols,* 129–148 (2014).

40. Zhang, B. *et al.* DNA-based hybridization chain reaction for amplified bioelectronic signal and ultrasensitive detection of proteins. *Analytical chemistry* **84,** 5392–5399 (2012).

41. Zhou, J. *et al.* Nanogold-based bio-bar codes for label-free immunosensing of proteins coupling with an in situ DNA-based hybridization chain reaction. *Chemical Communications* **48,** 12207–12209 (2012).

Chapter 4

MULTIPLEXED MAPPING OF BACTERIAL SPECIES IN MOUSE COLON TISSUE SECTIONS WITH HIGH SPECIFICITY AND SELECTIVITY

4.1 Introduction

The biodiversity among microbes in the gastrointestinal (GI) system of humans and other mammals is a unique function of a complex series of interactions and events over the course of an individual's lifetime. Although detailed understanding of this process to the point when predictions become possible eludes us, current research efforts have established several key drivers of gut biogeography, including diet and nutrition [1–5], the effects of antimicrobials [6–9], the presence of mucus [10, 11], and interactions with the native immune system [12–14]. Additionally, dysbiosis, or imbalance in the abundance or composition, of these microbes is increasingly being linked to various immune, metabolic, and neurological disorders, such as inflammatory bowel diseases [15–17].

Key to understanding how microbial biogeography may impact human or host health is developing a catalog of tools to survey the abundance and composition of the GI tract and of microhabitats within, such as the crypts embedded within the wall of the colon. These tools generally require choosing between maintaining sample integrity or studying a comprehensive scope of microbes. While attaining either goal in isolation can result in novel discovery, a tool that advances both goals simultaneously would prove invaluable.

Next-generation sequencing is a valuable tool for polling a sample for all present microbes, and it can portray the diversity, specificity, stability, and developmental dynamics of gut microbiota. Despite recent advances to localize this dissection [18, 19], these techniques ultimately cannot retain exact spatial information.

Current methods for performing *in situ* hybridization to identify bacteria within mouse colon samples are consistently able to preserve sample integrity and localize cells to microhabitats therein [20–24]. Indeed, probes against unique regions of ribosomal RNA have been shown to be species-specific in bacteria

extracted from caecal samples [25, 26]. Yet the current state-of-the-art has not enabled effective multiplexing of multiple species-specific probes [20], and autofluorescence can be a significant issue to contend with (Figure 4.3).

Hybridization chain reaction (HCR) has been demonstrated as a superior amplification method for *in situ* hybridization [27, 28]. Relative to current methods for surveying gut biogeography, HCR offers key advantages: the ability to multiplex target detection and signal amplification, a modular design that allows for the substitution of optimized probes, and high signal-to-background to enable signal to overcome significant autofluorescence present in samples extracted from the GI tract.

Here, we demonstrate *in situ* HCR as a tool that improves upon the virtues of traditional *in situ* hybridization with increased signal-to-background and expands the technique's ability to multiplex, allowing for simultaneous, species-specific detection of multiple *Bacteroides* ribosomal RNA targets.

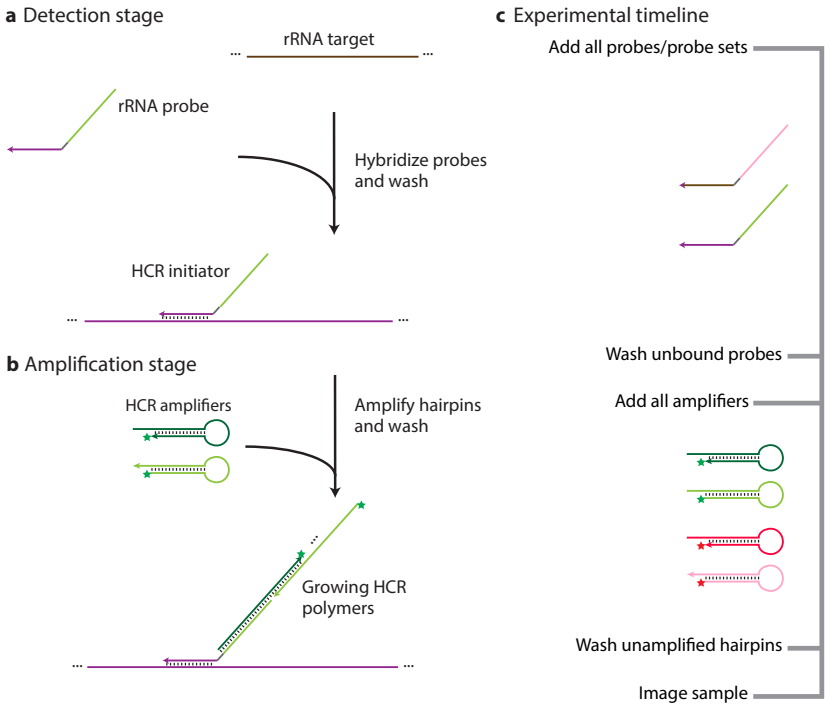

Figure 4.1: **Multiplexed in situ amplification via hybridization chain reaction (HCR). (a)** Detection stage. Probe sets are hybridized to rRNA targets and then unused probes are washed from the sample. **(b)** Amplification stage. Initiators trigger self-assembly of tethered HCR polymers and then unused hairpins are washed from the sample. **(c)** Experimental timeline. The same two-stage protocol is used regardless of number of target miRNA/mRNA targets. For multiplexed experiments (single color example depicted), probe sets for different target rRNAs carry orthogonal initiators that trigger orthogonal HCR amplification cascades labeled by spectrally distinct fluorophores.

4.2 Validation of Literature Probe Sequences in Cell Culture

In order to validate probe sequences sourced from prior work [25, 26], we sought to replicate results with cell culture samples. Figure 4.2 demonstrates the results of four such species-specific probes with *Bacteroides fragilis* grown in cell culture. Probes used were specific to *B. fragilis*, *B. ovatus*, *B. theta*, *B. vulgatus*, and the universal 16S ribosomal RNA sequence EUB338.

Table 4.2 shows signal-to-background analysis for these images. Images were thresholded based upon DAPI, and the resultant mask was applied to the EUB338 (green) and species-specific probe (red) channels to calculate intensities. Slide background was calculated by inverting the DAPI mask and applying it to the other channels. Mean and standard deviation are calculated

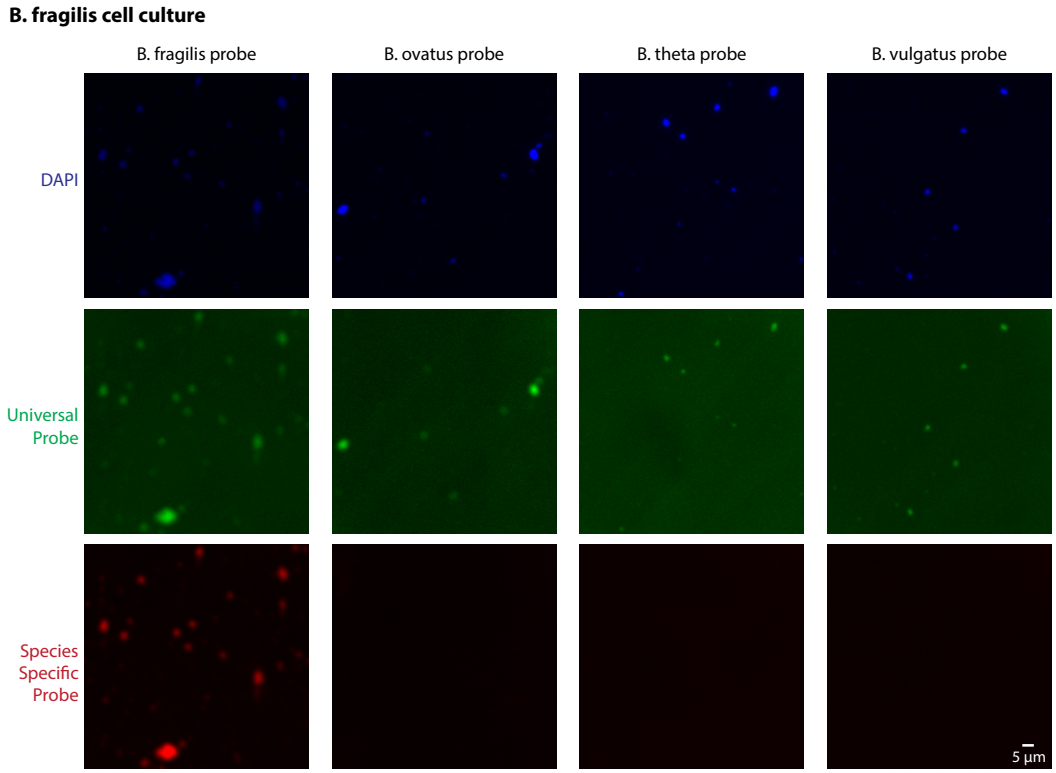

Figure 4.2: **Discrimination ability of literature species-specific probes in cell culture.** Sample: Cell cultures of *B. fragilis*, *B. vulgatus*. Probes: one fluorescent-labeled DNA probe per target.

over three replicates. Normalized signal is the species-specific signal across species-specific probes normalized the signal observed from adding a probe targeting *B. fragilis* to *B. fragilis* cell culture. Data confirms that sequences demonstrate high specificity across four probes and *Bacteroides* species (other species' data not shown). Additionally, direct-labeled probes provide sufficient signal-to-background with cell culture.

Target Species	EUB338 Signal	Species-Specific Signal	Normalized Signal
Bacteroides fragilis	3,000 ± 3,000	10,000 ± 5,000	1
Bacteroides ovatus	4,000 ± 3,000	300 ± 400	0.03
Bacteroides theta	4,000 ± 5,000	800 ± 2,000	0.08
Bacteroides vulgatus	6,000 ± 4,000	600 ± 300	0.06

4.3 Direct-labeled vs HCR Probes in Mouse Colon Tissue Sections

Building on the previous result, to demonstrate the necessity of HCR amplification, we show that while current techniques are sufficient for discriminating bacterial species in cell culture (see 4.2), they fail to generate signal-to-background sufficient enough to overcome autofluorescence of the mouse in tissue section samples. Figure 4.3 shows tissue sections obtained from singly-germinated mice (with *B. fragilis*) that were hybridized with probes direct-labeled with Alexa Fluor 488 compared to the same probe amplified with an Alexa Fluor 488 labeled HCR system. Although bacterial cells are identifiable in both images, the high signal-to-background conferred by HCR amplification completely overcomes sample autofluorescence (left panel) and enables significantly easier detection of bacterial cells.

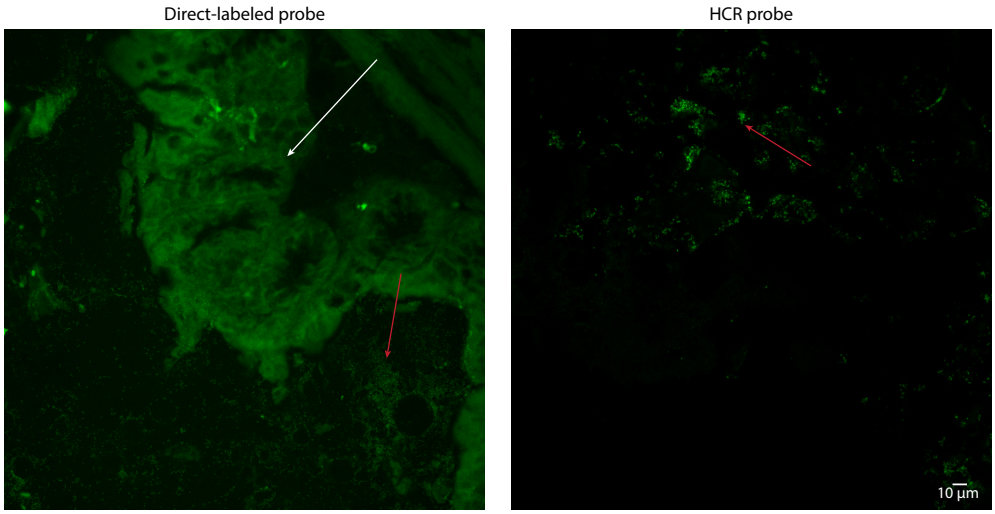

Figure 4.3: **Motivation for HCR amplification for detecting bacteria in mouse colon tissue sections.** White arrow indicates autofluorescent regions of the mouse colon, and red arrows indicate bacterial cells stained by probes *in situ*. Note the high signal-to-background of HCR amplification overcomes sample autofluorescence. Sample: Mouse colon tissue sections singly-colonized with *B. fragilis*. Probe: one fluorescent-labeled DNA probe targeting a universal 16S region direct-labeled with Alexa Fluor 488 (left) or amplified with HCR (right).

4.4 Specificity of in situ HCR Probes in Mouse Colon Tissue Sections

Prior art established that short probes (17-20 nt) are able to discriminate *Bacteroides* species controlled samples [25, 26] and our work reinforced this (Figure 4.2). Due to the modularity inherent in HCR amplification, the optimal solution is to couple state-of-the-art probes with state-of-the-art signal amplification. With this model, hybridization conditions for the probe could be borrowed from prior art, and amplification conditions for HCR could be recycled.

However, significant optimization for probe hybridization was necessary to achieve high signal-to-background (see Appendix C for key optimization steps). A protocol is presented here for multiplexed species-specific detection of *Bacteroides* species in fresh frozen mouse colon tissue sections (Appendix C.3).

Figure 4.4 demonstrates this species-specificity in regards to probes specific to four *Bacteroides* species present in mouse colon sections colonized with each of two *Bacteroides* species. Figure 4.4a involves mouse colon tissue sections extracted from a mouse singly-colonized with *B. fragilis*, and stained with *in situ* HCR with each of the four species-specific probes targeting unique 16S rRNA regions of *B. fragilis*, *B. ovatus*, *B. theta*, and *B. vulgatus* (from left to right). The top row of images shows HCR signal obtained from the species-specific probe, and the bottom row of images shows HCR signal obtained from the universal 16S probe. Figure 4.4b depicts the same set of experimental samples but with sections taken from a mouse colonized singly with *B. vulgatus*. As is evident qualitatively, these probes show species-specificity among these four species, consistent with prior findings [25, 26]. For histogram analysis of individual cells, refer to Appendix C.

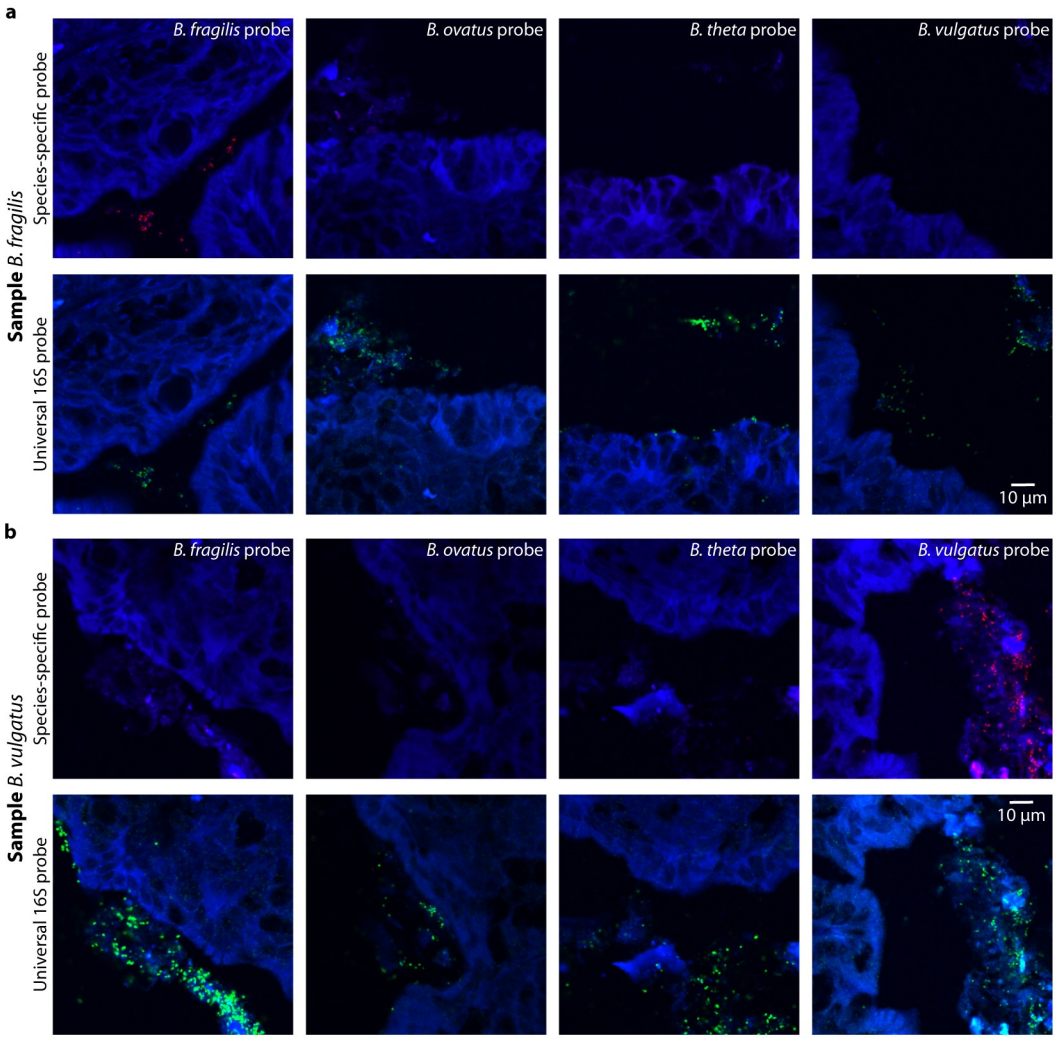

Figure 4.4: **Species-specific detection of Bacteroides species by in situ HCR.** All samples were stained with Phalloidin488 (blue), an HCR probe targeting a universal 16S sequence (green), and an HCR probe targeting a species-specific region of 16S (red). Note red dots appear only when the probe is matched to its appropriate cell line. This was conducted for colon tissue sections extracted from mice singly-colonized with each of *B. fragilis* (a) and *B. vulgatus* (b). Probes: 1 single-initiator DNA probe per target. Amplifiers: two orthogonal DNA HCR amplifiers carrying spectrally distinct fluorophores. Sample: singly-colonized mouse colon tissue sections. Mice were colonized with each *B. fragilis* and *B. vulgatus* prior to sectioning.

4.5 Histogram Analysis of Single Bacterial Cells in Mouse Colon Tissue Sections

In reference to Figure 4.6, Figure 4.5 details histogram analysis of individual bacterial cells in the mouse colon tissue sections. 4.5a corresponds to *B. fragilis* cells, and 4.5b to *B. vulgatus* cells stained within a dual-colonized mouse.

Signal is extracted by applying a threshold mask to raw data. Background is extracted by applying the mask generated from images of the first species to images of the second species. This ensures that the background corresponds to bacterial cells, rather than slide background or mouse cells. Signal histograms between replicates show variability due to the number and intensity of signal observed between bacterial cells. Regardless, all histograms show near-complete separation from background.

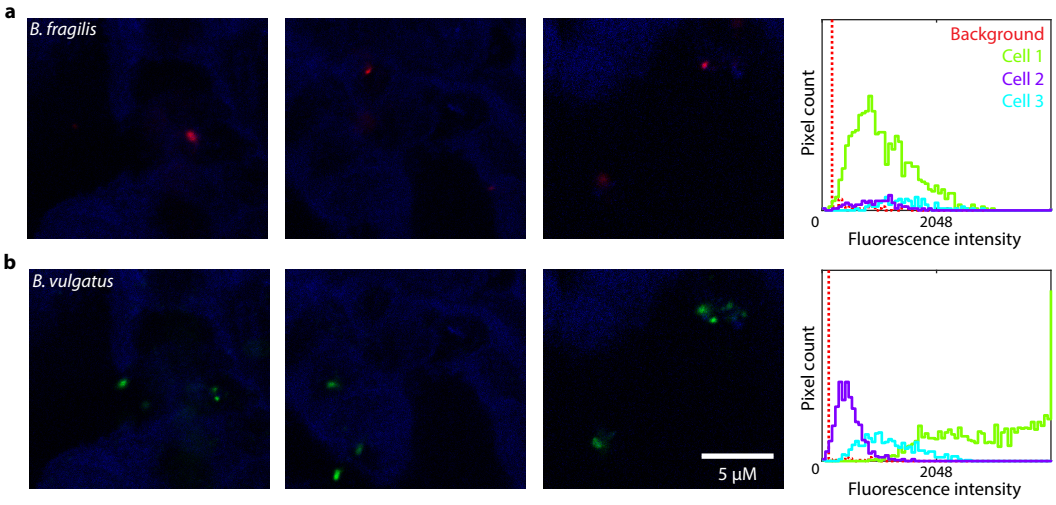

Figure 4.5: **Histogram analysis of single cells in mouse colon tissue sections.** Sample: Mouse colon tissue sections dual-colonized with *B. fragilis* and *B. vulgatus*. Probes: one single-initiator DNA probe per target. Amplifiers: two orthogonal HCR amplifiers carrying spectrally distinct fluorophores.

Target Species	Signal	Background	Signal-to-Background
B. fragilis	1,000 ± 500	60 ± 50	20 ± 20
B. vulgatus	3,000 ± 900	60 ± 40	50 ± 30

Table 4.1: **Signal-to-background calculation for individual species.** Calculations made using data extracted from images in Figure 4.5.

4.6 Multiplexed Discrimination of Bacteroides Species in Mouse Colon Tissue Sections

Though the multiplexed target detection demonstrated in Figure 4.4 is an advancement relative to prior direct-labeled probe fluorescent *in situ* hybridization techniques due to HCR's high signal-to-background, we sought to extend our multiplexing ability to discriminate multiples species within a mouse colonized with multiple *Bacteroides* species. Figure 4.6 demonstrates multiplexed detection of all bacteria, *B. fragilis*, and *B. vulgatus* in mouse colon tissue sections. Additionally, Table 4.2 shows the high signal-to-background generated by HCR amplification.

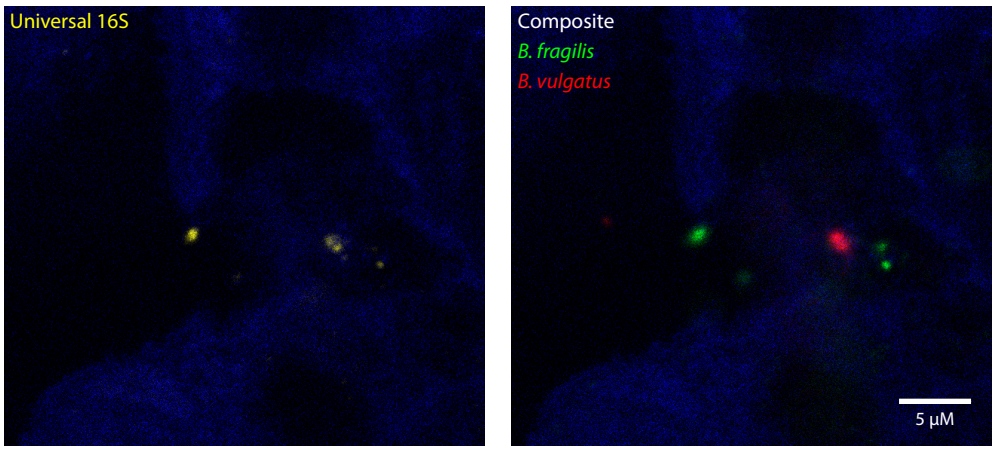

Figure 4.6: **Multiplexed mapping of Bacteroides species in fresh frozen, fixed mouse colon tissue sections.** *Bacteroides* localization within crypts along mouse colon wall. Probes targeting the universal 16S (left, yellow) and the two species (right, green and red) were added to the sample and amplified via HCR. Probes: 1 single-initiator DNA probe per target. Amplifiers: three orthogonal DNA HCR amplifiers carrying spectrally distinct fluorophores. Sample: dual-colonized mouse colon tissue sections. Mouse was colonized with both *B. fragilis* and *B. vulgatus* prior to sectioning.

Target Species	Signal	Background	Signal-to-Background
B. fragilis	1,000 ± 40	200 ± 10	5 ± 0.3
B. vulgatus	3,000 ± 100	500 ± 30	6 ± 0.4

Table 4.2: Signal-to-background analysis for individual targets. Calculations made using data extracted from images depicted in Figure 4.6. See Appendix C for image processing and calculation details.

4.7 Conclusion

The work presented here lays the groundwork for expanding multiplexed detection of closely related RNA targets in challenging samples. Specifically, we demonstrate multiplexed detection of two *Bacteroides* species within intact mouse colon tissue sections, along with a rigorous battery of control samples. Additionally, the sharp signal localization conferred by HCR amplification allows for the potential to localize bacteria within the mouse colon (e.g. differentiate between bacteria in crypts versus in mucus).

When coupled with spectral imaging and linear unmixing, optimized *in situ* HCR using short probes could allow for the immediate multiplexing of up to six fluorophores with high signal-to-background. Such a high degree of multiplexing would allow biologists to gain fresh perspective on how bacterial localization within the colon influences the environment.

4.8 Future Directions

Future work is planned in a few areas. First, it is important to expand our multiplexing ability. In order to validate highly multiplexed detection of bacterial species within the mouse colon, a range of control samples are required. We hope to demonstrate multiplexed discrimination of four *Bacteroides* species within the intact mouse colon sections.

Second, as shown in Chapters 2 and 3, HCR amplification allows for the detection of mRNA and microRNA targets. It should be possible to incorporate these kinds of RNA targets also. The techniques presented here combine to form a broad set of tools for detecting all types of RNA elements in a typical gene circuit. We have demonstrated detection of these elements (mRNA and microRNA), as well as employed detection to allow for species discrimination (via rRNA detection).

Third, that bacteria do not appear to co-localize spatially is suggestive that hyper-multiplexing may be possible using spatial or temporal barcoding of fluorophores [29, 30]. Standard *in situ* HCR enables straightforward multiplexing of n fluorophores, where n is the number of resolvable fluorescent dyes. Compared to this, temporal barcoding with r rounds allows for multiplexing of up to n^r fluorescent dyes. For example, with $n = 4$ dyes and $r = 3$ rounds, up to 64 targets can be multiplexed. This would potentially enable the discrimination of many closely-related species of bacteria.

References

1. Koropatkin, N. M., Cameron, E. A. & Martens, E. C. How glycan metabolism shapes the human gut microbiota. *Nature Publishing Group* **10,** 323–335 (May 2012).
2. Sonnenburg, E. D. *et al.* Specificity of Polysaccharide Use in Intestinal Bacteroides Species Determines Diet-Induced Microbiota Alterations. *Cell* **141,** 1241–1252 (June 2010).
3. David, L. A. *et al.* Diet rapidly and reproducibly alters the human gut microbiome. *Nature . . .* **505,** 559–563 (Jan. 2014).
4. El Kaoutari, A., Armougom, F., Gordon, J. I., Raoult, D. & Henrissat, B. The abundance and variety of carbohydrate-active enzymes in the human gut microbiota. *Nature Reviews Microbiology* **11,** 497–504 (July 2013).
5. Kashyap, P. C. *et al.* Genetically dictated change in host mucus carbohydrate landscape exerts a diet-dependent effect on the gut microbiota. *Proceedings of the National Academy of Sciences of the United States of America* **110,** 17059–17064 (Oct. 2013).
6. Cullen, T. W. *et al.* Gut microbiota. Antimicrobial peptide resistance mediates resilience of prominent gut commensals during inflammation. *Science* **347,** 170–175 (Jan. 2015).
7. Needham, B. D. & Trent, M. S. Fortifying the barrier: the impact of lipid A remodelling on bacterial pathogenesis. *Nature Publishing Group* **11,** 467–481 (July 2013).
8. Gallo, R. L. & Hooper, L. V. Epithelial antimicrobial defence of the skin and intestine. *Nature Reviews Immunology* **12,** 503–516 (July 2012).
9. Vaishnava, S. *et al.* The antibacterial lectin RegIIIgamma promotes the spatial segregation of microbiota and host in the intestine. *Science* **334,** 255–258 (Oct. 2011).
10. Navarro-Garcia, F. *et al.* Pic, an autotransporter protein secreted by different pathogens in the Enterobacteriaceae family, is a potent mucus secretagogue. *Infection and Immunity* **78,** 4101–4109 (Oct. 2010).
11. Luo, Q. *et al.* Enterotoxigenic Escherichia coli secretes a highly conserved mucin-degrading metalloprotease to effectively engage intestinal epithelial cells. *Infection and Immunity* **82,** 509–521 (Feb. 2014).
12. Kubinak, J. L. *et al.* MyD88 Signaling in T Cells Directs IgA-Mediated Control of the Microbiota to Promote Health. *Cell host & microbe* **17,** 153–163 (Feb. 2015).
13. Palm, N. W. *et al.* Immunoglobulin A Coating Identifies Colitogenic Bacteria in Inflammatory Bowel Disease. *Cell* **158,** 1000–1010 (Aug. 2014).

14. Peterson, D. A., McNulty, N. P., Guruge, J. L. & Gordon, J. I. IgA Response to Symbiotic Bacteria as a Mediator of Gut Homeostasis. *Cell host & microbe* **2,** 328–339 (Nov. 2007).

15. Ott, S. J. Reduction in diversity of the colonic mucosa associated bacterial microflora in patients with active inflammatory bowel disease. *Gut* **53,** 685–693 (2004).

16. Manichanh, C. *et al.* Reduced diversity of faecal microbiota in Crohn's disease revealed by a metagenomic approach. *Gut* **55,** 205–211 (Feb. 2006).

17. Gophna, U., Sommerfeld, K., Gophna, S., Doolittle, W. F. & Veldhuyzen van Zanten, S. J. O. Differences between tissue-associated intestinal microfloras of patients with Crohn's disease and ulcerative colitis. *Journal of Clinical Microbiology* **44,** 4136–4141 (Nov. 2006).

18. Nava, G. M., Friedrichsen, H. J. & Stappenbeck, T. S. Spatial organization of intestinal microbiota in the mouse ascending colon. *The ISME Journal* **5,** 627–638 (Oct. 2010).

19. Hooper, L. Laser microdissection: exploring host–bacterial encounters at the front lines. *Current Opinion in Microbiology* **7,** 290–295 (2004).

20. Pedron, T. *et al.* A crypt-specific core microbiota resides in the mouse colon. *mBio* **3,** e00116–12–e00116–12 (2012).

21. Swidsinski, A., Loening-Baucke, V. & Lochs, H. Spatial organization of bacterial flora in normal and inflamed intestine: a fluorescence in situ hybridization study in mice. *World J ...* **11,** 1131 (2005).

22. Poulsen, L. K., Lan, F., Kristensen, C. S. & Hobolth, P. Spatial distribution of Escherichia coli in the mouse large intestine inferred from rRNA in situ hybridization. *Infection and ...* **114,** 303–311 (1994).

23. Urieli-Shoval, S. *et al.* Preservation of RNA for in situ hybridization: Carnoy's versus formaldehyde fixation. *Journal of Histochemistry & Cytochemistry* **40,** 1879–1885 (1992).

24. Propheter, D. C. & Hooper, L. V. Bacteria Come into Focus: New Tools for Visualizing the Microbiota. *Cell host & microbe* **18,** 392–394 (2015).

25. Rigottier-Gois, L., Rochet, V., Garrec, N., Suau, A. & Doré, J. Enumeration of Bacteroides Species in Human Faeces by Fluorescent in situ Hybridisation Combined with Flow Cytometry Using 16S rRNA Probes. *Systematic and Applied Microbiology* **26,** 110–118 (Jan. 2003).

26. Momose, Y., Park, S. H., Miyamoto, Y. & Itoh, K. Design of species-specific oligonucleotide probes for the detection of Bacteroides and Parabacteroides by fluorescence in situ hybridization and their application to the analysis of mouse caecal Bacteroides-Parabacteroides microbiota. *Journal of Applied Microbiology* **111,** 176–184 (May 2011).

27. Choi, H. M. T. *et al.* Programmable in situ amplification for multiplexed imaging of mRNA expression. *Nature Biotechnology* **28,** 1208–1212 (Oct. 2010).

28. Choi, H. M. T., Beck, V. A. & Pierce, N. A. Next-Generation in SituHybridization Chain Reaction: Higher Gain, Lower Cost, Greater Durability. *ACS Nano* **8,** 4284–4294 (May 2014).

29. Lubeck, E., Coskun, A. F., Zhiyentayev, T., Ahmad, M. & Cai, L. Single-cell in situ RNA profiling by sequential hybridization. *Nature Methods* **11,** 360–361 (Mar. 2014).

30. Weber, T. S., Dukes, M., Glaser, S., Naik, S. & Duffy, K. R. Site-specific recombinatorics: in situ cellular barcoding with the Cre Lox system. *arXiv preprint arXiv:1602.02190* (2016).

Appendix A

SUPPLEMENTARY INFORMATION FOR CHAPTER II

A.1 Materials and Methods

A.1.1 Cell Maintenance and Preparation

Three cell lines were used in this study: the wild-type HEK293T line and two transgenic lines, HEK293 + *d2egfp* (*Tg(d2egfp)*) and HEK293 + *dsRed2* (*Tg(dsRed2)*), which express *d2egfp* and *dsRed2* mRNAs, respectively. HEK293T cell line was obtained from ATCC, HEK293 + *d2egfp* was gifted by Dr. Christopher Beisel (NIH), and HEK293 + *dsRed2* was created using wild-type HEK293 (ATCC) and the pdsRed2-C1 expression vector (Clontech). Due to imperfect vector integration process, the HEK293 + *dsRed2* contains a small fraction of wild-type cells. Transgenic protein fluorescence was confirmed by flow cytometry (data not shown).

A.1.2 HCR Probes and Amplifiers

RNA HCR probes are 174-nt long (4x (26-nt initiator, 5-nt spacer) + 50-nt mRNA recognition sequence). mRNA targets are addressed by probe sets containing one or more probes that hybridize at 50-nt binding sites. RNA probes were received in individual aliquots resuspended in ultrapure water, normalized to a concentration of 1 μM.

RNA HCR amplifiers are 52-nt long hairpins (10-nt toehold, 16-bp stem, 10-nt loop). RNA HCR amplifiers were conjugated to appropriate fluorophores (Life Technologies Alexa Fluor® Dyes, heretofore referred to as AlexaNNN to denote the dye's excitation wavelength). Hairpin pairs were received as individual aliquots resuspended in ultrapure water, normalized to a concentration of 3 μM.

For each target mRNA, a kit containing an RNA probe set, an RNA HCR amplifier, and hybridization, wash, and amplification buffers was purchased from Molecular Instruments (www.molecularinstruments.org). See Table A.1 for a summary of probe set, amplifier, and fluorophore details and Section A.4 for probe sequences.

Target Type	Target	Probes	Probe Set	HCR Amplifier	Fluorophore	Figures
mRNA	*actb*	5	2-6	A2	Alexa488	2.13
		2	1,2	A2	Alexa647	2.3a
		1	2	A2	Alexa647	2.3b
		4	3-6	A5	Alexa488	2.3
	d2egfp	1	1	A3	Alexa647	2.6a,2.8a,2.2a,2.4
		1	10	A3	Alexa647	2.2b
		1	1	A3	Alexa488	**??**a
		3	4,7,8	A2	Alexa647	**??**a
		3	1,4,8,10	A3	Alexa647	2.2c
		3	1,4,8	A3	Alexa647	2.13,2.2d,2.5
	dsRed2	2	1,2	A2	Alexa647	2.6b,2.8b
		3	4-6	A3	Alexa488	**??**b
		2	1,2	A2	Alexa647	**??**b
		3	1,2,6	A5	Alexa546	2.13

Table A.1: Probe set, HCR amplifier, and fluorophore for each target.

A.1.3 Experimental Design

All protocols and reagents can be found in Appendix A.3. All probe and amplifier sequences can be found in Appendix A.4.

Figure 2.6a includes wild-type cells (background) and *Tg(d2egfp)* cells (signal + background). A single HCR probe was used along with the A3 HCR amplifier conjugated to Alexa647. Figure 2.6b includes wild-type cells (background) and *Tg(dsRed2)* cells (signal + background). A single HCR probe was used along with the A3 HCR amplifier conjugated to Alexa647.

Figure 2.8 is composed of varying mixtures of wild-type and transgenic cells. For each transgene, 5 mixtures were artificially created after fixation and permeabilization but before HCR. These mixtures were created by volume and do not necessarily relate to total cell count. Mixtures included wild-type only, transgene only, and the following ratios of wild-type to transgene: 1:1, 1:3, and 3:1. For 2.8a, *d2egfp* was detected with a single HCR probe, and for 2.8b, *dsRed2* was also detected with a single HCR probe. The A3 HCR amplifier conjugated to Alexa647 was used in both cases.

Figure **??** includes only transgenic cells. For each transgene, two orthogonal probe sets and HCR amplifiers were used to perform redundant detection of the mRNA target. For **??**a, *d2egfp* was redundantly detected with: one HCR probe initiating the A3 HCR amplifier (conjugated to Alexa488) and three HCR probes initiating the A2 HCR amplifier (conjugated to Alexa647). For **??**b, *dsRed2* was redundantly detected with: three HCR probes initiating the A3 HCR amplifier (conjugated to Alexa488) and two HCR probes initiating the A5 HCR amplifier (conjugated to Alexa647).

Figure 2.13a is made up of individual cell lines. Figure 2.13b is composed of a mixture of all cell lines (wild-type and both transgenes). Figure 2.13c is analysis of the cells sorted using the gating indicated in 2.13b (quadrants). *Tg(d2egfp)* was detected with three HCR probes and the A3 HCR amplifier conjugated to Alexa647. *Tg(dsRed2)* was detected with three HCR probes and the A5 HCR amplifier conjugated to Alexa488.

A.1.4 Flow Cytometry

Transgenic and wild-type cell lines were checked for protein fluorescence on the BD Accuri^{TM} C6. For detection of *d2egfp* (laser 488 nm, filter 533 $\pm$

30 nm) and *dsRed2* (laser 488 nm, filter 585 $\pm$ 40 nm), protein fluorescence was compared between all three cell lines to verify protein presence in the appropriate samples (data not shown).

Similarly, protein fluorescence was determined to be denatured after the HCR protocol was completed due to the chemical and heat treatment. Cells were resuspended in 500 μL 1x PBS following the *in situ* protocol. Acquisition for Figures 2.6-**??** was completed on the BD Accuri^{TM} C6 for the detection of the Alexa488- (laser 488 nm, filter 533 $\pm$ 30) and Alexa647-labeled (laser 640 nm, filter 675 $\pm$ 25 nm) HCR amplifiers. For each sample, 50,000 events were counted within the selected gate (based on forward and side scatters to filter out debris).

A.1.5 Fluorescence Activated Cell Sorting

Cell sorting for Figure 2.13 was performed using a BD FACSAria^{TM} I located at University of Southern California's Flow Cytometry Core Facility. HCR amplifiers were detected with both Alexa488- (laser 488 nm, PMT 2D, mirror 505 LP, filter 510 $\pm$ 20) and Alexa647-labels (laser 633 nm, PMT 4C, filter 660 $\pm$ 20). Sorted cells were deposited into 1.7 mL micro-centrifuge tubes and re-analyzed on the same machine for checking purity. Entire samples were sorted, and approximately 10,000 cells were analyzed.

A.1.6 Statistical Analysis

All plots were created and statistical analyses completed using MATLAB®.

A.2 Technical Replicates

This section contains technical replicates for all figures presented in Chapter 2. Technical replicates refer to *in situ* HCR performance; biological samples are taken from the same batch of prepared cell lines to maintain consistency.

A.2.1 Single Color Validation of in situ HCR

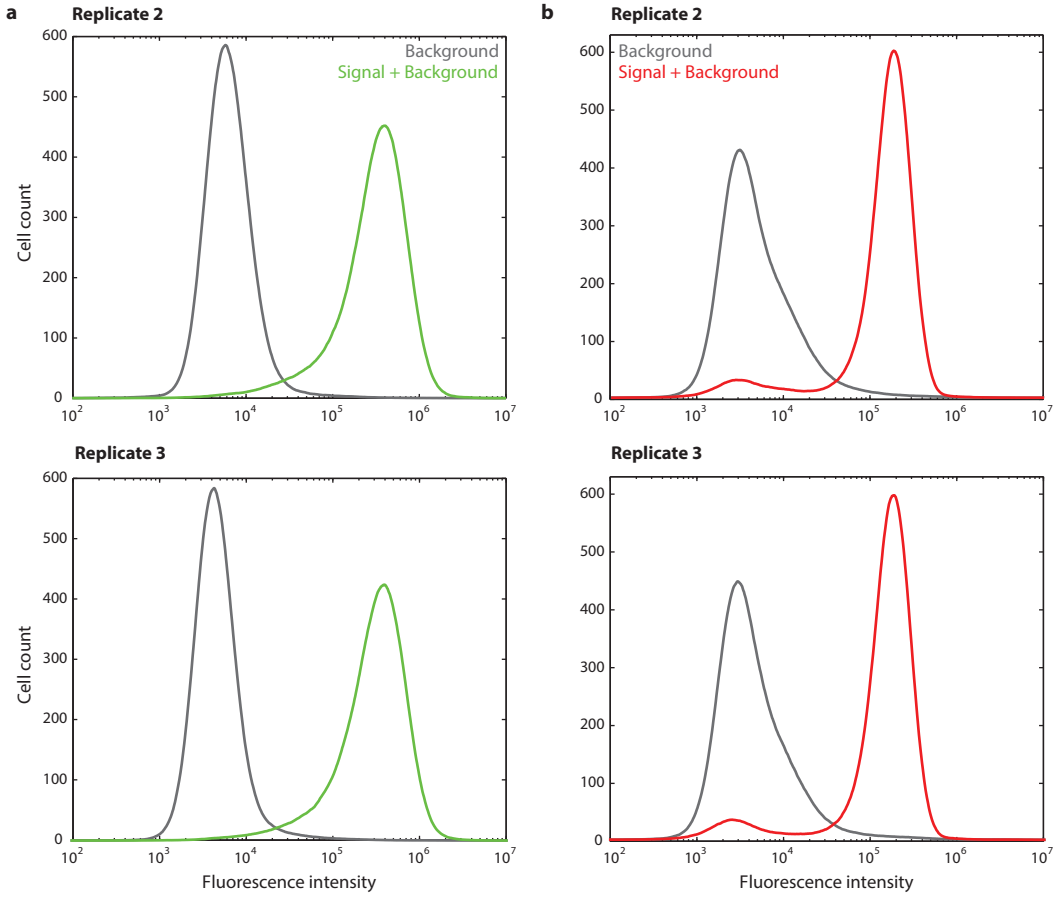

Figure A.1: **Technical replicates corresponding to Figure 2.6.** Samples: HEK293T, HEK293 + *d2egfp*, HEK293 + *dsRed2*. Targets: transgenic mRNAs: (a) *Tg(d2egfp)* and (b) *Tg(dsRed2)*. Probe sets: single HCR probe per target. Due to impurities in the vector integration process, a small population of wild-type cells are observed in the *Tg(dsRed2)* cell line. Each histogram is composed of 50,000 cells.

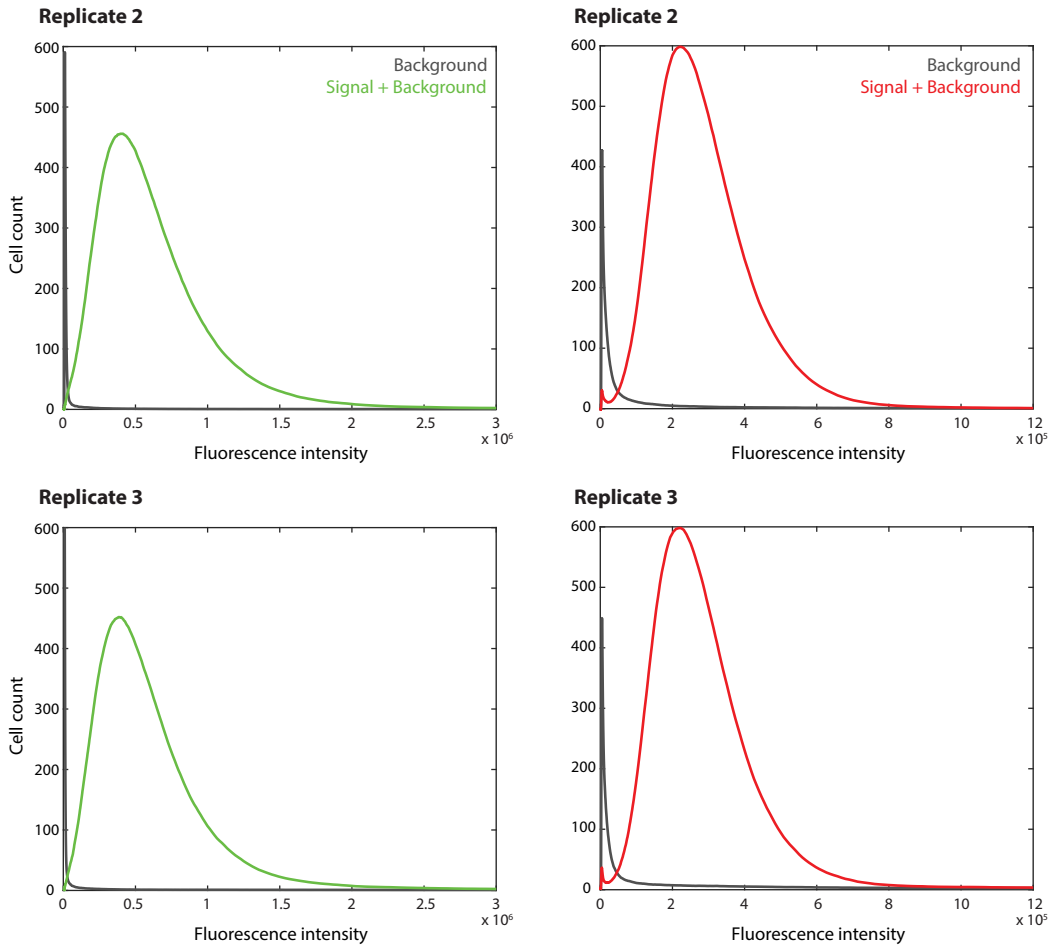

Figure A.2: **Technical replicates corresponding to Figure 2.7.** Samples: HEK293T, HEK293 + *d2egfp*, HEK293 + *dsRed2*. Targets: transgenic mRNAs: (a) *Tg(d2egfp)* and (b) *Tg(dsRed2)*. Probe sets: single HCR probe per target. Due to impurities in the vector integration process, a small population of wild-type cells are observed in the *Tg(dsRed2)* cell line. Each histogram is composed of 50,000 cells.

A.2.2 Single Color Validation of in situ HCR with Heterogeneous Mixtures

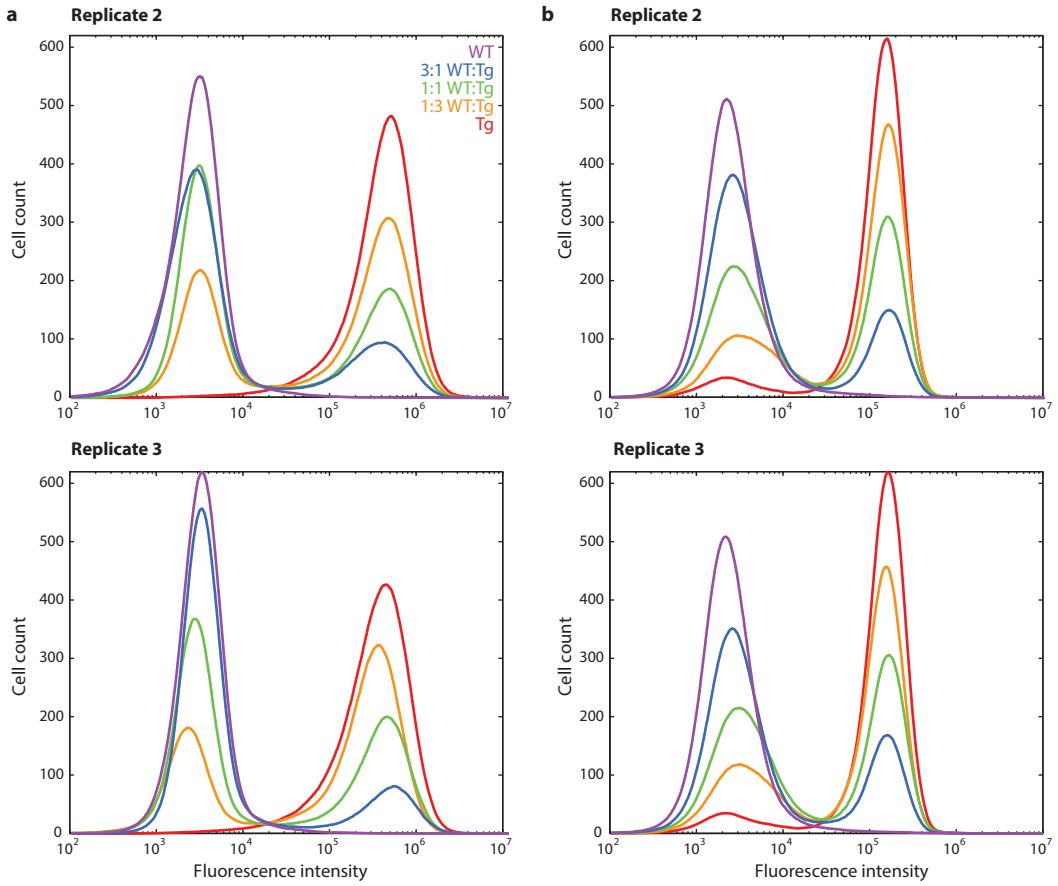

Figure A.3: **Technical replicates corresponding to Figure 2.8.** Cell lines: HEK293T, HEK293 + *d2egfp*, HEK293 + *dsRed2*. Targets: transgenic mRNAs: (a) *Tg(d2egfp)* and (b) *Tg(dsRed2)*. Probe sets: single HCR probe per target. Due to impurities in the vector integration process, a small population of wild-type cells are observable in the 100% *Tg(dsRed2)* sample and contribute to all mixtures of wild-type and *Tg(dsRed2)* cells. Each histogram is composed of 50,000 cells.

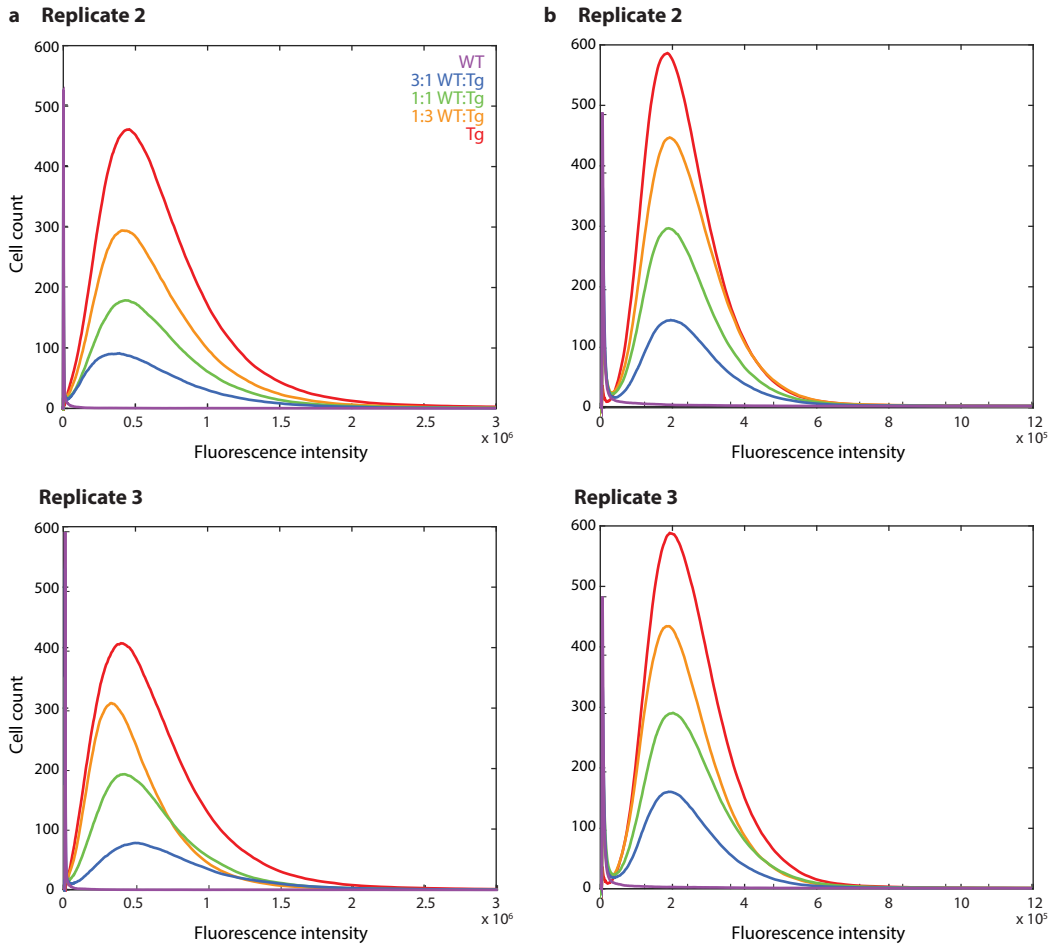

Figure A.4: **Technical replicates corresponding to Figure 2.9.** Cell lines: HEK293T, HEK293 + *d2egfp*, HEK293 + *dsRed2*. Targets: transgenic mRNAs: (a) *Tg(d2egfp)* and (b) *Tg(dsRed2)*. Probe sets: single HCR probe per target. Due to impurities in the vector integration process, a small population of wild-type cells are observable in the 100% *Tg(dsRed2)* sample and contribute to all mixtures of wild-type and *Tg(dsRed2)* cells. Each histogram is composed of 50,000 cells.

A.2.3 Relative Quantitation of mRNA Abundance by Redundant Detection

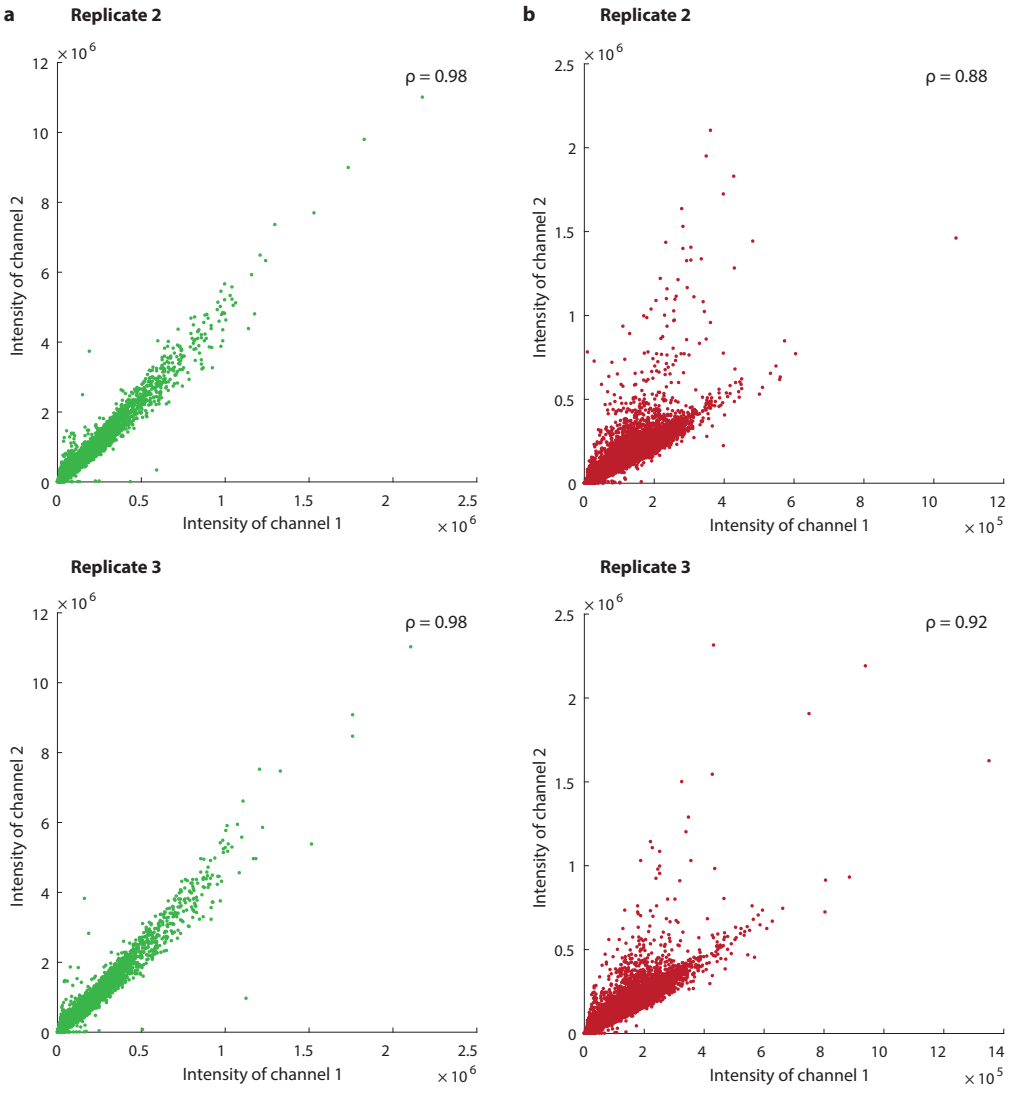

Figure A.5: **Technical replicates corresponding to Figure 2.11.** Samples: HEK293 + *d2egfp*, HEK293 + *dsRed2*. Targets: transgenic mRNAs: (a) *Tg(d2egfp)* and (b) *Tg(dsRed2)*. Probe sets: (a) three HCR probes for channel 1, single HCR probe for channel 2 and (b) two HCR probes for channel 1, three HCR probes for channel 2. Due to impurities in the vector integration process, a small population of wild-type cells are observable in the *Tg(dsRed2)* cell line (cluster near origin in (b)).

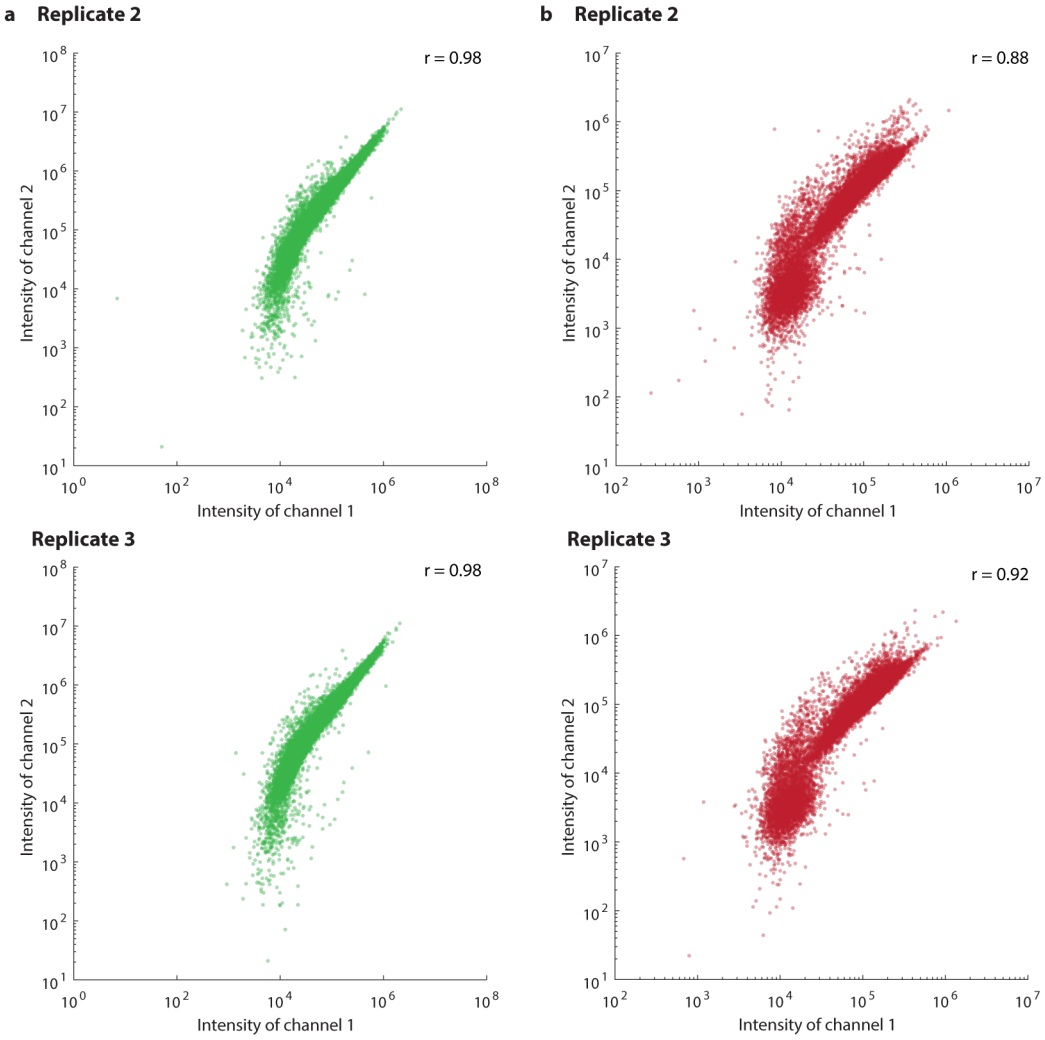

Figure A.6: **Technical replicates corresponding to Figure 2.12.** Samples: HEK293 + *d2egfp*, HEK293 + *dsRed2*. Targets: transgenic mRNAs: (a) *Tg(d2egfp)* and (b) *Tg(dsRed2)*. Probe sets: (a) three HCR probes for channel 1, single HCR probe for channel 2 and (b) two HCR probes for channel 1, three HCR probes for channel 2. Due to impurities in the vector integration process, a small population of wild-type cells are observable in the *Tg(dsRed2)* cell line (cluster near origin in (b)).

A.3 Protocols

A.3.1 Media Preparation

Growth Media

1. Heat inactivate a bottle of FBS at 50 °C for 30 m and aliquot the bottle into 50 mL Falcon tubes.
2. Remove 50 mL of media from fresh 500 mL bottle of Dulbecco's Eagle Modified Medium (DMEM).
3. Add 50 mL of FBS for 10% final concentration.
4. Media must be pre-warmed to 37 °C prior to adding to live cells[1].

Cell Freezing Media

- 90% growth media
- 10% dimethyl sulfoxide (DMSO)

A.3.2 Cell Thawing

1. Add 9 mL of warmed (37 °C) growth medium to a 15 mL Falcon tube.
2. Thaw frozen cells by placing cryogenic storage vial in 37 °C water bath with floating styrofoam.
3. Remove the tube when cells begin to thaw ($\approx$ 2 m).
4. Add 1 mL growth medium to melt ice completely.
5. Transfer cells back to 15 mL tube (making 10 mL total).
6. Centrifuge for 5 m at 1.0 RCF (relative centrifugal force) to remove DMSO.
7. Aspirate supernatant carefully.
8. Add 0.5 mL growth medium to resuspend cell pellet.
9. Add 9.5 mL growth medium to 10 cm cell culture plate.

[1] Be sure to make fresh media every 1-2 months.

10. Add 0.5 mL cells in growth medium to cell culture plate.
11. Store plate at 37 °C.

A.3.3 Cell Passaging

1. Warm up trypsin, phosphate buffered saline (PBS), and growth medium to 37 °C.
2. Remove culture plate from 37 °C incubator.
3. Wash plate with 5 mL PBS.
4. Add 3 mL trypsin to detach cells.
5. Incubate plate for 5 m at 37 °C.
6. Add 3 mL growth medium to quench trypsin.
7. Transfer cells to 15 mL Falcon tube.
8. Centrifuge for 5 m at 1.0 RCF.
9. Aspirate medium, and resuspend cells in 10 mL fresh growth medium.
10. Add 0.5 mL cells to 9.5 mL in fresh cell culture plate.
11. Store plate at 37 °C.

A.3.4 Cell Freezing

1. Grow four extra plates of cell line.
2. Prepare 5 mL freezing medium.
3. Follow steps 1-8 from cell passaging protocol.
4. Instead of growth medium, resuspend cells in freezing medium[2].
5. Aliquot cells in freezing medium into 5 cryogenic storage vials.
6. Place vials in styrofoam box inside -80 °C to slowly chill cells.
7. After 16 h, move cells into liquid nitrogen for long-term storage.

[2]Be sure to begin freezing process within 5 m of adding DMSO to cells

A.3.5 Cell Fixation

Follow steps 1-8 from cell passaging protocol.

1. Aspirate, and resuspend cells in 20 mL growth medium.
2. Centrifuge for 5 m at 1.0 RCF.
3. Aspirate, and resuspend cells in freshly made 4% PFA in PBST.
4. Fix for 1 h at RT.
5. Centrifuge for 5 m at 1.0 RCF.
6. Aspirate, and resuspend cells in 10 mL PBST.
7. Repeat previous two steps two more times.
8. Aspirate, and resuspend cells in 10 mL 70% ethanol.
9. Store overnight at 4 °C.

A.3.6 Multiplexed in situ Hybridization Chain Reaction in Cell Culture

Detection Stage

1. For each sample, move ≈500,000 cells to a 1.5 mL eppendorf tube.
2. Pre-hybridize with 100 μL of 50% hybridization buffer (HB50) for 10 min at 55 °C.
3. Prepare probe solution by adding 10 pmol of each probe (1 μL of 10 μM stock per probe) to 400 μL of HB50 at 55 °C.
4. Add the probe solution directly to samples in HB50.
5. Incubate samples 4 h at 55 °C.
6. Remove excess probes by washing at 55 °C with 1 mL of:
   a) HB50 for 30 min
   b) HB50 for 30 min

   Solutions should be pre-heated to 55 °C before use. Remove HB50 between washes by centrifugation (5 m at 1.0 RCF).

Amplification Stage

1. Pre-amplify samples with 100 μL of 40% hybridization buffer (HB40) for 10 min at 45 °C.
2. Prepare 30 pmol of each fluorescently-labeled hairpin by snap cooling in 10 μL of 5× SSC buffer (heat at 95 °C for 90 seconds and cool to room temperature on the benchtop for 30 min).
3. Prepare hairpin solution by adding all snap-cooled hairpins to 400 μL of HB40 at 45 °C.
4. Add the hairpin solution directly to samples in HB40.
5. Incubate samples overnight (12–16 h) at 45 °C.
6. Remove excess hairpins by washing with at 45 °C with 1 mL of:
   a) 75% HB40 and 25% 2× SSCT for 5 m

b) 50% HB40 and 50% 2× SSCT for 5 m

c) 25% HB40 and 75% 2× SSCT for 5 m

d) 100% 2× SSCT for 5 m

7. Resuspend in 2× SSCT at RT.

A.3.7 Buffer Recipes

Cell Growth Media	For 500 mL of solution
10% fetal bovine serum (FBS)	50 mL of FBS
1× penicillin streptomycin (pen strep)	5 mL 100× pen strep
	Fill up to 500 mL with Dulbecco's Modified Eagle Medium

PBST	For 50 mL of solution
1× PBS	5 mL of 10× PBS
0.1% Tween 20	500 μL of 10% Tween 20
	Fill up to 50 mL with ultrapure H_2O

4% Formaldehyde (FA)	For 40 mL of solution
4% FA	10 mL 16% methanol-free FA
1× PBST	30 mL of 1× PBST

50% Hybridization Buffer (HB50)	For 40 mL of solution
50% Formamide	20 mL of Formamide
2× Sodium Chloride Sodium Citrate (SSC)	4 mL of 20× SSC
9 mM Citric Acid (pH 6.0)	360 μL of 1 M Citric Acid (pH 6.0)
0.1% Tween 20	400 μL of 10% Tween 20
500 μg/mL tRNA	200 μL of 100 mg/mL tRNA
50 μg/mL Heparin	200 μL of 10 mg/mL Heparin
	Fill up to 40 mL with ultrapure H_2O

40% Hybridization Buffer (HB40)	For 40 mL of solution
40% Formamide	16 mL of Formamide
2× Sodium Chloride Sodium Citrate (SSC)	4 mL of 20× SSC
9 mM Citric Acid (pH 6.0)	360 μL of 1 M Citric Acid (pH 6.0)
0.1% Tween 20	400 μL of 10% Tween 20
500 μg/mL tRNA	200 μL of 100 mg/mL tRNA
50 μg/mL Heparin	200 μL of 10 mg/mL Heparin
	Fill up to 50 mL with ultrapure H_2O

A.3.8 Reagents and Supplies

Dimethyl sulfoxide (DMSO) (Sigma Aldrich Cat. # D8418)
Dulbecco's Modified Eagle Medium (DMEM) (Thermo Fisher Cat. # 11995-065)
Dulbecco's Phosphate Buffered Saline (DPBS) (Thermo Fisher Cat. # 14190-094)
Fetal Bovine Serum (FBS) (Thermo Fisher Cat. # 16140-071)
Formaldehyde (16%) (Polysciences Cat. # 18814-10)
HCR Amplifiers and Buffers (Molecular Instruments)
Penicillin Streptomycin (Pen Strep) (Thermo Fisher Cat. # 15140-122)
Round Bottom Test Tubes (Flow Cytometry) (VWR Cat. # 21008-948)
Trypsin-EDTA (0.25%) (Thermo Fisher Cat. # 25200-072)
10× Phosphate-buffered saline (PBS) (Ambion Cat. # AM9625)
20× Sodium chloride sodium citrate (SSC) (Invitrogen Cat. # 15557-044)
50% Tween 20 (Invitrogen Cat. # 00-3005)

A.4 Sequences

A.4.1 Probe Sequences

Sequences for all target mRNAs used in this paper were obtained from the Universal Protein Resource (UniProt) and Addgene. All sequences are listed 5′ to 3′. For full quad-initiator probe sequences, four repeat initiator + spacer sequences were appended to the 5′ end of the probe sequence. For brevity, full probe sequences are not shown.

Target: **beta actin (actb)**

Probe #	Probe Sequence
1	CCgACUgCUgUCACCUUCACCgUUCCAgUUUUUAAAUCCUgAgUCAAgCC
2	CAAUgUgCAAUCAAAgUCCUCggCCACAUUgUgAACUUUgggggAUgCUC
3	CCAUUCUCCUUAgAgAgAAgUggggUggCUUUUAggAUggCAAgggACUU
4	AUUUACACgAAAgCAAUgCUAUCACCUCCCCUgUgUggACUUgggAgAgg
5	CACUCCCAgggAgACCAAAAgCCUUCAUACAUCUCAAgUUgggggACAAA
6	UUUAUUCAACUggUCUCAAgUCAgUgUACAggUAAgCCCUggCUgCCUCC

Table A.2: Probe sequences targeting mammalian mRNA transcript: *actb*

Target: **destabilized enhanced green fluorescent protein # 2 (d2egfp)**

Probe #	Probe Sequence
1	gUUCUUCUgCUUgUCggCCAUgAUAUAgACgUUgUggCUgUUgUAgUUgU
4	ACgCUgCCgUCCUCgAUgUUgUggCggAUCUUgAAgUUCACCUUgAUgCC
7	gCgggUCUUgUAgUUgCCgUCgUCCUUgAAgAAgAUggUgCgCUCCUggA
8	CgUAgCCUUCgggCAUggCggACUUgAAgAAgUCgUgCUgCUUCAUgUgg
10	ggUgggCCAgggCACgggCAgCUUgCCggUggUgCAgAUgAACUUCAggg

Table A.3: Probe sequences targeting mRNA transcript: *d2egfp*

Target: **optimized red fluorescent protein (dsRed2)**

Probe #	**Probe Sequence**
1	AAgUUCAUCACgCgCUCCCACUUgAAgCCCUCggggAAggACAgCUUCUU
2	gAAgUUCACgCCgAUgAACUUCACCUUgUAgAUgAAgCAgCCgUCCUgCA
4	gACUUgAACUCCACCAggUAgUggCCgCCgUCCUUCAgCUUCAgggCCUU
5	CCACgUAgUAgUAgCCgggCAgCUgCACgggCUUCUUggCCAUgUAgAU
6	ggUACCgUCgACUgCAgAAUUCgAAgCUUgAgCUCgAgAUCUCAggAACA

Table A.4: Probe sequences targeting mRNA transcript: *dsRed2*

A.4.2 Amplifier Sequences

Sequences for RNA HCR initiators were obtained from Molecular Instruments (MI). All sequences are listed 5′ to 3′.

System #	Initiator	Spacer
A2	gACCCUAAgCAUACAUCgUCCUUCAU	UUUUU
A3	gACUACUgAUAACUggAUUgCCUUAg	AAUUU
A5	UACgCCCUAAgAAUCCgAACCCUAUg	AAAUA

Table A.5: RNA HCR initiator sequences

Appendix B

SUPPLEMENTARY INFORMATION FOR CHAPTER III

B.1 Materials and Methods

B.1.1 HCR Probes and Amplifiers

For each target miRNA, probes were ordered as chimeric 2'-O-methylated RNA sequences appended by the appropriate DNA HCR initiator sequence from Integrated DNA Technologies (www.idtdna.com). For each target mRNA, a kit containing a DNA probe set, a DNA HCR amplifier, and hybridization, wash, and amplification buffers was purchased from Molecular Instruments (www.molecularinstruments.org). See Table B.1 for a summary of probe set, amplifier, and fluorophore details and Appendix B.6 for probe sequences.

Target Type	Target	Probes	HCR Amplifier	Fluorophore	Figures
mRNA	*hbae3*	7	B1	Alexa546	3.3, 3.4, B.2-B.3
microRNA	miR-9	1	B3	Alexa488	3.3, 3.4, B.2-B.3
	miR-96	1	B4	Alexa647	3.3, 3.4, B.2-B.3
	miR-206	1	B2	Alexa514	3.3, 3.4, B.2-B.3
		1	B1	Alexa647	B.1
	miR-10	1	B1	Alexa647	B.1
	miR-144	1	B1	Alexa647	B.1

Table B.1: Probe set, HCR amplifier, and fluorophore for each target.

B.1.2 Experimental Design

Procedures for the care and use of zebrafish embryos were approved by the Caltech IACUC. Embryos were fixed and permeabilized using the protocol of Sections B.5.1. *In situ* hybridization experiments were performed using the protocols of Section B.5.2. Samples were mounted for imaging as described also in Section B.5.2.

B.1.3 Standard Confocal Microscopy

A Zeiss 710 NLO inverted confocal microscope was used to image whole-mount embryos and larva. An LD LCI Plan-Apochromat 25x/0.8 Imm Korr DIC objective was used to acquire all images. See Table B.2 for a summary of excitation laser sources, beam splitters, and tuned emission bandpass filters used for each target when using standard confocal microscopy.

Target	Fluorophore	Laser (nm)	Beam Splitter	Filter (nm)	Figure
hbae3	Alexa647	633	488/561/633	638–755	3.2
miR-9	Alexa546	561	458/561	563–641	3.2
miR-96	Alexa488	488	488/561/633	493–530	3.2
miR-206	Alexa514	514	458/514	534–563	3.2
	Alexa647	647	488/561/633	638–755	B.1
miR-10	Alexa647	647	488/561/633	638–755	B.1
miR-144	Alexa647	647	488/561/633	638–755	B.1

Table B.2: Standard confocal microscopy settings for each target.

B.1.4 Spectral Confocal Microscopy

The same Zeiss 710 NLO inverted confocal microscope hardware was used to image when using spectral confocal microscopy. See Table B.3 for a summary of imaging parameters.

Target	Fluorophore	Laser (nm)	Beam Splitter	Filter (nm)	Figures
hbae3	Alexa647	633	488/561/633	631–728	3.3, 3.4, 3.2, B.3
miR-9	Alexa546	561	488/561	563–728	3.3, 3.4, B.2-B.3
miR-96	Alexa488	488	488	495–728	3.3, 3.4, B.2-B.3
miR-206	Alexa514	514	458/514	514–728	3.3, 3.4, B.2-B.3

Table B.3: Spectral confocal microscopy settings for each target.

B.1.5 Image Analysis

Image analysis protocols have been outlined in previous work [1]. For each target miRNA/mRNA, background (BACK) is characterized for pixels in one representative region without gene expression, and signal plus background (SIG + BACK) is characterized for pixels in one representative region with high gene expression (Figures 3.4a, B.1b). For pixels within these regions, distributions are characterized by plotting pixel intensity histograms (Figure 3.4b, B.1c) and characterize performance by calculating mean pixel intensity (x_{BACK} and $x_{SIG+BACK}$). Performance across technical replicates (N = 3 for each target in Figure 3.4) is characterized by calculating sample means ($\bar{x}_{BACK}$ and $\bar{x}_{SIG+BACK}$) and sample standard deviations (σ_{BACK} and $\sigma_{SIG+BACK}$) (See Table 3.3). The mean signal is then estimated as (Equation B.1):

$$\bar{x}_{SIG} = \bar{x}_{SIG+BACK} - \bar{x}_{BACK} \tag{B.1}$$

and the standard deviation, accounting for the propagation of uncertainty as (Equation B.2):

$$\sigma_{SIG} \leq \sqrt{\sigma^2_{SIG+BACK} + \sigma^2_{BACK}}. \tag{B.2}$$

Then, the result from Equation B.1 is used to calculate signal-to-background (Equation B.3):

$$\bar{x}_{SB} = \frac{\bar{x}_{SIG}}{\bar{x}_{BACK}} \tag{B.3}$$

with standard deviation, accounting for the propagation uncertainty as (Equation B.4):

$$\sigma_{SB} \leq \bar{x}_{SB} \cdot \sqrt{\left(\frac{\sigma_{SIG}}{\bar{x}_{SIG}}\right)^2 + \left(\frac{\sigma_{BACK}}{\bar{x}_{BACK}}\right)^2} \tag{B.4}$$

Estimates for background ($\bar{x}_{BACK} \pm \sigma_{BACK}$), signal ($\bar{x}_{SIG} \pm \sigma_{SIG}$), and signal-to-background ($\bar{x}_{SB} \pm \sigma_{SB}$) are displayed for each target miRNA/mRNA in Table 3.3.

For Figure 3.2, autofluorescence in characterized for pixels in a representative region within blood vessels. Pixels in these regions are analyzed as outlined previously. Figure 3.2a demonstrates these representative regions and the corresponding histograms. See Table 3.2 for quantitative comparisons.

B.2 MicroRNA Detection in Early Stage Embryos

Experiments were also performed using younger zebrafish embryos (26 hpf). For these embryos, the protocol outlined in Section B.5 was used, but proteinase K digestion was not required. Figure B.1 demonstrates a minimal set of *in situ* HCR images and analysis of microRNA targets expressing at this younger stage. It also serves to show the flexibility of the protocol with respect to sample stage and tissue complexity.

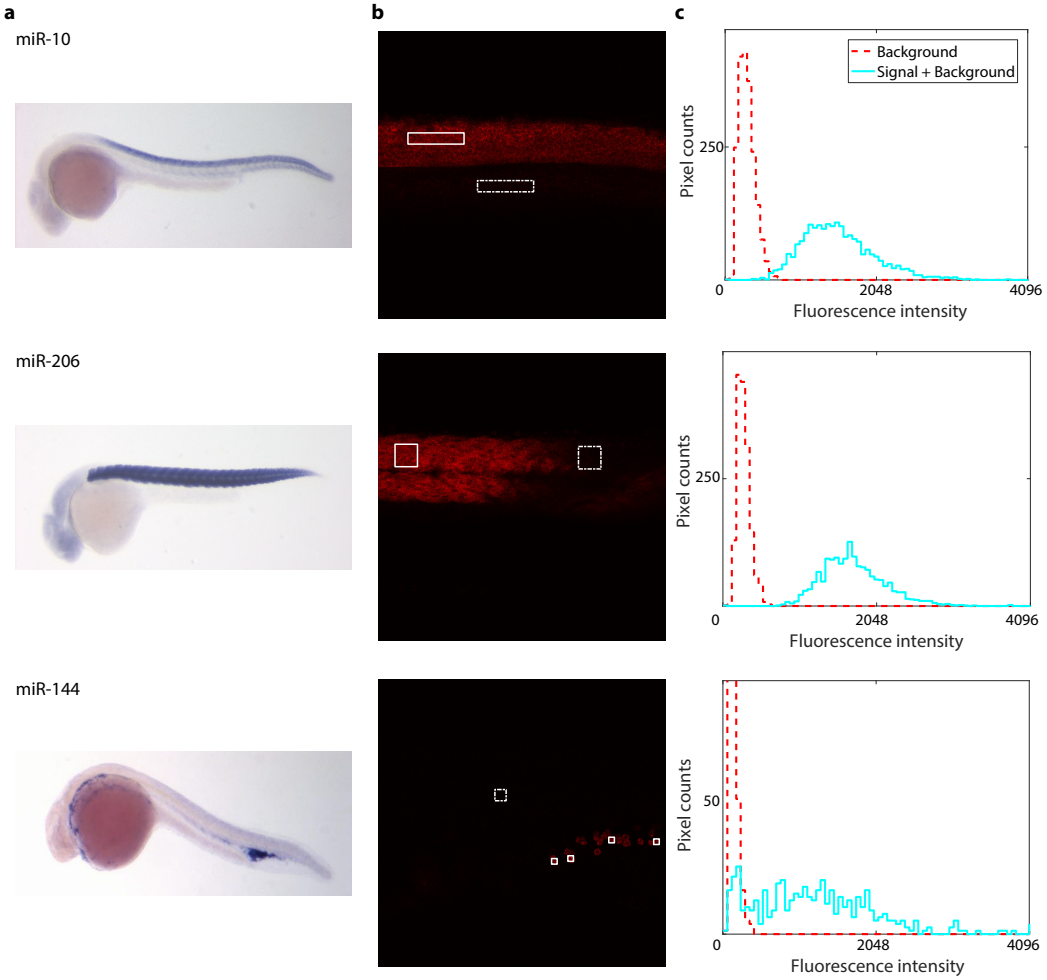

Figure B.1: **MicroRNA detection with early stage zebrafish embryos. a.** Traditional *in situ* images of three microRNA targets. **b.** *In situ* HCR images of three microRNA target. **c.** Histogram analysis of HCR images. Solid box in (b) indicates "Signal + Background" and dotted box indicates "Background." Sample: Wild-type zebrafish fixed at 26 hpf. Probes: one single-initiator DNA probe per target.

B.3 Reference Images for microRNA Targets

Reference images were obtained for each microRNA target studied from prior work in the field[2]. HCR images were compared to these reference images to ensure competitive and correct target staining. Figure B.2 depicts traditional *in situ* images for each microRNA target detected alongside respective signal obtained with *in situ* HCR.

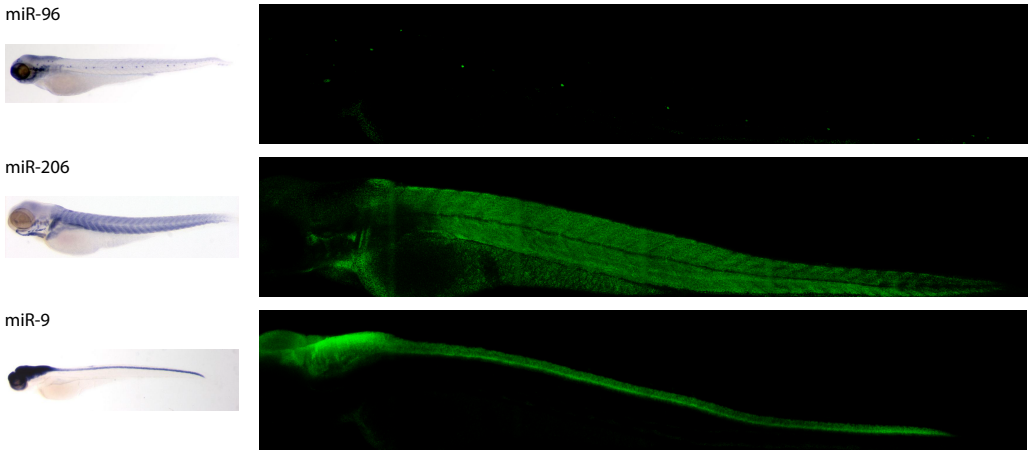

Figure B.2: **Reference images for microRNA targets.** Images in right column are maximum intensity projections of images obtained via spectral confocal microscopy and processed with linear unmixing. Sample: Casper zebrafish fixed at 72 hpf. Probes: one single-initiator DNA probe per target.

B.4 Reference Spectra for Alexa Fluor Dyes

In order to determine which dyes would require linear unmixing, we spectrally imaged each dye of interest, exciting with each laser source of interest. Figure B.3 shows the spectral overlap of the dyes used, as well as the extent to which each dye is excited by various excitation sources.

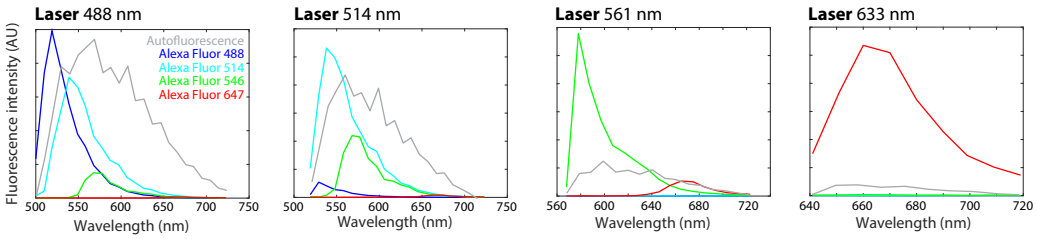

Figure B.3: **Observed emission spectra for embryo autofluorescence and Alexa Fluor dyes.** Plots depict acquired emission spectra for embryo autofluorescence and four Alexa Fluor dyes, excited with each of four laser sources.

Additionally, Table B.4 quantifies the observed excitation of efficiency depicted in Figure B.3. Histograms are integrated and normalized to the emission observed with a dye's optimal laser source (e.g. Alexa Fluor 488 excited by a 488 nm laser source). Data suggests Alexa Fluor 546 and Alexa Fluor 647 do not require unmixing in their respective channels. Imaging Alexa Fluor 488 and 514 requires linear unmixing.

Dye/Excitation	488 nm	514 nm	561 nm	633 nm
Alexa Fluor 488	100%	93%	17%	1%
Alexa Fluor 514	7%	100%	37%	2%
Alexa Fluor 546	<1%	<1%	100%	12%
Alexa Fluor 647	<1%	<1%	<1%	100%

Table B.4: **Excitation efficiency of source and dye pairs.** Columns refer to excitation source and rows refer to specific dye. Data in fields represent the efficiency relative to the optimal source/dye pair (e.g. 488 nm laser exciting Alexa Fluor 488).

B.5 Protocols

B.5.1 Preparation of Fixed Whole-Mount Zebrafish Embryos

1. Collect embryos and incubate at 28 °C in a petri dish with egg H_2O until they reach 70 hr post-fertilization (70 hpf).

2. Transfer ∼80 embryos (72 hpf) to a 2 mL eppendorf tube and remove excess egg H_2O.

3. Fix embryos in 1 mL of 4% paraformaldehyde (PFA)[1] for 24 hr at 4 °C .

4. Wash embryos 3 × 5 min with 1 mL of 1× phosphate-buffered saline (PBS) to stop the fixation. Fixed embryos can be stored at 4 °C at this point.

5. Dehydrate and permeabilize with a series of methanol (MeOH) washes (1 mL each):

   a) 100% MeOH for 4 × 10 min

   b) 100% MeOH for 1 × 50 min.

6. Rehydrate with a series of graded 1 mL MeOH/PBST washes for 5 min each:

   a) 75% MeOH / 25% PBST

   b) 50% MeOH / 50% PBST

   c) 25% MeOH / 75% PBST

   d) 5 × 100% PBST.

7. Digest embryos with 1 μg/mL proteinase K for 15 min[2].

8. Immediately post-fix embryos in 4% PFA for 20 min[3].

9. Wash embryos 5 × 5 min with 1 mL of tris-buffered saline (TBST) to stop the fixation and wash out phosphate.

10. Wash embryos 3 × 15 min with 1 mL of 1-Methylimidazole buffer (1-MIB).

[1] Use fresh PFA to avoid increased autofluorescence.
[2] Be sure to optimize exact proteinase K digestion conditions per batch.
[3] PFA made earlier can be reused during post-fixation.

11. Fix embryos in 1 mL of 0.16 M 1-ethyl-3-(3-dimethylaminopropyl) carbodiimide (EDC) in 1-MIB[4] for 2 hr at RT.

12. Wash embryos 4 $\times$ 5 min with 1 mL TBST.

13. Store embryos at 4 °C before use[5].

[4] Add dry EDC to 1-MIB immediately before adding to sample.
[5] Prepare embryos every two weeks to avoid increased autofluorescence.

B.5.2 Multiplexed in situ Hybridization Chain Reaction

Detection stage

1. For each sample, move 8 embryos to a 1.5 mL eppendorf tube.
2. Pre-hybridize with 500 μL of probe hybridization buffer for 30 min at 45 °C.
3. Prepare probe solution by adding 1 pmol of each probe (1 μL of 1 μM stock per probe) to 500 μL of probe hybridization buffer at 45 °C.
4. Remove the pre-hybridization solution and add the probe solution.
5. Incubate the embryos overnight (12–16 hr) at 45 °C.
6. Remove excess probes by washing at 45 °C with 500 μL of:
   a) 75% of probe wash buffer / 25% 5× SSCT for 15 min
   b) 50% of probe wash buffer / 50% 5× SSCT for 15 min
   c) 25% of probe wash buffer / 75% 5× SSCT for 15 min
   d) 100% 5× SSCT for 15 min
   e) 100% 5× SSCT for 30 min.

   Wash solutions should be pre-heated to 45 °C before use.

Amplification stage

1. Pre-amplify embryos with 500 μL of amplification buffer for 30 min at room temperature.
2. Prepare 30 pmol of each fluorescently-labeled hairpin by snap cooling in 10 μL of 5× SSC buffer (heat at 95 °C for 90 seconds and cool to room temperature on the benchtop for 30 min).
3. Prepare hairpin solution by adding all snap-cooled hairpins to 500 μL of amplification buffer at room temperature.
4. Remove the pre-amplification solution and add the hairpin solution.
5. Incubate the embryos overnight (12–16 hr) at room temperature.

6. Remove excess hairpins by washing with 500 μL of 5$\times$ SSCT at room temperature:

   a) 2 $\times$ 5 min

   b) 2 $\times$ 30 min

   c) 1 $\times$ 5 min

B.5.3 Buffer Recipes

4% Paraformaldehyde (PFA)	For 25 mL of solution
4% PFA	1 g of PFA powder
1× PBS	25 mL of 1× PBS

PBST	For 50 mL of solution
1× PBS	5 mL of 10× PBS
0.1% Tween 20	500 μL of 10% Tween 20
	Fill up to 50 mL with ultrapure H_2O

TBST	For 50 mL of solution
1× TBS	5 mL of 10× TBS
0.1% Tween 20	500 μL of 10% Tween 20
	Fill up to 50 mL with ultrapure H_2O

1-Methylimidazole buffer (1-MIB)	For 20 mL of solution
300 mM NaCl	2 mL of 3M NaCl
0.13 M 1-methylimidazole	200 μL 1-methylimidazole
	Add 56 μL 12 M HCl to pH 8.0
	Fill up to 20 mL with ultrapure H_2O

EDC fixation buffer[6]	For 10 mL of solution
0.16 M EDC	0.163 g EDC
	Fill up to 10 mL with 1-MIB

[6]Prepare EDC fixation buffer immediately prior to use.

[6]Prepare EDC fixation buffer immediately prior to use.

B.5.4 Reagents and Supplies

EDC (Thermo Scientific Pierce Cat. # PI22980)

HCR Amplifiers and Buffers (Molecular Instruments)

Hydrochloric Acid (HCl) (EMD Millipore Cat. # HX0603-75)

Methanol (Mallinckrodt Chemicals Cat. # 3016-16)

Paraformaldehyde (PFA, 16% methanol free) (Alfa Aesar Cat. # 43368)

Proteinase K solution (Ambion Cat. # AM2546)

1-Methylimidazole (MP Biomedicals, LLC Cat. # 0215165580)

10× Phosphate-buffered saline (PBS) (Ambion Cat. # AM9625)

20× Sodium chloride sodium citrate (SSC) (Invitrogen Cat. # 15557-044)

20× Tris-buffered saline (TBS) (Pierce Cat. # 28358)

22 mm × 50 mm No. 1 coverslip (VWR Cat. # 48393-048)

25 mm × 75 mm glass slide (VWR Cat. # 48300-025)

50% Tween 20 (Invitrogen Cat. # 00-3005)

B.6 Sequences

Sequences for the all target microRNAs and mRNAs used in this paper were obtained from the Zebrafish Information Network (ZFIN). All sequences are listed 5′ to 3′.

B.6.1 Probes for microRNA Targets

Each microRNA probe carries a single initiator for HCR.

Target: **microRNA-9 (miR-9)**

Amplifier: **HCR B3**

Fluorophore: **Alexa Fluor 546**

Probe Sequence	Spacer	Initiator
mUmCmAmUmAmCmAmgmCmUmAmgmAmUmAmAmCmCmAmAmAmgmA	TAAAA	AAAgTCTAATCCgTCCCTgCCTCTATATCTCCACTC

Target: **microRNA-96 (miR-96)**

Amplifier: **HCR B4**

Fluorophore: **Alexa Fluor 488**

Probe Sequence	Spacer	Initiator
mAmgmCmAmAmAmAmUmgmUmgmCmUmAmgmUmgmCmCmAmAmA	ATTTT	CACATTTACAgACCTCAACCTACCTCCAACTCTCAC

Target: **microRNA-206 (miR-206)**

Amplifier: **HCR B2**

Fluorophore: **Alexa Fluor 514**

Probe Sequence	Spacer	Initiator
mCmCmAmCmAmCmAmCmUmUmCmCmUmUmAmCmAmUmUmCmCmA	AAAAA	AgCTCAgTCCATCCTCgTAAATCCTCATCAATCATC

B.6.2 Probes for mRNA Target

mRNA probe set consists of multiple probes, each carrying two initiators for HCR.

Target: **hemoglobin alpha embryonic-3 (hbae3)**

Amplifier: **HCR B1**

Fluorophore: **Alexa Fluor 647**

Initiator 1	Spacer	Probe #	Spacer	Initiator 2
gAggAgggCAgCAAACgggAAgAgTCTTCCTTTACg	ATATT	1	ATATA	gCATTCTTTCTTgAggAgggCAgCAAACgggAAgAg
gAggAgggCAgCAAACgggAAgAgTCTTCCTTTACg	ATATT	2	ATATA	gCATTCTTTCTTgAggAgggCAgCAAACgggAAgAg
gAggAgggCAgCAAACgggAAgAgTCTTCCTTTACg	ATATT	3	ATATA	gCATTCTTTCTTgAggAgggCAgCAAACgggAAgAg
gAggAgggCAgCAAACgggAAgAgTCTTCCTTTACg	ATATT	4	ATATA	gCATTCTTTCTTgAggAgggCAgCAAACgggAAgAg
gAggAgggCAgCAAACgggAAgAgTCTTCCTTTACg	ATATT	5	ATATA	gCATTCTTTCTTgAggAgggCAgCAAACgggAAgAg
gAggAgggCAgCAAACgggAAgAgTCTTCCTTTACg	ATATT	6	ATATA	gCATTCTTTCTTgAggAgggCAgCAAACgggAAgAg
gAggAgggCAgCAAACgggAAgAgTCTTCCTTTACg	ATATT	7	ATATA	gCATTCTTTCTTgAggAgggCAgCAAACgggAAgAg

Probe #	Probe Sequence
1	ATCAgCCCgACggCAgTCAAAACTCCgTTTATCACCgTggTTCCgTgCTT
2	gTCCTTTgCggAAAgACTCATggTTgCTTggTTAgCTgTgggCAggCTgA
3	AAgAgTCTCACggCCgATCTCCTCAgCTTTgggTgCAACCTTgTCAAAgA
4	CACCAgCAgATTgTggTTgATgATCTTgAAgTTTgCggggTCCACgCgCA
5	ggCTgACCTgggCCAggAACTTgTCCACggAAACATgCACCTCAggAgTg
6	gAggAgAgTTggggCTTAggTCTgCCCAgTgggAgAAgTATgTCTTCgTC
7	CATCAgAgATgAAggCAAgCTgCAgCTTTAgCggTACTTCTCggACAggg

B.6.3 Amplifier Sequences

Sequences for DNA HCR initiators were obtained from Molecular Instruments (MI). All sequences are listed 5′ to 3′.

System #	Initiator 1	Spacer 1	Spacer 2	Initiator 2
B1	gAggAgggCAgCAAACgggAAgAgTCTTCCTTTACg	ATATT	ATATA	gCATTCTTTCTTgAggAgggCAgCAAACgggAAgAg
B2	CCTCgTAAATCCTCATCAATCATCCAgTAAACCgCC	AAAAA	AAAAA	AgCTCAgTCCATCCTCgTAAATCCTCATCAATCATC
B3	gTCCCTgCCTCTATATCTCCACTCAACTTTAACCCg	TACAA	TAAAA	AAAgTCTAATCCgTCCCTgCCTCTATATCTCCACTC
B4	CCTCAACCTACCTCCAACTCTCACCATATTCgCTTC	TAAAA	ATTTT	CACATTTACAgACCTCAACCTACCTCCAACTCTCAC

Table B.5: DNA HCR initiator sequences.

Appendix C

SUPPLEMENTARY INFORMATION FOR CHAPTER IV

C.1 Materials and Methods

C.1.1 HCR Probes and Amplifiers

Probes were ordered as DNA sequences appended by the appropriate DNA HCR initiator sequence from Integrated DNA Technologies (www.idtdna.com). Kits containing a DNA HCR amplifier and hybridization, wash, and amplification buffers were purchased from Molecular Instruments (www.molecularinstruments.org). See Table C.1 for a summary of probe set, amplifier, and fluorophore details and Appendix C.4 for probe sequences.

Target Type	Target Organism	HCR Amplifier	Fluorophore	Figures
16s rRNA	All *Bacteroides*	B1	Alexa488	4.6, 4.5, 4.3, C.1
		None	Alexa488	4.3
		B1	Alexa546	4.4
		None	Alexa546	4.2
	Bacteroides fragilis	B3	Alexa647	4.4a, 4.6, 4.5
		None	Alexa647	4.2
	Bacteroides ovatus	None	Alexa647	4.2
	Bacteroides theta	None	Alexa647	4.2
	Bacteroides vulgatus	B2	Alexa546	4.6, 4.5
		B2	Alexa647	4.4b
		None	Alexa647	4.2

Table C.1: Probe, HCR amplifier, and fluorophore for each *Bacteroides* species. All targets detected with single probe each.

C.1.2 Experimental Design

Mice were handled and sectioned by trained personnel in the Mazmanian Lab following IACUC guidelines. Fresh frozen colon tissue sections were fixed and permeabilized using the protocol of Sections C.3.1. *In situ* hybridization experiments were performed using the protocols of Section C.3.2. Samples were prepared for imaging as described also in Section C.3.2.

C.1.3 Microscopy

Images were acquired using either a ZEISS Axio Observer Z1 fluorescent microscope or a ZEISS LSM 800 confocal microscope. For fluorescent microscopy images, an EC Plan-NeoFluar 40x/0.75 Ph2 M27 objective was used with 1.6x Optovar for a final magnification of 64x. For confocal images, a Plan-Apochromat 63x/1.40 Oil DIC M27 objective was used to acquire all images. See Tables C.2 and C.3 for a summary of excitation sources, beam splitters, and tuned emission bandpass filters used for each fluorophore on both types of microscopes.

Fluorophore	Excitation (nm)	Beam Splitter (nm)	Filter (nm)
Alexa546	545 ± 30	570	620 ± 60
Alexa647	640 ± 30	660	690 ± 50

Table C.2: Fluorescent microscope settings for each fluorophore channel.

Fluorophore	Laser (nm)	Beam Splitter (nm)	Filter (nm)
Alexa405	405	None	400–450
Alexa488	488	488/561/633	490–530
Alexa546	561	488/561/633	561–580
Alexa647	633	488/561/633	645–700

Table C.3: Confocal microscope settings for each fluorophore channel.

C.1.4 Image Analysis

Image analysis presented here is based upon aforementioned work (Appendix B.1.5) [1]. For each acquired image, thresholds are applied using Otsu's method to automatically determine threshold by exhaustively searching for the threshold that minimized intra-class variance in signal and background. Once this threshold is applied, a binary mask is created. This binary mask is used to extract pixels corresponding to signal plus background (SIG + BACK). Background (BACK) is characterized for pixels in a representative region not containing bacterial cells (as determined by universal 16S staining).

Once this data is extracted from images, calculations are performed similar to those found in Appendix B.1.5.

Figure 4.5 demonstrates raw images and corresponding histograms obtained from analysis. Estimates for background ($\bar{x}_{BACK} \pm \sigma_{BACK}$), signal ($\bar{x}_{SIG} \pm \sigma_{SIG}$), and signal-to-background ($\bar{x}_{SB}$) are displayed for each target species in Table 4.1.

Additionally, Figure 4.2 and related Table 4.2 demonstrate raw images and quantitative analysis. Estimates for universal 16S (EUB) signal, species-specific signal, and the normalized signal (discrimination ratio) are displayed for each target species in Table 4.2.

C.2 Comparison of Literature in situ vs Optimized HCR Protocol

Figure C.1 compares current methodology for short probe hybridization[3] compared to optimized conditions presented in Appendix C.3. Key differences between the protocols include hybridization temperature, hybridization and wash buffers, and wash protocol. Detailed descriptions of these can also be found in Appendix C.3.3.

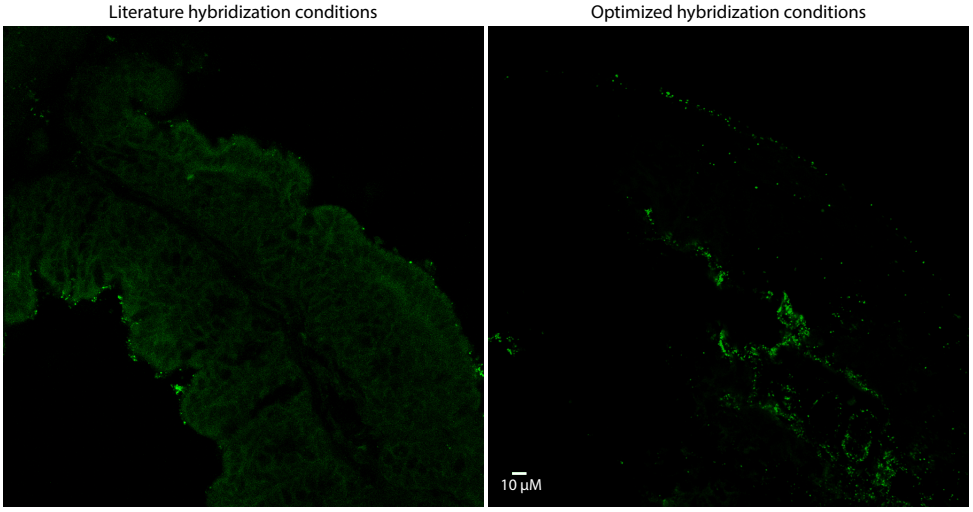

Figure C.1: **Comparing literature in situ protocol to optimized HCR protocol.** Sample: Mouse colon tissue sections singly-colonized with *B. fragilis*. Probe: one HCR probe targeting a universal 16S region amplified with Alexa488-labeled HCR using literature conditions (left) versus optimized conditions (right).

C.3 Protocols

C.3.1 Preparation of Fresh Frozen Mouse Colon Tissue Sections

1. Remove slides from -80 °C, and allow to thaw and air dry to RT.
2. Wipe down slide as much as possible with Kimwipe without disturbing sections.
3. Fix sections by placing slides in Coplin jar filled with 30 mL of 4% paraformaldehyde (PFA)[1] for 20 m at RT.
4. Remove fixative, and wash slides twice in PBST for 5 m at RT.

[1] Use fresh PFA to avoid increased autofluorescence.

C.3.2 Multiplexed in situ Hybridization Chain Reaction

Detection stage

1. Pre-hybridize with 150 μL of 20% hybridization buffer for 1 h at 65 °C.
2. Prepare probe solution by adding 0.2 pmol of each probe (2 μL of 0.1 μM stock per probe) to 100 μL of 20% hybridization buffer at 37 °C.
3. Wipe down slide without disturbing tissue sections to remove the pre-hybridization solution and add 75 μL of the probe solution.
4. Place cover slip over tissue sections to minimize evaporation.
5. Incubate slides overnight (12–16 hr) at 37 °C in a humidified chamber.
6. Gently remove the cover slip by immersing slide in a Coplin jar filled with 30 mL of 20% probe wash buffer at RT.
7. Remove excess probes by washing at 37 °C in a Coplin jar filled with 30 mL each of:
   a) 75% of 20% probe wash buffer / 25% 5× SSCT for 15 min
   b) 50% of 20% probe wash buffer / 50% 5× SSCT for 15 min
   c) 25% of 20% probe wash buffer / 75% 5× SSCT for 15 min
   d) 100% 5× SSCT for 15 min

   Wash solutions should be pre-heated to 37 °C before use.
8. Immerse slides in 5× SSCT at RT for 5 m.

Amplification stage

1. Pre-amplify with 150 μL of amplification buffer for 1 h at RT.
2. Prepare 6 pmol of each fluorescently-labeled hairpin by snap cooling in 2 μL of 5× SSC buffer (heat at 95 °Cfor 90 seconds and cool to room temperature on the benchtop for 30 min).
3. Prepare hairpin solution by adding all snap-cooled hairpins to 100 μL of amplification buffer at RT.

4. Wipe down slide without disturbing tissue sections to remove the pre-amplification solution and add 75 μL of the hairpin solution.

5. Place cover slip over tissue sections to minimize evaporation.

6. Incubate slides overnight (12–16 hr) at RT in a humidified chamber.

7. Gently remove the cover slip by immersing slide in a Coplin jar filled with 30 mL of 5× SSCT at RT.

8. Remove excess amplifier by washing at RT in a Coplin jar filled with 30 mL each of:

   a) 2 × 30 min

   b) 1 × 5 min

Tissue Section Staining and Mounting

1. Prepare phalloidin staining buffer by diluting 1:40 stock into PBST.

2. Add 150 μL staining buffer to cover tissue sections on slide.

3. Incubate slides 1–24 h at RT in a humidified chamber.[2]

4. Remove staining buffer by washing twice at RT in a Coplin jar filled with 30 mL of 5× SSCT.

5. Wipe down slide without disturbing tissue sections to remove 5× SSCT.

6. Add 75 μL ProLong Gold mounting media to cover tissue sections, and immediately place cover slip.

7. Slides can be stored in the dark at RT indefinitely.

[2]For longer incubation, consider using a cover slip to minimize evaporation.

C.3.3 Buffer Recipes

4% Paraformaldehyde (PFA)	For 40 mL of solution
4% PFA	10 mL of 16% Methanol-Free PFA
1× PBS	30 mL of 1× PBS

PBST	For 50 mL of solution
1× PBS	5 mL of 10× PBS
0.1% Tween 20	500 μL of 10% Tween 20
	Fill up to 50 mL with ultrapure H_2O

SSCT	For 50 mL of solution
5× Sodium Chloride Sodium Citrate (SSC)	12.5 mL of 20× SSC
0.1% Tween 20	500 μL of 10% Tween 20
	Fill up to 50 mL with ultrapure H_2O

20% Hybridization Buffer	For 40 mL of solution
20% Formamide	8 mL of Formamide
5× SSC	10 mL of 20× SSC
9 mM Citric Acid (pH 6.0)	360 μL of 1 M Citric Acid (pH 6.0)
0.1% Tween 20	400 μL of 10% Tween 20
50 μg/mL Heparin	200 μL of 10 mg/mL Heparin
1× Denhardt's Solution	800 μL of 50× Denhardt's Solution
10% Dextran Sulfate	10 mL of 50% Dextran Sulfate
	Fill up to 40 mL with ultrapure H_2O

20% Probe Wash Buffer	For 40 mL of solution
20% Formamide	8 mL of Formamide
5× Sodium Chloride Sodium Citrate (SSC)	10 mL of 20× SSC
9 mM Citric Acid (pH 6.0)	360 μL of 1 M Citric Acid (pH 6.0)
0.1% Tween 20	400 μL of 10% Tween 20
50 μg/mL Heparin	200 μL of 10 mg/mL Heparin
	Fill up to 40 mL with ultrapure H_2O

Amplification Buffer	For 40 mL of solution
5× Sodium Chloride Sodium Citrate (SSC)	10 mL of 20× SSC
0.1% Tween 20	400 μL of 10% Tween 20
10% Dextran Sulfate	10 mL of 50% Dextran Sulfate
	Fill up to 40 mL with ultrapure H_2O

Phalloidin Staining Buffer	For 200 μL of solution
1× Phalloidin	5 μL of stock Phalloidin
	Fill up to 200 μL with PBST

Literature Hybridization Buffer

Probes hybridized at 35 °C.

30% Formamide

900 mM NaCl

20 mM Tris-HCl

0.1% Sodium Dodecyl Sulfate

Literature Wash Buffer

Probes washed at 37 °C.

64 mM NaCl

20 mM Tris-HCl

5 mM EDTA

0.1% Sodium Dodecyl Sulfate

C.3.4 Reagents and Supplies

Alexa Fluor 488 Phalloidin (Thermo Fisher Cat. # A12379)
CytoPainter Phalloidin-iFluor 405 (Abcam Cat. # AB176752)
HCR Amplifiers and Buffers (Molecular Instruments)
Paraformaldehyde (PFA, 16% methanol free) (Alfa Aesar Cat. # 43368)
ProLong Gold Antifade Mountant (Thermo Fisher Cat. # P36930)
Wheaton Coplin Staining Jar (Sigma Aldrich Cat. # S6016)
10× Phosphate-buffered saline (PBS) (Ambion Cat. # AM9625)
20× Sodium chloride sodium citrate (SSC) (Invitrogen Cat. # 15557-044)
25 mm x 25 mm No. 1 coverslip (VWR Cat. # 48393-)
25 mm x 75 mm glass slide (VWR Cat. # 48393-048)
50% Tween 20 (Invitrogen Cat. # 00-3005)

C.4 Sequences

Sequences for the all target rRNAs used in this paper were obtained from prior studies in the field[3, 4]. All sequences are listed 5′ to 3′.

C.4.1 Direct-Labeled Probes

Target	Fluorophore	Probe
Universal 16S	FITC	/5FluorT/TgCTgCCTCCCgTAggAgTT
Bacteroides fragilis	Cy5	/5Cy5/gTTTCCACATCATTCCACTg
Bacteroides ovatus	Cy5	/5Cy5/CAACAgCCTTACggCTA
Bacteroides theta	Cy5	/5Cy5/CATTTgCCTTgCggCTA
Bacteroides vulgatus	Cy5	/5Cy5/AgATgCCTTgCggCTTACggC

C.4.2 HCR Probes

The universal 16S rRNA probe set consists of five probes, each carrying a single initiator for HCR. Species are detected using single probes, each carrying a single initiator for HCR.

Target	Amplifier	Probe	Spacer	Initiator
Universal 16S Probe	HCR B1	CATTgACCAATATTCCTCAC	ATATA	gCATTCTTTCTTgAggAgggCAgCAAACgggAAgAg
Bacteroides fragilis	HCR B5	gTTTCCACATCATTCCACTg	ATTTT	CACTTCATATCACTCACTCCCAATCTCTATCTACCC
Bacteroides ovatus	HCR B2	CAACAgCCTTACggCTA	AAAAA	AgCTCAgTCCATCCTCgTAAATCCTCATCAATCATC
Bacteroides theta	HCR B3	CATTTgCCTTgCggCTA	TAAAA	AAAgTCTAATCCgTCCCTgCCTCTATATCTCCACTC
Bacteroides vulgatus	HCR B4	AgATgCCTTgCggCTTACggC	ATTTT	CACATTTACAgACCTCAACCTACCTCCAACTCTCAC

C.4.3 Amplifier Sequences

Sequences for DNA HCR initiators were obtained from Molecular Instruments (MI). All sequences are listed 5′ to 3′.

System #	Initiator 1	Spacer 1	Spacer 2	Initiator 2
B1	gAggAgggCAgCAAACgggAAgAgTCTTCCTTTACg	ATATT	ATATA	gCATTCTTTCTTgAggAgggCAgCAAACgggAAgAg
B2	CCTCgTAAATCCTCATCAATCATCCAgTAAACCgCC	AAAAA	AAAAA	AgCTCAgTCCATCCTCgTAAATCCTCATCAATCATC
B3	gTCCCTgCCTCTATATCTCCACTCAACTTTAACCCg	TACAA	TAAAA	AAAgTCTAATCCgTCCCTgCCTCTATATCTCCACTC
B4	CCTCAACCTACCTCCAACTCTCACCATATTCgCTTC	TAAAA	ATTTT	CACATTTACAgACCTCAACCTACCTCCAACTCTCAC
B5	CTCACTCCCAATCTCTATCTACCCTACAAATCCAAT	AAAAA	ATTTT	CACTTCATATCACTCACTCCCAATCTCTATCTACCC

Table C.4: DNA HCR initiator sequences.